2015

Design, Fabrication, and Characterization of Pseudomorphic and Quasi-Pseudomorphic AlGaN Based Deep Ultraviolet Light Emitting Diodes Over Sapphire

Fatima Asif
University of South Carolina - Columbia

Design, Fabrication, and Characterization of Pseudomorphic and Quasi-Pseudomorphic AlGaN Based Deep Ultraviolet Light Emitting Diodes Over Sapphire

by

Fatima Asif

Bachelor of Science
University of Engineering and Technology, Lahore 2003

Master of Science
University of South Carolina 2011

Submitted in Partial Fulfillment of the Requirements

for the Degree of Doctor of Philosophy in

Electrical Engineering

College of Engineering and Computing

University of South Carolina

2015

Accepted by:

Asif Khan, Major Professor

Mohammod Ali, Committee Member

Enrico Santi, Committee Member

Jamil Khan, Committee Member

Lacy Ford, Vice Provost and Dean of Graduate Studies

Dedication

Dedicated to my loving family.

Acknowledgments

I would like to express my sincere gratitude to my advisor, Professor Asif Khan, from whom I have learned so much, about life and research. He has been a true inspiration, and I thank him for his guidance in helping me develop into a better researcher and human being. Next, I would like to thank the members of my dissertation committee: Prof. Enrico Santi, Prof. Jamil Khan, and Prof. Mohammod Ali, for their many insightful comments and suggestions that have helped improve this dissertation. I would also like to acknowledge and thank Nitek, Inc. for their collaboration and help in this research. This research is the outcome of a team effort and would not have succeeded without the help of many kind and brilliant researchers. I would especially like to thank Dr. Vinod Adivarahan, Dr. Mohamed Lachab, Dr. Iftikhar Ahmed, Dr. Qhalid Fareed, Bin Zhang, and Dr. Alex Lunev from Nitek. I wish to thank my fellow colleagues and researchers over the years, Ahmad Heidari, Dr. Monirul Islam, Dr. Seongmo Hwang, Dr. Joe Dion, Dr. Hung-Chi Chen, Sho Sugiyama, Mahbuba Sultana, Sakib Muhtadi, Antwon Coleman, Morgan Gauthreaus, Daniel Morgan, Josh Raiborde, Blythe Johnson, and many others, for their friendship, help, and camaraderie. I would also like to thank the friendly staff at department of electrical engineering including Nat Paterson, Ashley Burt, Heather Covey, and Alicia Williams. Most importantly, I wish to thank my family: my parents, my husband, my brothers and sisters, for loving me, for believing in me, and for supporting me every step of the way.

Abstract

III-Nitride based deep ultraviolet (UV) light emitting diodes (LEDs) emitting below 280nm has the potential to replace mercury lamps currently used in the systems for water/air purification, germicidal and medical instruments sterilization applications. However, this potential has not yet been fully realized as the output power, quantum efficiency and lifetime of deep UV-LEDs have been limited by the large number of dislocations in the active region of the devices, arising from the lattice mismatched sapphire substrate, which has been the substrate of choice due to its high transparency to deep UV radiation. To reduce dislocations in the active region of the DUV LEDs grown on sapphire, AlN/AlGaN short period superlattice is usually grown to manage strain and filter the dislocations. However, the growth of these thick superlattice is not only time consuming but it can also cause severe substrate bowing making device fabrication a challenge. An alternative method for reducing the dislocation density in deep UV-LEDs structure is the use of low defect density bulk AlN substrates, which has more than two orders of magnitude low defect density than sapphire/AlN template. In spite of such a lower density of defects, the quantum efficiency values for DUV LEDs on bulk AlN substrate are very similar to that of DUV LEDs on sapphire. This is due to the high absorption coefficient of AlN substrate in the deep UV region; also the high cost and limited availability are important issues. This dissertation focuses on the design, fabrication and characterization of Deep UV LEDs employing the pseudomorphic structure similar to those grown on bulk AlN, in order to keep the active layers crystalline quality very close to that of the underlying AlN/Sapphire template. Other LED designs, with different degree of relaxation of the n-AlGaN

current spreading layer were also investigated with the main target of achieving a cost-effective design without compromising the resulting device performance, namely output power and reliability.

Table of Contents

List of Figures

Chapter 1

Introduction

After decades of technological advancements and reduction in manufacturing costs, semiconductor fabrication technologies are finally in a position to replace the traditional incandescent light bulb. Light emitting diodes (LED) are emerging as the technology of choice in a wide range of applications, including but not limited to residential and commercial illumination, solid-state displays, non-line-of-sight communication, automotive lighting, and biomedical sterilization. The current generation of LEDs have higher tolerance to shock, temperature and humidity, have higher efficiencies, longer life spans, and much lower environmental impact than fluorescent or incandescent light sources.

Due to the large number of applications, a greater research focus has been placed on LEDs with light emission in the visible light spectrum. However, a number of technologically important applications require LEDs with shorter wavelength emissions in the ultraviolet (UV) range. Ultraviolet Light emitting diodes (UVLED) emit light in the UV region of electromagnetic spectrum with wavelengths ranging from 10-400 nm. Deep UV LEDs (DUV-LED) have light emissions with wavelengths in the 200-290 nm range. The primary focus of this research is on the design, fabrication, and characterization of DUV-LEDs particularly those based on pseudomorphic and quasi-pseudomorphic growth of Aluminum-Gallium-Nitride (AlGaN) epilayers over sapphire.

This introductory chapter starts with a brief introduction to the applications of DUV-LEDs. Section 1.2 presents LEDs based on group III-nitrides which include

the AlGaN-based LEDs. Section 1.3 describes the injection, extraction, and internal quantum efficiencies of these LEDs and introduces the different parameters that have been used to quantify these efficiencies. A brief survey of research literature capturing the evolution of the design of DUV-LEDs is presented in Section 1.4.

Chapter 2 introduces the established techniques and terminologies used to characterize these materials and devices. The underlying issues responsible for the low optical output power and low quantum efficiency of DUV-LEDs are also discussed in this chapter. Chapter 3 begins with an analysis of AlGaN based multiple quantum wells (MQW) quality using photo-pumping and presents the fabrication process and characterization schemes for pseudomorphic DUV-LEDs. Chapter 4 describes the development of quasi-pseudomorphic LEDs and provide a detailed comparison with pseudomorphic and standard SPSL LEDs with superlattice structure. A novel approach based on selective area material deposition is proposed in Chapter 5, along with the preliminary results. Chapter 6 concludes the dissertation with a detailed discussion of the outcomes of various experiments and the conclusions derived from them.

1.1 Applications of Ultraviolet Light Emitting Diodes

Ultraviolet Light emitting diodes emit light in the UV region of electromagnetic spectrum. UV radiations can be further subdivided into four distinct regions: UV-A (320–400 nm); UV-B (290-320 nm); UV-C or deep UV (200-290 nm); and vacuum UV (10-200 nm) [1].

UV LEDs have been used in a wide range of applications that take advantage of uniques characteristics of these electromagnetic radiations. Devices with emission in the UV-A range, particularly with wavelengths in 365-375 nm range, are generally used in low-power applications such as photo-catalytic deodorizing units in air conditioners and refrigerators. These devices range in power between 3-10 mW. UV-A

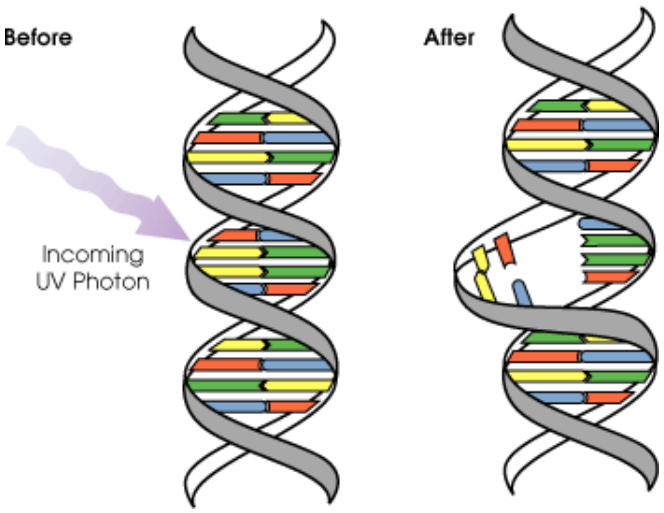

Figure 1.1: The UV radiation damages the DNA of microorganisms [3].

radiations are also used for detecting counterfeit bank-notes.

High powered variants of UV-A LEDs are used in applications such as hardening or curing of plastics and resins. These devices generally operate around the 365 nm wavelength point. The assembly process for plastic lenses in digital cameras often use a UV-A LED. These high powered devices are also used as optical pickups in digital versatile discs (DVD) and compact discs (CD). These devices require higher output power typically in the range of 100 mW to over 5 W. These LEDs have also been used as replacements for mercury lamps in modern inkjet printing and mask-aligners in photolithography sector.

The applications for UV-B are mostly in the area of medical instrumentations. These devices have been successfully used in phototherapy for the treatment of skin disorders such as psoriases [2]. This UV-B light exposure can be absorbed by the epidermis and has a significant effect on psoriasis.

Ultraviolet radiations with wavelengths ranging from 220 nm to 280 nm can disrupt chemical bonds within the Ribonucleic acid (RNA) and Deoxyribonucleic acid (DNA) of microorganisms, as shown in Figure 1.1. This leads to the destruction of their genetic information and prevents their reproduction. Without the ability to

reproduce, these microorganisms are rendered harmless when consumed by humans [4]. Hence, the primary applications for UV-C emitters are in the area of air/water purification and surface sterilization.

In water purification systems, the water is irradiated with UV light to clear bacterias and viruses. The peak absorbance of these radiations by DNA takes place at approximately 260 nm. However, the optimal wavelength for disinfection varies with the target microorganism. For the eradication of pathogens such as E-coli in water, the optimal wavelength for radiations is reported to be 269 nm [5]. UV LED based water purification systems have already been demonstrated for standing and running water [6], [7].

The III-nitride-based DUV-LEDs have also been used in defense applications, such as non-line-of-sight (NLOS) communication and bio-agent detection. NLOS communication utilizes the spectrum with wavelengths shorter than 280 nm. This frequency range has also been called as the solar blind region since the radiations in this region are absorbed by the ozone layer. This property leads to a dual benefits for NLOS communication. The absorption of extra-terrestrial radiations results to low background noise in this frequency range[8]. Hence, a higher signal to noise ratio allows for easy signal detection. Due to high absorption, the signal cannot be detected from a distance, allowing for covert communications. Furthermore, the UV light generated near earth's surface are strongly scattered by atmospheric gases. This scattering facilitate the signal to be transmitted without direct line of sight restrictions. The system would consist of a transmitter unit with a UV source (λ<280 nm) and a receiver with a solar-blind detector, as shown in Figure 1.2. The receiver would be able to detect a signal from the transmitter as long as the distance between them is between 10 and 250 meters.

The deep UV-C region of the spectrum is also ideal for detection of the fluorescence of chemical compounds in bacteria present in the environment. The unknown agent

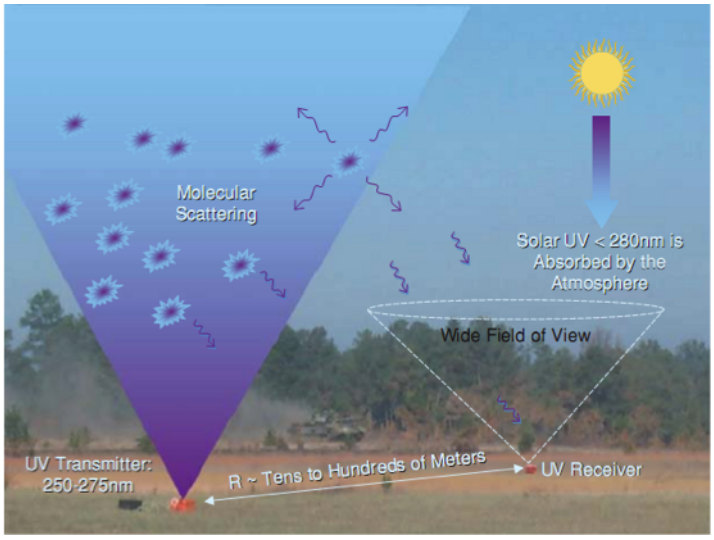

Figure 1.2: Depiction of NLOS deep UV communication.

is illuminated by the UV light source, and the emitted fluorescence spectrum can then be used to identify the presence of certain dangerous biological agents [9].

The combined market for UV LEDs is fairly large. The water purification market alone is estimated to be worth more than $5 billion [10]. With rapid technological advancement, UV LEDs are poised to replace the traditional UV mercury lamps in a large number of applications. UV mercury lamps are bulky, fragile, environmentally hazardous, have lower life spans, require regular maintenance and high voltage to operate. With fast turn on/off speeds, small footprint, low voltage operation and the ability to operate in cold environments, UV-LEDs based on III-nitrides offer many advantages over traditional mercury lamps as shown in Figure 1.3.

Different applications may require a light source with light emissions at varying wavelengths. Consequently, it is essential to fabricate an optoelectronic device with emission frequencies that can be tailored to the requirements of different applications. A ternary alloy between Gallium Nitride (GaN) and Aluminum Nitride (AlN) can be tuned to emit light at every wavelength across the ultraviolet spectrum. These devices are part of a larger family of light emitting diodes, known as the III-nitride LEDs, introduced in the next section.

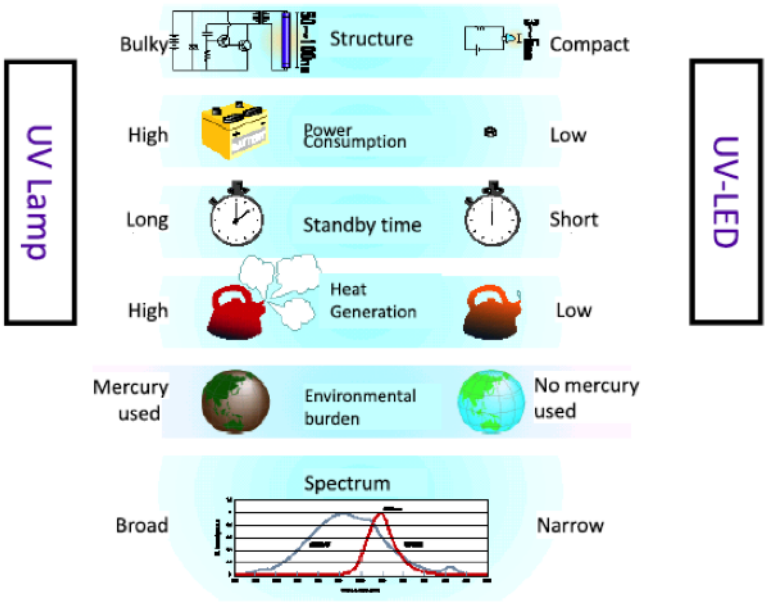

Figure 1.3: Features of UV-LEDs in comparison with mercury UV lamps [11].

1.2 History of III-Nitride Light Emitting Diodes

The III-nitride material system has direct band gap, making it an ideal candidate for the development of optoelectronic devices. The wide band gap of this material system allows us to tune the band gap energies from 0.7 eV for Indium nitride (InN) to 3.4 eV for GaN to 6.2 eV for AlN to form a ternary or quaternary III-nitride alloy system (AlInGaN) [12]. This covers the wavelength range from infrared to deep ultraviolet region of spectrum, making it the only semiconductor material system that covers the deep ultraviolet part of the spectrum.

The material properties of these devices such as high thermal conductivity, high melting point and high breakdown voltage, in addition to small size and light weight, make III-nitrides invaluable for many electronic and optoelectronic applications. Although the report on the initial synthesis of GaN, AlN and InN came out in early twentieth century, the search for material system that can be used to develop blue LEDs started in 1960s after green and red LEDs were fully realized.

In 1971, GaN single crystal based on metal-insulator-semiconductor (MIS) was

developed by Pankove et al. [13]. The growth of high quality single crystal III-nitride materials became possible after the introduction of low temperature nucleation layer by Akasaki and co-workers in 1986 [14]. The next major breakthrough was the realization of p-type material by using low energy electron beam irradiation (LEEBI) of Magnesium-doped material in 1989 [15].

In 1991, Nakamura et al. [16] pioneered the growth of low-temperature GaN buffer layer and proceeded to developed a high temperature post growth annealing method for the activation of p-type Magnesium-doped GaN film [17], which proved to be more efficient and reproducible than LEEBI. This breakthrough led Nakamura et al. to the realization of high brightness blue and green LEDs [18], [19], and laser diodes [20], [21].

After extensive research efforts, visible LEDs with high external quantum efficiencies as high as 62% at 20mA for chip size of 1x1 mm^2 have been achieved [22]. InGaN based high performance visible LEDs are already being used in many applications such as, solid-state full color display, residential, commercial and automotive lighting. As visible LED technology was reaching its maturity, the research focus was shifted towards the development of shorter wavelength UV devices mainly to replace the existing UV tube technology. Light emitting diodes with emission wavelength longer than 365 nm wavelengths are fabricated from InGaN or GaN quantum wells, while those with shorter wavelengths have AlGaN quantum wells in their active region.

The first demonstration of AlGaN-GaN-AlGaN multiple quantum wells was reported in 1990 [23]. Subsequently, the first AlGaN based UVLED with emission at 353 nm was fabricated by J. Han et al in 1998 [24]. Several research groups have used AlGaN/AlGaN MQWs, double heterostructure, quaternary AlInGaN, Mg doped AlGaN/GaN Superlattice [25]–[29], to bring the emission wavelength below 350 nm.

In 2002, the first DUV-LED with emission at 285 nm was published by Khan

et. al. [30]. These developments have been followed by multiple efforts leading to emissions below 285 nm [31]–[34]. In 2006, AlN based wavelength of 210 nm was reported by Taniyasu et al [35]. Despite these developments, AlGaN based DUV-LEDs lag in performance when compared to its visible counterparts.

1.3 Quantum Efficiency of III-Nitride Light Emitting Diodes

The emission of photons by light emitting diodes is a complex process that is shaped and influenced by a number of different processes. The first phase in this process involves the injection of electrons into the active region of the LED. Not all injected electrons make it to the active region. The injection efficiency (η_{inj}) represents the fraction of injected electrons that can be captured in the active region of the device.

A fraction of the injected electrons recombine radiatively, leading to emission of photons in the desired frequency range. The fraction of injected carriers that lead to the generation of photons, is measured by the recombination efficiency (η_r). The product of injection and recombination efficiencies is representative of the efficiency of the processes leading to light emission from the active region in the LED and is known as internal quantum efficiency ($\eta_{IQE} = \eta_{inj} \times \eta_r$).

The emitted photons must then be extracted out of the active region. The extraction efficiency (η_{ext}) is the fraction of the generated photons that survive re-absorption and make it out of the device.

The overall performance of a light emitting diodes is characterized by its external quantum efficiency (EQE). It is defined as the ratio of the number of photons emitted from a LED device to the electrons injected into the device. EQE can also be expressed as the product of injection, recombination and extraction efficiencies as shown below.

$$\eta_{EQE} = \eta_{inj} \cdot \eta_r \cdot \eta_{ext} = \eta_{IQE} . \eta_{ext} \tag{1.1}$$

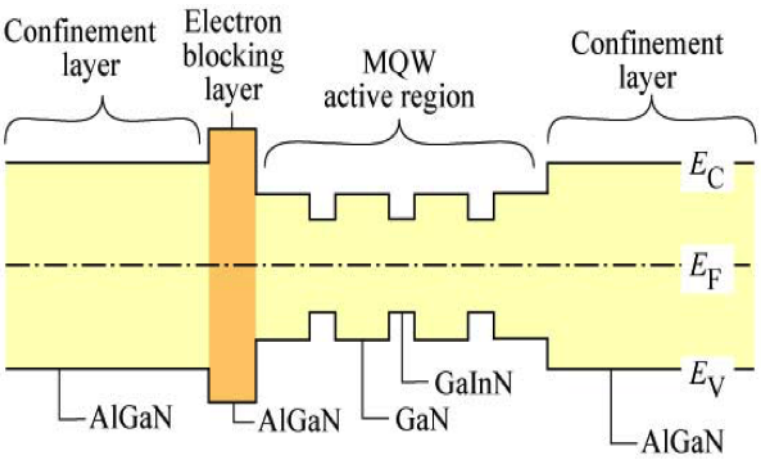

Figure 1.4: Band diagram for GaN/InGaN LED with electron blocking layer [39].

Additionally, the wall-plug efficiency (WPE) can also be used to determine the performance of a LED. Wall-plug efficiency, also known as power efficiency, is the optical output power of the device divided by the electrical power supplied to the LED.

The injected carriers can escape from the quantum wells to the confinement layers, decreasing the injection efficiency of the device. This loss of carriers can be observed as an emission peak at longer wavelength other than the desired peak of the LED. These peaks appear when electrons, instead of being captured in the active region, pass through it and recombine with holes in the p-type layer [36].

To reduce the carrier leakage out of the active region and to enhance the confinement of electrons in the quantum wells, an electron blocking layer (EBL) is inserted between the quantum wells and the p-type layer [37]. The electron blocking layer has a wider band gap and serves as a barrier to these electrons. An EBL is usually doped p-type, consequently, it offers no barrier to holes. The injection efficiency of LED device can also be influenced by the thickness of the EBL layer [38]. The band diagram of InGaN LED with electron blocking layer is shown in Figure 1.4.

The recombination efficiency depends on the ratio of radiative and non-radiative recombination of carriers. The radiative recombination happens when injected elec-

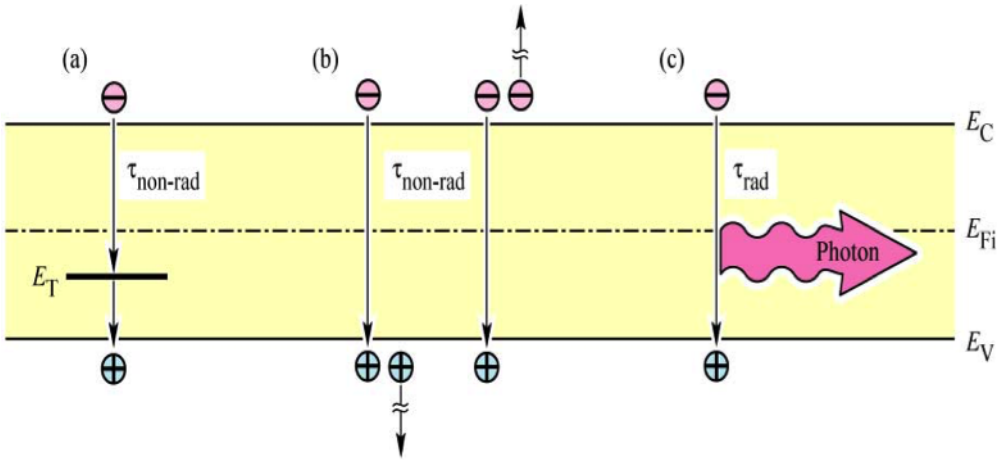

Figure 1.5: Band diagram illustrating non-radiative recombination (a) via defects/traps, (b) via auger processes and (c) radiative recombination via band-to-band recombination [39].

trons and holes recombine and emit light. The probability of radiative recombination increases with an increase in concentration of injected carriers. Multiple quantum wells are generally used to confine these carriers and to increase their concentrations.

Not every recombination leads to emission of photons in the desired frequency range. Non-radiative recombination occurs when injected carriers get trapped in the mid-gap defect states, leading to generation of phonons as heat energy. The number of these defect states in the active region is directly proportional to the dislocations/defects in the epilayer of the LED device.

Different mechanisms for carrier recombination is depicted in Figure 1.5. Part (a) in the figure depicts a non-radiative recombination where defects acts as traps for electrons and holes, causing phonon generation. In part (b), auger processes are responsible for non-radiative recombination, while part (c) illustrates band-to-band radiative recombinations, leading to generation of photons (light). Therefore, it is imperative to grow high quality epilayers in order to improve the radiative recombination efficiency.

The extraction efficiency can suffer from large differences in the refractive indices of AlGaN material, sapphire substrate, and air. A difference in refractive indices of

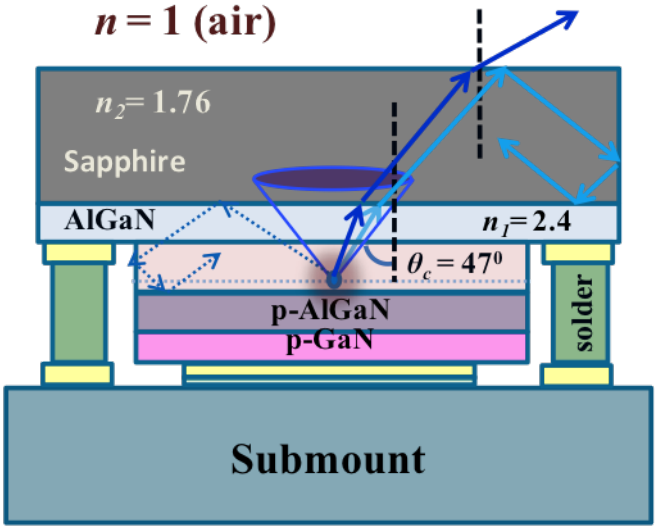

Figure 1.6: Diagram illustrating the effect of refractive index mismatch on light extraction.

adjacent layers determines the critical angle of a surface. According to Snell's law, if the emitted light is incident on a surface with an angle larger than the critical angle for that surface, it is reflected and get absorbed by the material, as shown in the Figure 1.6. To summarize, the amount of light that can be extracted from the device can be maximized by curtailing total internal reflection.

A number of different methods have been adopted by various research groups to increase the light extraction efficiency of LED devices. In [40], for example, the efficiency of the LED was improved by substrate backside roughening, while surface texturing of bottom epilayer in thin-film technology was used in [41]–[44]. Patterned sapphire substrate (PSS) has also been shown to improve the extraction efficiency of the LED device [45].

The wall plug efficiency is limited by the differential resistance of the LED device. This differential resistance arises from the cumulative effects of metal contact resistance, the n-AlGaN layer resistance, and the voltage drop across the p-n junction of LED device. An increase in the voltage drop across the device will increase the amount of energy needed to push the carriers to the active region, thereby decreas-

ing the wall plug efficiency of the device. The resistance of n-AlGaN layer must be minimized to reduce the operating voltage of a LED. A reduction in resistance can be achieved by either increasing the doping or increasing the thickness of this layer, without compromising the crystal quality.

There is tremendous room for improvement in the wall plug efficiency of DUV-LEDs. For comparison, the wall plug efficiencies for AlGaN-based UV LEDs are around 1% [46] while the efficiencies for InGaN based red and blue visible LEDs have reached or exceeded 60% [22].

1.4 Review of III-Nitride Deep Ultraviolet Light Emitting Diodes

The external quantum efficiencies for current state-of-the-art UV LEDs are shown in Figure 1.7. It is evident from the diagram that InGaN based LEDs, with emission wavelengths longer than 365 nm, have EQEs of around 14%. However, EQEs remain low for LEDs based on AlGaN quantum wells; with an EQE of approximately 3% for LEDs with wavelengths in 280-285 nm range [33], [47], and below 2% for LEDs with emissions in the UV-C region (200-280 nm). A significant degradation in the EQE has been reported for devices with shorter wavelengths [48], [49].

There are a number of factors contributing to this low value of EQE for DUV-LEDs. The high level of defect densities in AlGaN layers lead to a reduced radiative recombination efficiency. The major contributing factor to the high level of defect density can be attributed to an unavailability of lattice-matched native substrates.

The AlN substrate, while a high quality substrate, is not readily available nor is it a cost effective solution. Sapphire is the most suitable substrate commercially, due to its low cost and sufficient transparency to UV light (down to 150 nm). However, a downside of using sapphire substrate is the resulting large lattice and thermal mismatches between sapphire and AlN layers [51]. These lattice and thermal mismatches, together with the low surface mobility of Al atoms, can lead to large number

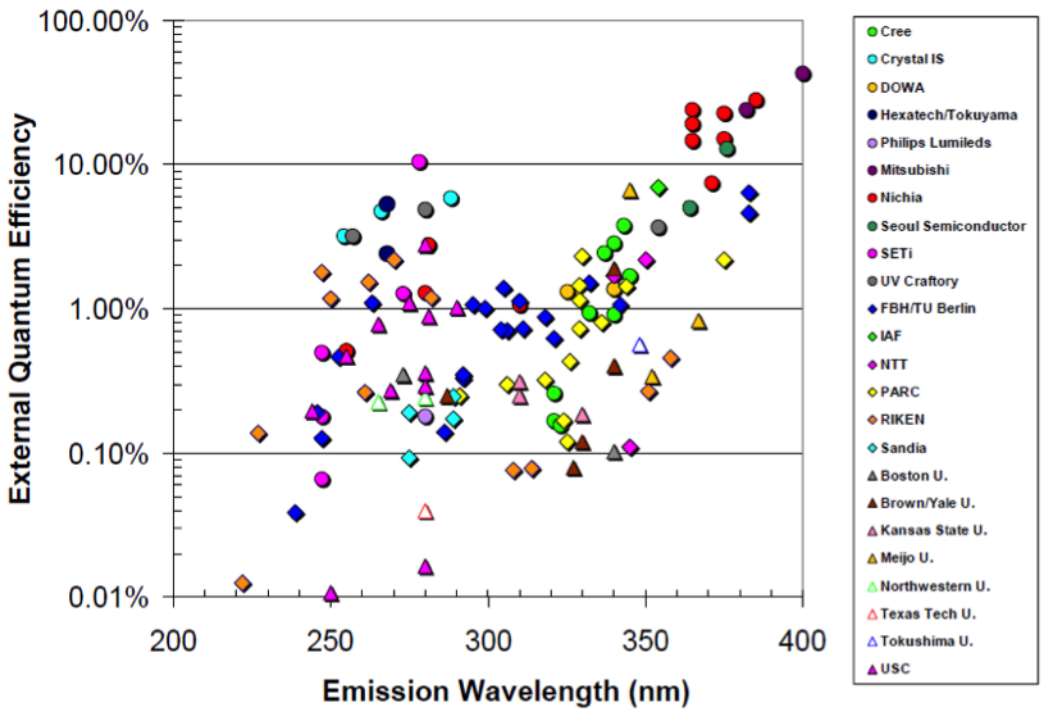

Figure 1.7: State-of-the-art in EQE for near UV and DUV-LEDs [50].

of threading dislocations in the epilayer. These threading dislocations can penetrate deep into the active region of the LED and can increase the concentration of mid-gap defect states. The presence of these defect states can lead to higher number of trapped electrons, thereby decreasing the radiative recombination efficiency.

The plot of simulated IQE as a function of the dislocation density for 280 nm UVLEDs is shown in Figure 1.8. It is evident from the plot that threading dislocation densities of less than 10^9 cm^{-2} are required for internal quantum efficiency to exceed the 50% point [52].

Different approaches have been proposed by many researchers to improve the crystal quality of the AlGaN layer. Zhang et. al. [53]–[55] employed migration enhanced metal-organic chemical vapor deposition (MEMOCVD) to grow high quality AlN layer on sapphire. Alternately, the growth of AlN layer at high temperatures with simultaneous source supply has been proposed by Pernot et al. [40], [56]. An ammo-

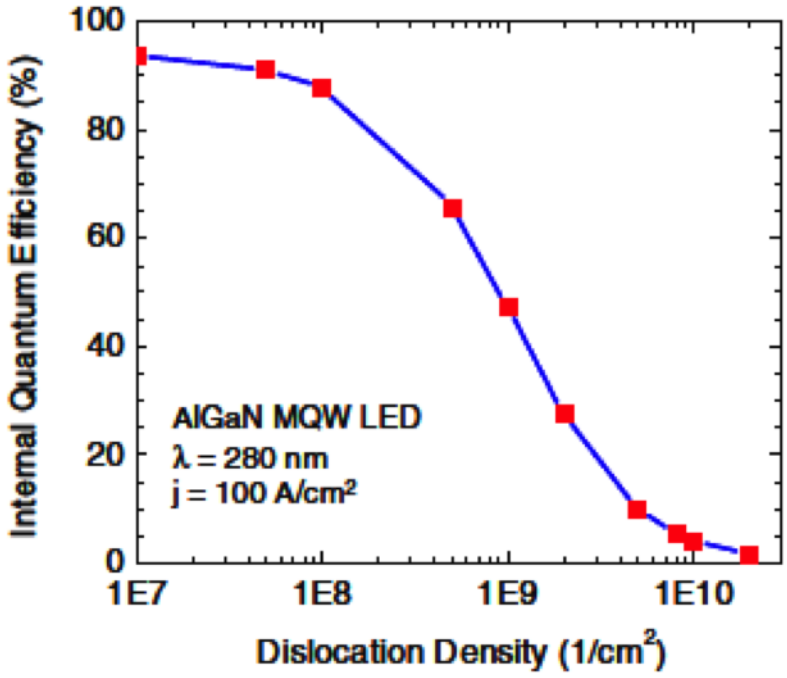

Figure 1.8: Simulated internal quantum efficiency versus the dislocation density for 280 nm DUV-LEDs.

nia pulsed-flow multilayer growth has been introduced by Hirayama et al. [49], [57], [58]. Similarly, AlN layers grown by metal-organic vapor phase epitaxy (MOVPE) at high temperature, with an optimized nucleation layer, was also demonstrated to reduce dislocation density [59].

In addition to the growth of high quality AlN buffer layer, AlN/AlGaN or AlGaN/AlGaN superlattice (SL) [54], [60] layers have also been used to further filter the defects and to enable the growth of thick n-AlGaN layer without cracking. Rough/smooth AlGaN [61] technique has been shown to reduce the defects when grown before the SL layer. Although these research efforts have brought down the overall dislocation densities from 10^{10} cm^{-2} down to $5x10^{8}cm^{-2}$ for AlGaN layers, the internal quantum efficiencies for these devices still remain below 50%.

The doping of AlGaN layers with high Al content is another challenge in DUV-LEDs. As the aluminum concentration increases, the bandgap of AlGaN layers also increases, thereby increasing the ionization energy of silicon in the case of n-AlGaN

and of magnesium for p-AlGaN layer. The activation energy for Mg dopants in GaN is already high at 250 meV. This value reaches close to 400 meV with Al content of 70%, resulting in very low conductivity and poor injection of hole carriers.

This low conductivity creates a number of issues in the design of efficient DUV-LEDs. An increase in the layer resistance results in higher joule heating in the device, further reducing the device efficiency and reliability. Since it is difficult to make ohmic contacts directly on p-AlGaN layer, a p-GaN layer is deposited on top of this layer to serve as a contact layer. This additional layer increases the rate of absorption of the UV emissions. The p-GaN layer also serves as a potential barrier to the injected holes before they can be transported across the p-AlGaN layer down to the active region. The trapped holes at the interface set up an electric field, which attracts the electrons and allows a fraction of them to bypass the QWs and recombine non-radiatively in the p-GaN layer, further reducing the injection efficiency. A multi-quantum barrier electron-blocking layer was employed in [49] to improve the injection efficiency. The barrier for hole injection can be reduced by grading the composition of p-AlGaN layer [62].

A number of research efforts have tried to address the issues of light absorption in the p-GaN contact layer and total internal reflection due to high refractive indices. The refractive index for AlGaN layers is relatively high with values between 2-2.5. Consequently, more than 92% of the produced photons are reflected back into the semiconductor. An encapsulation epoxy with high refractive index can be introduced to improve light extraction. A disadvantage of this approach is that majority of encapsulation polymers deteriorate when exposed to UV light for long durations.

Laser lift-off, together with epilayer texturing/roughening, have been employed in a number of configurations to improve light extraction. Notable variants of this technique include vertical injection thin-film UVLEDs [63], [64] and lateral injection thin-film flip-chip UVLEDs [65]–[67]. Other important techniques include moth-eye

structures [40], [56], and nano-pixel contact design with Al reflector [68].

The highest reported EQE of 10.4%, at a wavelength of 278 nm, is achieved by a combination of these techniques [69]. In the first step, the internal quantum efficiency was maximized by a reduction in dislocation density. Maximum light extraction was then ensured by using a combination of UV-transparent p-type contact layers, and UV reflecting ohmic contacts. The transparent p-type contact layer minimizes light absorption and allow the photons to reach the ohmic contacts which was made reflective to collect these photons and reflect them back into the device. Finally, an encapsulation of the device with an epoxy layer, with optimized shape and refractive index, allowed for maximum extraction of light from the device.

Chapter 2

Problem Identification and Characterization Techniques

2.1 Problem Identification

Sapphire is the substrate of choice for deep ultraviolet light emitting diodes (UV-LEDs). Sapphire is primarily used due to its low cost, high availability, and optical transparency to UV radiations down to 150 nm range.

The large lattice and thermal mismatches between sapphire and high Al-content AlGaN epilayers, however, lead to the formation of a large number of threading dislocations and cracks in the LED structure. Upon reaching the active region of the LED, these defects act as non-radiative recombination centers for the injected carriers, hence reducing the device output power.

In addition to reduced efficiency, the non-radiative recombination process is directly related to lifetime degradation of LEDs [70]. The energy emitted through the non-radiative recombination of carriers is usually in the form of phonon (heat), which dissipates into crystal lattice and accelerate the degradation of the device.

Due to poor doping efficiency of high Al-content n-AlGaN layer, DUV-LEDs exhibit high series resistance, which subsequently leads to higher operating voltage, and results in low wall-plug efficiency.

The focus of this research is to improve the design of DUV-LEDs, leading to more efficient growth and fabrication processes, increasing its commercial feasibility without sacrificing the optical output power or reliability of these devices.

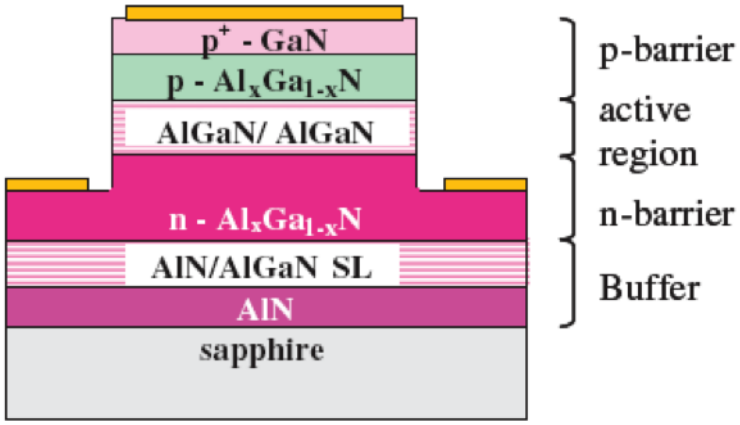

Figure 2.1: A typical schematic of DUV-LEDs [73].

In order to reduce dislocations in the active region of the DUV-LEDs grown on sapphire, an AlN buffer layer is first deposited [53]–[55]. This deposition is followed by the growth of AlN/AlGaN short-period superlattice, introduced in [54], [60], to manage strain in the epilayer and filter the dislocations. The introduction of the superlattice allows for the growth of thick n-AlGaN layer without the formation of cracks. This fully-relaxed device structure, first developed by [54], has since been adopted by a number of researchers including [33], [71], [72].

The growth of superlattice is an effective strain management techniques, however, it suffers from a number of issues. It is a complex and time consuming process that suffers from the problem of reproducibility, resulting in lower yields and commercial feasibility. Furthermore, the growth of thick superlattice structures is often plagued by the introduction of bowing in the resulting wafer which further complicates the fabrication process. The device schematic for a DUV-LED with superlattice structure is shown in Figure 2.1.

Another source for reductions in the dislocation density in DUV-LEDs structure is the use of low defect density bulk AlN substrates instead of sapphire [74]. The defect density in homoepitaxial AlN buffer layer grown on bulk AlN substrate is more than 2 orders of magnitude lower than the AlN buffer layers grown on sapphire. The

bulk AlN based devices generally employ pseudomorphic structures to avoid epilayer relaxation. The pseudomorphic structures keep the layers strained which otherwise could lead to increase in defect density from less than 10^6 cm^{-2} to over 10^8 cm^{-2}. The resulting pseudomorphic AlGaN multi-quantum well structures exhibited dislocation densities well below 10^7 cm^{-2} [75], [76].

The highest reported EQEs for small periphery DUV-LEDs on bulk AlN substrate are very similar to that of DUV-LEDs on sapphire in spite of lower defect densities. The EQEs were reported to be in the 2.0–3.0% range for LEDs with bulk AlN substrates [77], [78] while this value is between 3.0–3.5% for those on sapphire [40], [69].

The lower quantum efficiencies for DUV-LEDs on bulk AlN can be attributed to a number of factors. The absorption coefficients for AlN substrates is very high in the deep UV region. Furthermore, these devices generally experience higher stress due to the substrate thinning process after device fabrication. Moreover, the diameters of bulk AlN substrates are generally much smaller than sapphire. For comparison, sapphire substrates are readily available in a wide range of diameters up to 8 inches while typical values are around 1 inch for bulk AlN. The size limitation for bulk AlN significantly lowers the yield for high volume device production.

Most importantly, the manufacturing cost for bulk AlN is much higher than sapphire. At the time of publication of this dissertation, the market price for a 4-inch sapphire wafer is approximately $18 while the price for an 1-inch bulk AlN is close to $5000, making it commercially infeasible for the development of DUV-LEDs.

Consequently, sapphire is the substrate of choice for the development of DUV-LEDs in high volume production. In this context, a new approach has been developed by our group to grow high-quality thick (3-5 μm) AlN buffer layers over sapphire substrates using pulsed metal-organic chemical vapor deposition (MOCVD) [61]. The devices developed using this approach have threading dislocation densities between

(1-5)x10^8 cm^{-2}.

In this research, these templates have been used to grow the DUV-LEDs employing the pseudomorphic structure. These pseudomorphic structures, very similar to those grown on bulk AlN, brings the crystalline quality of active layers closer to that of the underlying AlN/sapphire template.

In addition to pseudomorphic DUV-LEDs, other designs, based on various degrees of relaxation of the n-AlGaN layers, have also been investigated in this research. The primary objective of this research is to achieve an optimal design that attains the required device characteristics, namely output power and reliability, while simultaneously being cost-effective leading to commercial feasibility.

2.2 Material Characterization

In this section, a brief introduction to various material characterization techniques is presented. These measurements are carried out during the different phases of device growth and fabrication and can convey vital information regarding the quality of the fabricated devices.

Sheet Resistance Mapping

The Lehighton contactless sheet resistance mapping system is used in this research for a fast and nondestructive sheet resistance measurements after the growth of an LED structure. The sample is placed between two RF coils and eddy currents are generated by the RF power. The eddy currents are generated primarily in the n-AlGaN layer owing to its higher conductivity compared to other layers in the LED structure.

A typical mapping for n-AlGaN sheet resistance can be seen in Figure 2.2. The sheet resistance has been evaluated at different locations on the wafer surface. The measurements also provide the average sheet resistance. The standard deviation for

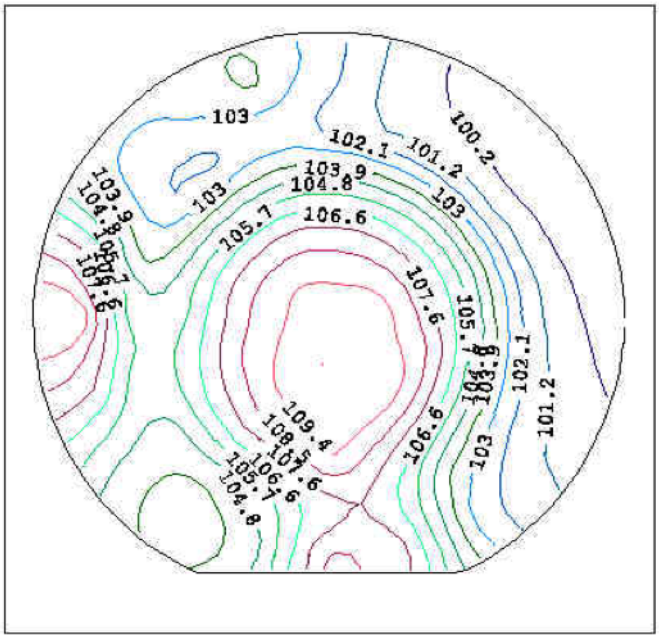

Figure 2.2: Sheet resistance mapping of n-AlGaN layer with average sheet resistance of 105 Ω/sq.

these measurements can then be calculated, which corresponds to the conductivity and Si-doping concentration uniformity of n-AlGaN across the wafer. This method was first proposed and demonstrated by Miller et al [79].

Photoluminescence

Photoluminescence (PL) is the measurement of spontaneous emission spectrum of a direct bandgap material, when excited by a laser. The light from a laser source is directed on the sample. If the incident laser energy is higher than the bandgap of the sample, it gets absorbed in the material and leads to the generation of electron hole pairs. These electrons and holes will undergo radiative and non-radiative recombination. For these measurements, photons generated through radiative recombinations are measured as a function of wavelength of the emitted light.

The measured spectrum conveys useful information about the bandgap of the material and can also be used to estimate the mid-gap defect states. The intensity of

the emitted light and the full width at half maximum (FWHM) values are typically related to the crystalline quality of the material. A better quality epilayer will have a higher intensity spectrum and narrower FWHM.

The following equation can be used as a guideline for the selection of laser wavelength when measuring photoluminescence for a material with a particular direct bandgap.

$$E_g = 1249.8/\lambda. \tag{2.1}$$

In Equation 2.1, λ denotes the wavelength of a laser in nanometers while Eg represents the bandgap energy of the material in electron volts. For instance, a 193 nm excimer laser can be used for photoluminescence characteristics measurement of III-nitrides with bandgap energy up to 6.47 eV.

Atomic Force Microscopy

An atomic force microscope (AFM) generates the surface morphology of an epitaxial layer with a resolution in the nano-scale range.

For non-destructive measurement, AFM is used in tapping mode (intermittent contact mode), as shown in Figure 2.3.

During this process, a micro-cantilever with a sharp tip is driven by a piezoelectric crystal material. The cantilever oscillates (with amplitude of more than 10 nm) up and down on top of the sample surface with its resonance frequency of about 200 Hz to 400 KHz. The tip experiences a Van der Waals force when it comes in close proximity to the measured surface. The resulting force decreases the amplitude of oscillation.

Surface irregularities in the epitaxial layer can be estimated by measuring the variations in the amplitude of oscillations. When the tip passes a depression in the surface, the distance between the surface and the cantilever tip increases, which leads

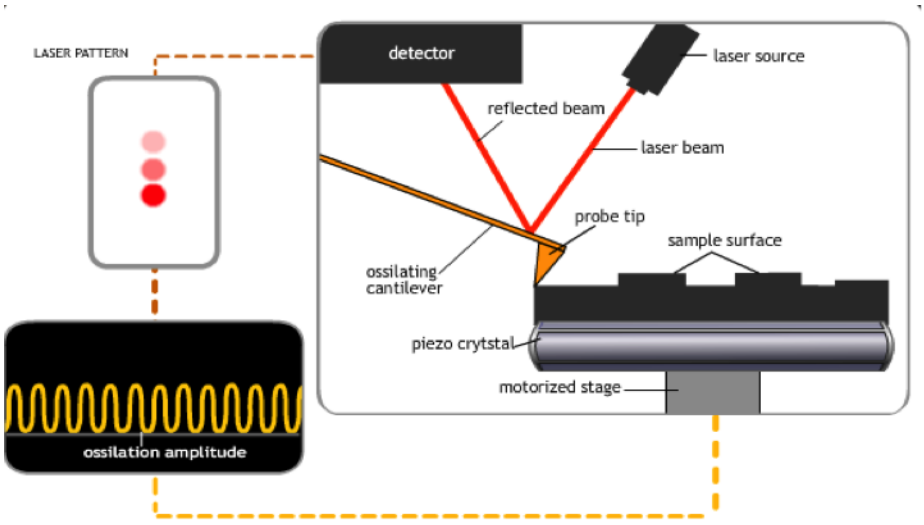

Figure 2.3: AFM in tapping mode [80].

to a larger amplitude of oscillation due to lower Van der Waals forces. In contrast, an increase in this amplitude will be observed when the tip passes over an elevated point on the surface.

This change in amplitude is measured by a deflecting laser beam attached to a detector. A feedback system adjusts the height to maintain the oscillation amplitude of the cantilever as it scans over the sample. The relationship between Van der Waals forces and inter-atomic spacing is depicted in Figure 2.4 [81]. In tapping mode, an image is created by imaging the force of intermittent contacts of the cantilever tip with the surface of the sample [82]. Consequently, any damage to the surface and tip is decreased as compared to the contact mode of operation. Furthermore, image resolution is greatly improved due to the elimination of lateral forces between the tip and the sample.

The AFM image is used to evaluate surface morphologies like surface pits, grain boundaries and surface atomic steps. The quality of a sample with linear atomic steps in the AFM image is deemed higher than one with curving, intersecting atomic steps. The intersection of atomic steps, and the presence of black pits at these intersection are generally an indication of dislocations. The topographic map of the sample surface

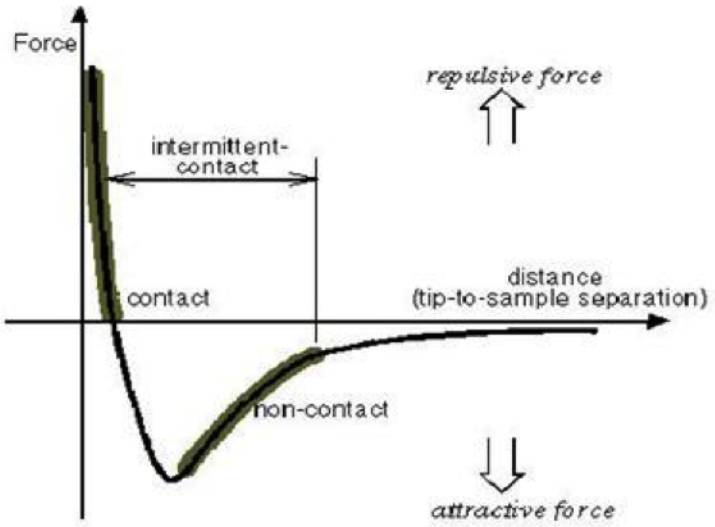

Figure 2.4: The Van der Waals forces regime versus distance.

can also be used to derive the root mean square (RMS) of surface roughness.

Etch Pit Density

In this work, etch pit density (EPD) method has been used to acquire the dislocation density of n-AlGaN layer and AlN/sapphire template. EPD is a fast and simple technique that is extensively used during growth optimization of each layer of LED structure. It can be used to obtain the number and type of dislocation densities for the epitaxial layers based on the defect selective etching process.

In EPD analysis, the sample, cut in 2 cm x 2 cm blocks, is immersed in H_3PO_4 solution heated at $130°C$ for 3-5 minutes. The sample is then removed from the solution, cleaned thoroughly with de-ionized water, and is blow-dried by nitrogen. To remove the excess water, the sample is baked in oven for 10-15 minutes.

A high-resolution image is then extracted using atomic force microscopy for defect analysis and to obtain the dislocation density of the layer. An AFM image of AlN after etching is shown in Figure 2.5. The AFM image shows clear atomic steps with a small number of pits at the intersection and termination points of the atomic steps.

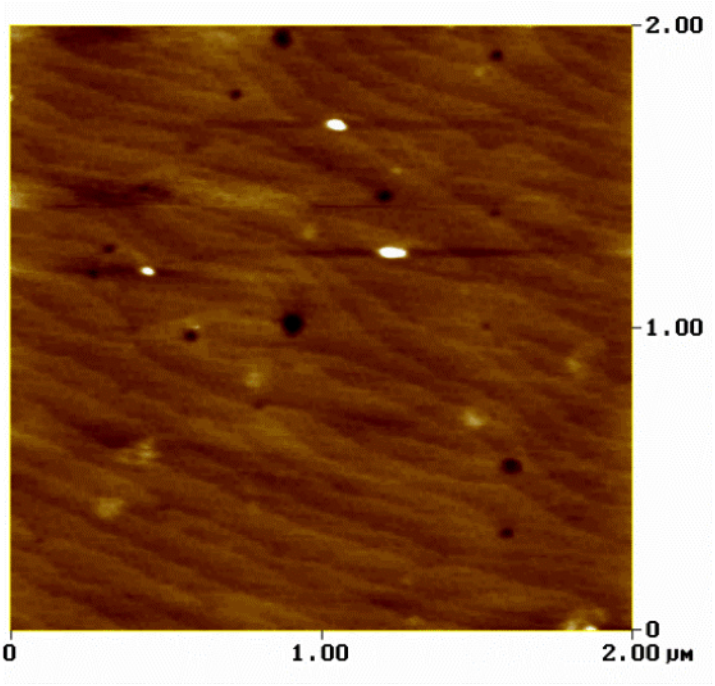

Figure 2.5: An AFM image of AlN/sapphire template after etching with EPD of $3x10^8$ cm^{-2}.

The size of the pits is related to the differences in defect energies for each type of dislocations, which is subsequently proportional to the etching rate.

To determine the overall etch pit density, including all types of dislocations, the number of pits in the scan area are counted. For instance, there are 12 pits in a scanned area of 2x2 μm^2 ($4x10^{-8}$ cm^2) in Figure 2.5. The number of pits divided by the scanned area will give us a etch pit density, and hence a dislocation density, of $3x10^8$ cm^{-2} for this layer.

X-Ray Diffraction

X-ray diffraction (XRD) is a convenient and nondestructive characterization techniques used for the determination of epitaxial parameters related to crystallographic structures. These parameters include thickness, composition, lattice mismatch, strain and relaxation of layers, and dislocations densities. In this work, the XRD data have been collected using Philips X'Pert Material Research Diffractometer with the X-ray

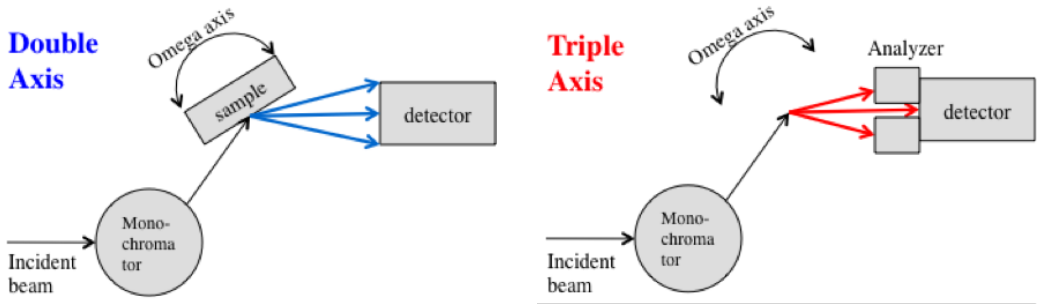

(a) Double Axis Diffractometer (b) Triple Axis Diffractometer

Figure 2.6: Different schemes of X-Ray diffractometers [83].

source wavelength of 1.54 Å.

The diffractometer consists of an X-ray tube, a sample holder, a monochromator, and an X-ray detector. The X-ray beam is generated in the X-ray tube by the heating of a filament. The X-rays are passed through a monochromator to get the desired wavelength. It is then directed to the sample mounted on the sample holder, and the diffracted beam is collected by a detector.

There are four axes, namely Omega (ω), 2Theta (2ϑ), Phi (φ) and Psi (ψ) in a diffractometer. This particular setup is known as a double axis instrument. A triple axis instrument, with good resolution in the 2ϑ, can also be made by adding an analyzer crystal before the detector. This addition, however, will result in an output with lower intensity. Double and triple axis diffractometers are illustrated in Figure 2.6.

The sample and detector are rotated, and the intensity of the reflected X-rays is recorded. If the geometry of the incident beam satisfies the condition defined by the Bragg's law ($2d \sin\theta = n\lambda$), a constructive interference occurs, appearing as a peak in intensity. Bragg's law is illustrated in Figure 2.7.

Mosaicity is created by slight mis-orientations of different crystals as they grow on the substrate. When the crystals join, they form low energy domain boundaries. To evaluate the crystal mosaicity of an epilayer, on-axis (002) and off-axis (102) rocking

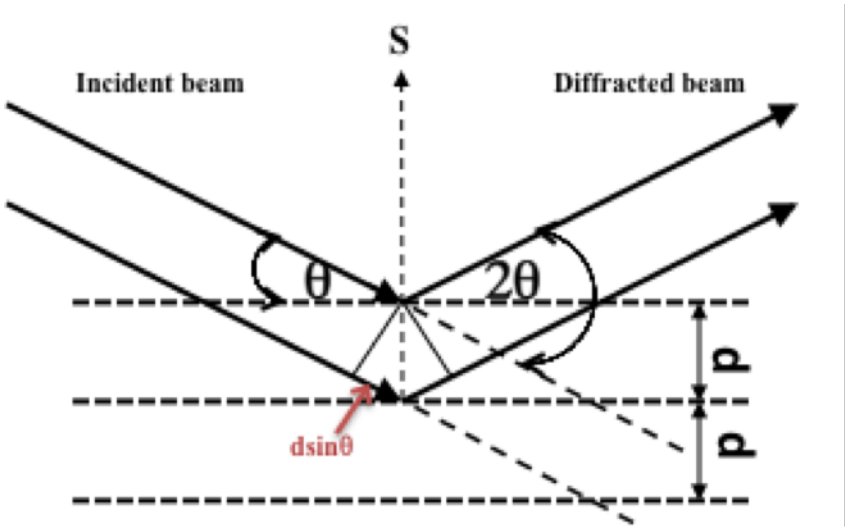

Figure 2.7: Mechanism of X-Ray diffraction.

curves are typically used. The broadening of the rocking curve is translated as the existence of different orientation grains, thus dislocation density.

The on-axis ω scan gives information about the screw and mixed type dislocations, which shows the tilt of the lattice planes. The off-axis scan reveals the twists in the lattice plane, which is an indication of edge type dislocations in a layer. X-ray diffraction is also used to estimate strain in the epitaxial layers of the LED structure. This information is crucial since high strain in epilayers can lead to formation of dislocation and cracks.

The reciprocal space Map (RSM) is a collection of several omega-2Theta coupled scans. Each coupled scan is collected with a slightly different tilt (offset) in the omega direction. In this work, RSM is used to characterize the strain in AlGaN layers of the LED structure.

A reciprocal space map of a fully strained AlGaN MQW structure is shown in Figure 2.8. The AlGaN peak is positioned on the vertical line drawn from the AlN peak. This exact alignment of adjacent peaks is an indication of 100% compressive strain in the layer. The broadening of the reciprocal lattice points indicate imperfections in the layer crystal, which otherwise should appear as a tiny spot. A detailed

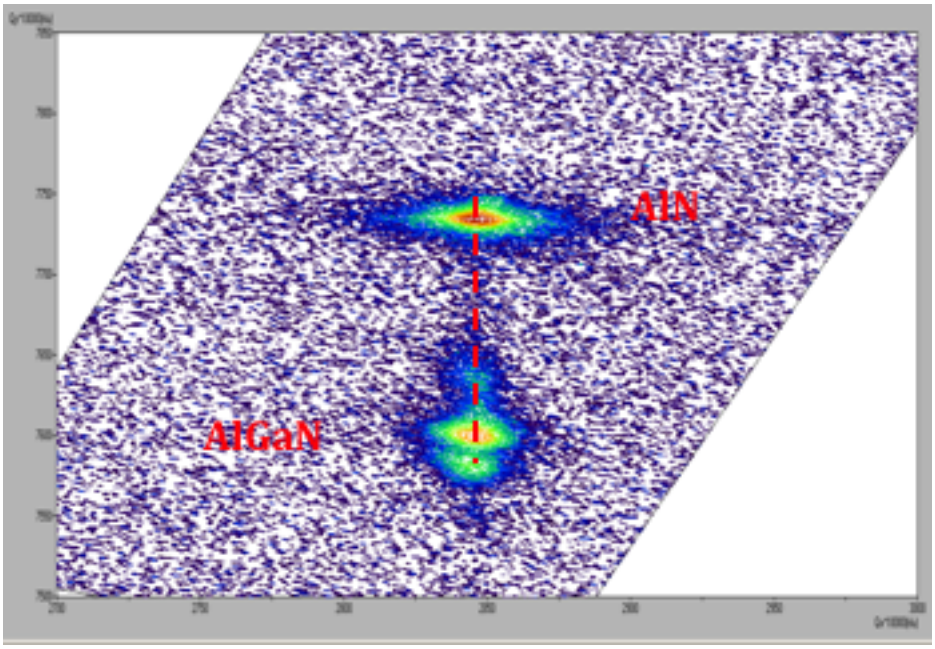

Figure 2.8: Reciprocal space mapping showing fully strained AlGaN layer.

discussion of strain in the DUV-LEDs and their manifestation in off-axis reciprocal space mapping has been discussed in [84].

2.3 Device Characterization

Electroluminescence

The electroluminescence (EL) spectrum is used to measure the peak emission wavelength of the LED device. In this work, electroluminescence measurements were carried out using a HORIBA Jobin Yvon Triax 550 spectrometer, equipped with a 600 gr/mm grating and a liquid nitrogen cooled Si CCD detector.

For most applications, a device with emissions concentrated in a small bandwidth is desired. Such a device must have narrow full width at half maximum (FWHM). The devices developed in this research have FWHM generally in the range of 10-11 nm. The spectrum is usually plotted on a semi-logarithmic scale, which allows to discern additional peaks that may be an indication of un-optimized electron blocking

layer and quantum wells. Furthermore, it is desirable to have a high (quantum well) main peak to parasitic peak ratio in a high quality device.

I-V Characteristics

The current-voltage (I-V) characteristics were measured using a Suss MicroTec probe station and HP parameter analyzer. Like most semiconductor diodes, the I-V characteristic curve is used to analyze the electrical performance of an LED device, such as turn-on voltage, differential resistance, reverse leakage, series resistance and ideality factor.

The slope of the linear portion of the I-V curve is equal to the differential resistance of the device. Moreover, the value at which the linear portion of the I-V curve, when extended, intercepts the x-axis is defined as the turn-on voltage of the LED. The turn-on voltage is approximately equal to the bandgap of the material used in the quantum wells of the LED. The reverse leakage current is typically measured at a fixed reverse voltage of -1V to -3V for LEDs. At higher values of current, the diode I-V curve becomes linear due to the dominance of the series resistance. The series resistance can be measured through an approximation of the I-V curve in the linear region using the ideal diode equation shown below.

$$\frac{dV}{dI}I = IR_s + \frac{kT}{q} \tag{2.2}$$

The slope of the curve from the $^{dV}/_{dI} \times I$ vs. I plot is the series resistance of LED device.

I-V-L Characteristics

In I-V-L measurements, the light output power is measured as a function of input current, while simultaneously measuring the voltage across the LED. For these

measurements, the device is mounted inside an integrating sphere with a calibrated UV-enhanced Si detector connected to a power meter, while biasing the device using a HP parameter analyzer.

The measurements can be carried out in two different modes. In the first mode, known as direct current (dc) or continuous wave (cw) mode, the current is kept at a constant value. In pulse mode, on the other hand, the current is pumped in, in the form of pulses. The pulses of current mitigate the self-heating effects, and allow the device to attain near optimal performance in absence of adverse effects of heating.

The slope of both dc and pulsed mode curves typically overlap at low currents. Ideally, the output power should increase linearly with an increase in input current. However, early power saturation (thermal roll-over) sets in as a consequence of heating effects. Consequently, the slope of the I-V-L curve is generally higher for the pulse mode measurements at higher values of current due to lower heating.

The I-V-L data can also be used to determine the external quantum efficiency and wall plug efficiency for an LED device and are generally measured as percentages.

Chapter 3

Pseudomorphic Deep Ultraviolet Light Emitting Diodes over Sapphire [1]

[1]F. Asif, M. Lachab, A. Coleman, I. Ahmad, B. Zhang, V. Adivarahan, and A. Khan, "Deep ultraviolet photopumped stimulated emission from partially relaxed AlGaN multiple quantum well heterostructures grown on sapphire substrates", *Journal of Vacuum Science and Technology B*, vol. 32, no. 6, 0612041, pp. 1-5, 2014.
Reprinted here with permission of publisher.

[1]F. Asif, H. Chen, A. Coleman, I. Ahmad, B. Zhang, J. Dion, A. Heidari, V. Adivarahan and A. Khan, "Pseudomorphic $Al_xGa_{1-x}N$ MQW based deep ultraviolet light emitting diodes over sapphire", *physica status solidi (c)* , vol. 11, no. 3-4, pp. 798-801, 2014.
Reprinted here with permission of publisher.

Milliwatt power AlGaN-based deep-ultraviolet light emitting diodes over sapphire substrates were first developed in [85] as part of research efforts to develop a potential replacement for UV mercury lamps. These devices have potential applications in air/water purification systems, bio-medical instrumentation and resin curing, among others.

Since their introduction, several research groups have been working extensively towards improving and commercializing these devices [33], [40], [58], [77], [86]. The majority of these studies have employed a relaxed device structure where the active region comprises of AlGaN multiple quantum wells. These MQWs are generally deposited over a thick n-AlGaN current spreading layers over short-period superlattice structure, which was grown on a high quality AlN buffer/c-sapphire templates.

More recently, the use of bulk AlN substrates have been explored to fabricate DUV-LEDs [77], [78]. The key developments include low-defect density (i.e. $<10^6$ cm^{-2}) for the substrates and the observation that for 50-80% Al composition, Si-doped n-AlGaN material could be grown fully-strained up to a thickness of 1.0 μm [87], and hence the active layers crystalline quality remains very close to that of the underlying bulk AlN. These resulted in the demonstration of UV-C LED devices that exhibit up to 60 mW dc output powers with external quantum efficiency (EQE) between 5 and 6 %.

A similar performance was also reported for LEDs grown on high quality AlGaN/sapphire templates [56]. This suggests that photons extraction and low p-type conductivity represent the other major factors limiting the EQE in nitride-based UV-C LEDs.

Consequently, sapphire is used as a substrate to fabricate AlGaN MQW based LEDs in this research. The choice of sapphire, over bulk AlN, is driven primarily due to cost and availability considerations. However, sapphire offers a number of unique growth challenges due to its lattice and thermal mismatch with the AlGaN layers.

resulting in high number of dislocations density in overlaying layers.

Since these dislocations generated from the heterostructure interface can propagate to the overlaying layers, a smooth and low defect density bottom layer is needed to reduce the overall defect density in the LED structure, particularly in the active region of LED. Hence, an thick AlN layer has been successfully used to serve as a buffer layer between the n-AlGaN layer and the substrate, in order to reduce the defect density and improve the crystal quality of the subsequent layers.

When growing n-AlGaN layer on AlN buffer layer, the in-plane lattice parameter of the AlGaN conforms to that of AlN if the thickness of the AlGaN layer is below a critical value. In this regime, the growth of AlGaN is referred to as pseudomorphic [88], and all of the strain induced at the hetero-interface is contained within the AlGaN film, keeping the crystalline quality of the active layer close to that of the underlying AlN template.

Once the AlGaN is grown beyond its critical thickness, layer cracking and misfit dislocations are introduced due to the strain in the film, leaving numerous non-radiative centers within the quantum well. These imperfections results in a decline in the LED internal quantum efficiency and lifetime affecting the device output power and reliability. This chapter starts with an investigation of the optical quality of the pseudomorphically-grown MQWs using photo-pumped stimulated emissions. This introductory discussion is followed by a detailed presentation of growth of full LED structure, and fabrication of pseudomorphic LED devices. The chapter is concluded with a detailed presentation of experiments and analysis of observations to evaluate the performance of pseudomorphic as compared with standard SPSL LED devices.

3.1 Investigation of Epilayer Quality Using Optical-Pumping

The significant progress achieved in deep-UV light emitting diodes over the last few years has recently re-ignited interests in low-threshold optically pumped sub-300 nm

lasing structures. The optical pumping experiments using pulsed excimer laser have been employed to analyze the optical quality of epilayers without growing and fabricating a complete electrically pumped laser diodes.

The new research efforts build on the prior demonstration of optically pumped lasing at 214 nm from high quality AlN layers grown by low-pressure metal-organic chemical vapor deposition (MOCVD) over sapphire substrates [89]. Nearly all the subsequent studies, however, primarily involved bulk AlN substrates despite its high cost [90]–[92].

The epilayers designs generally consist of undoped AlGaN QW structures grown pseudomorphically to prevent generation of new defects due to strain relaxation. This is because the threading dislocations density in the active region of Al-rich AlGaN heterostructures emitting in UV-B and UV-C strongly affect their lasing characteristics, and the lower the buffer AlN structural quality the higher the threshold power density (P_{th}) [93]–[95].

The total thickness of the top wave-guiding and/or clad layers are generally kept thin (< 20 nm) when using ArF excimer laser to avoid excessive absorption of the pump laser radiation away from the active region [91], [92], which invariably leads to increased threshold. The other parameter that affects the threshold level is the optical confinement factor [96], which requires a careful optimization of the epilayers thicknesses and materials compositions. With improvements of the materials quality and optimization of the heterostructures design, lasing actions with impressive threshold power densities as low as 84 kW/cm^2 were attained in UV-C [90], [91].

These optically pumped stimulated emission have been investigated previously using a slightly modified design of the MQW structures based on high-quality 285 nm emission DUV-LEDs [95]. The fully-relaxed structure with superlattice still featured both the n- and p-type doped clad layers to ensure a closer representation of electrically pumped laser diodes. The threshold power density for the sample in this

report was approximately 970 kW/cm^2. The threshold value large disparity with that of AlN substrate-based structures was shown to be primarily due to optical losses in the top p-clad.

Experiment Procedure

The optically pumped AlGaN heterostructure is schematically illustrated in Figure 3.1. It was grown on a 2-in. (0001) sapphire substrate by low-pressure MOCVD. It includes a 2.4 μm-thick high quality AlN buffer layer deposited at approximately 1200 ^{o}C on top of a low-temperature (LT) AlN nucleation layer. Typical line-width for the HT-AlN (102) off-axis X-ray diffraction rocking curve was 360-400 arcsec. The corresponding dislocation density was estimated to be in the mid-10^8 cm^{-2} using etch pit density technique.

The AlN buffer was followed by a 0.6 μm thick silicon-doped n-$Al_{0.60}Ga_{0.40}N$, a four-period undoped multiple quantum wells with 2.5 nm $Al_{0.44}Ga_{0.56}N$ wells separated by 21 nm $Al_{0.60}Ga_{0.40}N$ barriers. The active region was capped with $Al_{0.60}Ga_{0.40}N$ material grown to a thickness of 19 nm. This cap layer acts not only as cladding layer, but also as surface passivation layer for carrier confinement. Silane (SiH_4) was used for n-type doping.

The MQW wafer was characterized using Philips high-resolution X'Pert MRD system to determine the strain in the epilayers and room temperature (RT) edge photoluminescence measurements to study the emissions properties in the high pumping regime. To carry out the optical pumping experiments, laser bars were cleaved along the a-facet of sapphire substrate to form m-plane mirrors. No extra process step was undertaken to improve the quality of the mirrors or the quality value (Q-value) of the lasing cavity. In addition, no reflective coatings were used for the mirror facets. The cavity length (CL) of the cleaved bars was between 1.4 and 2.3 mm. A 193 nm ArF excimer laser with a pulse width of 10 ns and a repetition rate of 5 Hz was used as the

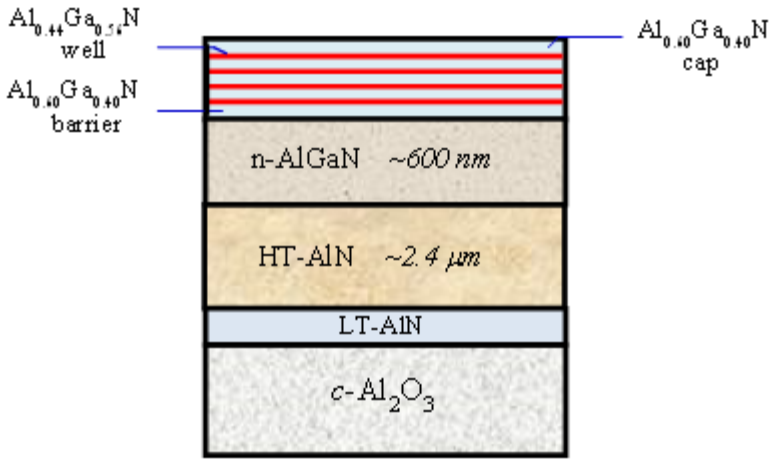

Figure 3.1: Schematic representation of the optically pumped AlGaN/AlGaN MQW structure grown on sapphire substrate.

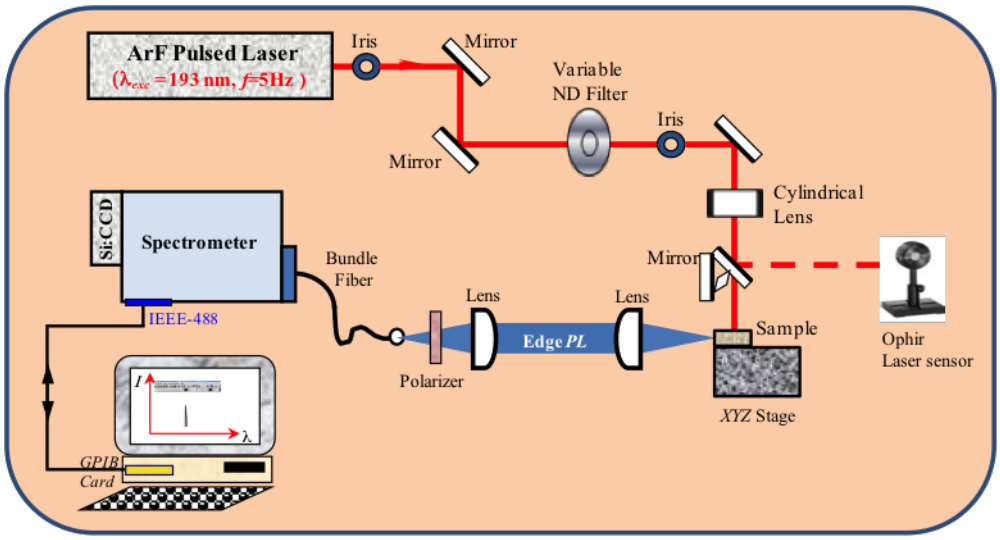

Figure 3.2: Schematic diagram of the setup used for optical pumping experiments.

excitation source. The samples were excited uniformly using a cylindrical lens. The emitted light was detected by an optical fiber attached to a Triax 550 spectrometer equipped with a 300gr/mm grating and a liquid nitrogen-cooled CCD detector. The optical setup schematic is illustrated in Figure 3.2. The detection system resolution was 0.5 nm.

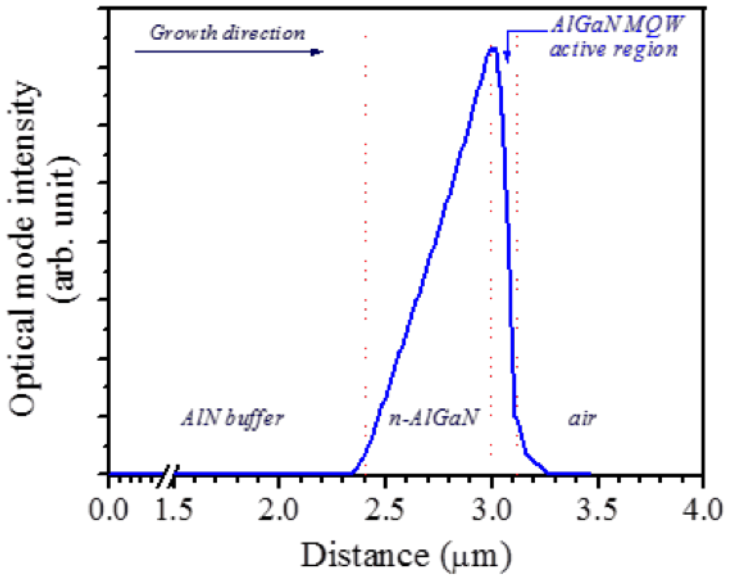

Figure 3.3: Calculated distribution of the optical mode amplitude.

Simulation of Field Distribution and Optical Confinement Factor Calculation

The optical confinement factor (Γ) of the fundamental transverse electric (TE) mode of the electromagnetic field for the MQW structure was calculated using a commercial simulation software. The distribution of the optical mode along the growth direction can be seen in Figure 3.3.

In the absence of optimized epilayers design, the optical mode was found to leak outside the active region (formed by the four QWs and three barrier layers) into the bottom n-AlGaN. Furthermore, the optical field maximum intensity was located away from the center of the MQWs region. As a result, the optical confinement factor in the active region was calculated to be about 2.1%. The refractive indices for the AlGaN compositions of interest were taken from [97].

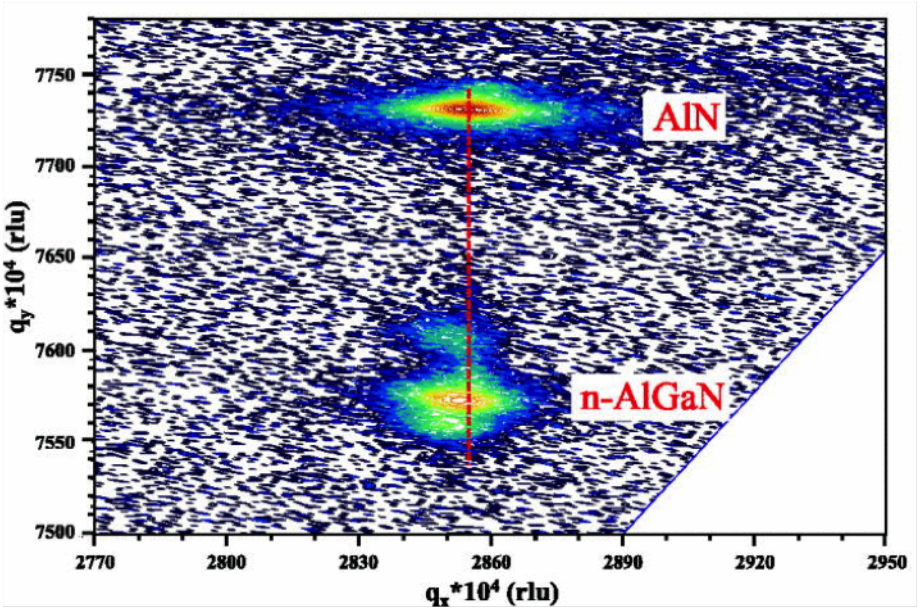

Figure 3.4: RSM of the asymmetric (105) reflection for the photo-pumped AlGaN MQW structure showing a partially relaxed n-AlGaN material with respect to the underlying AlN buffer layer.

Structural and Optical Characterization of MQW Structures

To analyze the lattice mismatch and stain in the epilayers forming the heterostructure grown on AlN/sapphire template reciprocal space mapping of the (105) asymmetric Bragg peak was carried out.

From Figure 3.4, it is evident that the n-AlGaN film reciprocal lattice points (RLP) do not fall exactly on the vertical line that is perpendicular to the q_x axis and include the RLP of AlN buffer. This indicates that n-AlGaN is not fully-strained with respect to the underlying AlN material. A partial relaxation of the doped layer, estimated to be of less than 10%, has thus taken place when grown to the thickness of 0.6 μm.

In Figure 3.5, the edge photoluminescence spectra for the MQW structure, acquired at room temperature for different laser power densities (PD) between ~53 and 472 kW/cm^2, can be seen. The resonator CL was 2.3 mm. At low PD, the PL spectra exhibited a relatively broad spontaneous emission peak at 274.5 nm with 9.7 nm

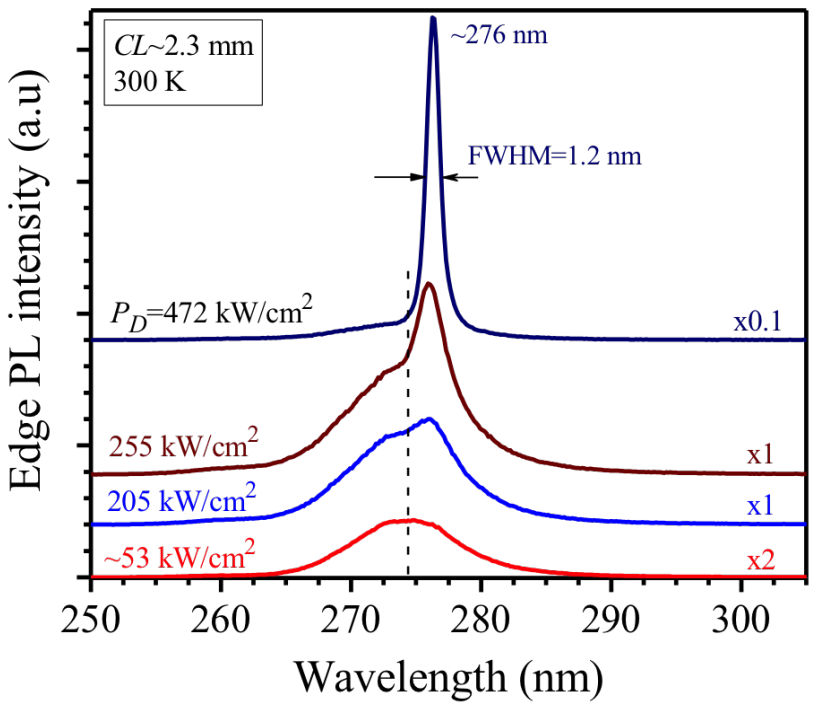

Figure 3.5: Edge PL spectra from the partially relaxed AlGaN/AlGaN MQWs measured at room temperature for different pump power densities.

line-width. As the power density approached 205 kW/cm^2, a narrow peak emerged on the higher wavelength side. The peak then developed into a sharp and strong emission located at ~276 nm with further increasing PD up to 472 kW/cm^2.

The integrated edge PL peak intensity is plotted against the pump power density in Figure 3.6. A superlinear increase of the emitted light intensity was observed beyond the threshold, which was estimated to be ~240 kW/cm^2. This behavior was accompanied by a rapid drop in the peak line-width down to 1.2 nm, as illustrated in Figure 3.6b. Beyond threshold, the peak wavelength exhibited a very small redshift ($\leq$ 0.5 nm) while the PL emission broadening was limited to less than 0.4 nm. Moreover, the optical output light intensity appeared to saturate when the laser source was raised above 800 kW/cm^2 (i.e. ~3.3 P_{th}), which is most likely due to materials

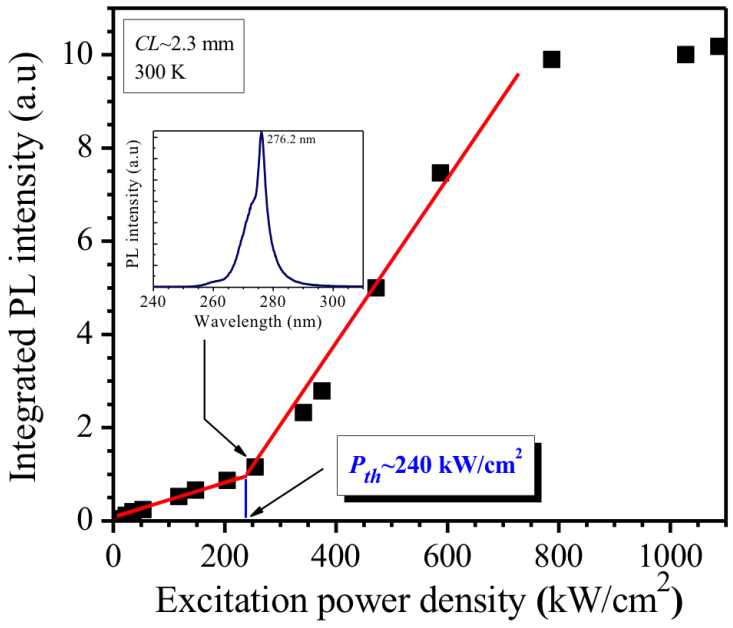

(a)

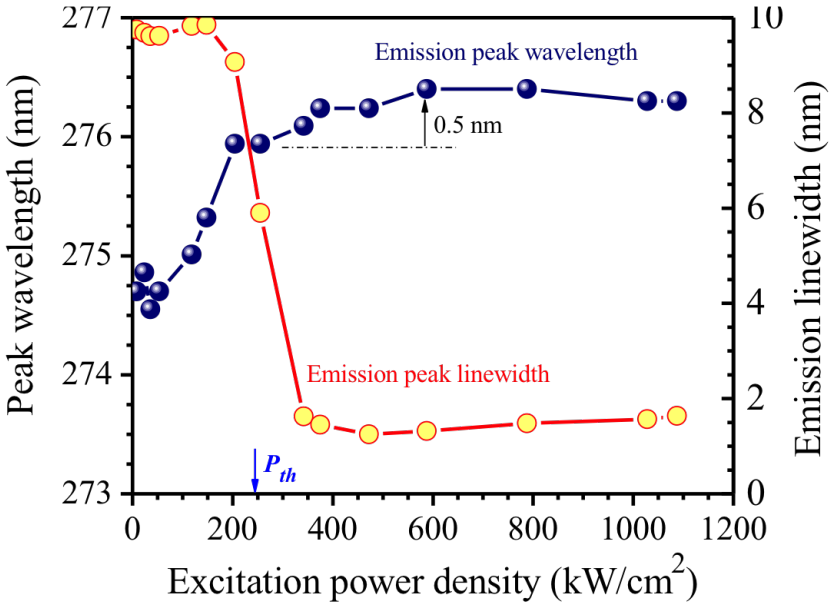

(b)

Figure 3.6: Plot of the integrated edge PL intensity (a) and both emission peak wavelength and line-width (b) as a function of the excitation source power density for a laser bar with a CL = 2.3 mm. The inset shows optically resolved PL emission measured just around the threshold.

degradation in the very high pumping regime.

The stimulated emission properties in laser bars with a smaller cavity were also measured. The output light-excitation power density at a sample CL of 1.4 mm is shown in Figure 3.7. As expected, the threshold increased to ~340 kW/cm^2. The simulated emission peak wavelength was in the range 277-278 nm, and similar to the larger laser bars, both the emission wavelength shift and peak broadening above P_{th} remained very small.

The optical properties observed for the partially-relaxed heterostructures clearly highlight the high quality of the AlN template and the subsequent AlGaN epilayers. For comparison, so far there have been only two reports on optically-pumped stimulated emission from AlGaN MQW structures on sapphire substrates emitting in the UV-C region [94], [98]. In one report the threshold for MOCVD-grown MQWs on epitaxially laterally overgrown (ELO) AlN/c-Al203 templates was greater than 5 MW/cm^2 at 272 nm (CL=1-2 mm) [94]. The other work was based on a single AlGaN QW grown asymmetrically within a 120 nm thick waveguide over planar AlN/c-Al_2O_3 using plasma-assisted molecular beam epitaxy (PAMBE) [98]. Their cleaved 400 μm long laser cavities exhibited simulated emissions with P_{th} between 280 and 300 kW/cm^2 in the wavelength range 276-278 nm. For both studies the edge PL was excited by a 266 nm laser source.

To further establish the occurrence of stimulated emission process in our samples we investigated the polarization properties of the output light for PD=2.3P_{th}. For this purpose, aGlan–Thompson polarizer was placed just before the fiber optics attached to the spectrometer entrance port. The results shown in Figure 3.8 indicates a strongly TE polarized PL emission above threshold. Despite using thicker bottom n-AlGaN clad and thicker barriers layers, the polarization of stimulated emission is in good agreement with that previously observed for AlGaN MQW heterostructures emitting in the range 243-291 nm, which were grown pseudomorphically either on

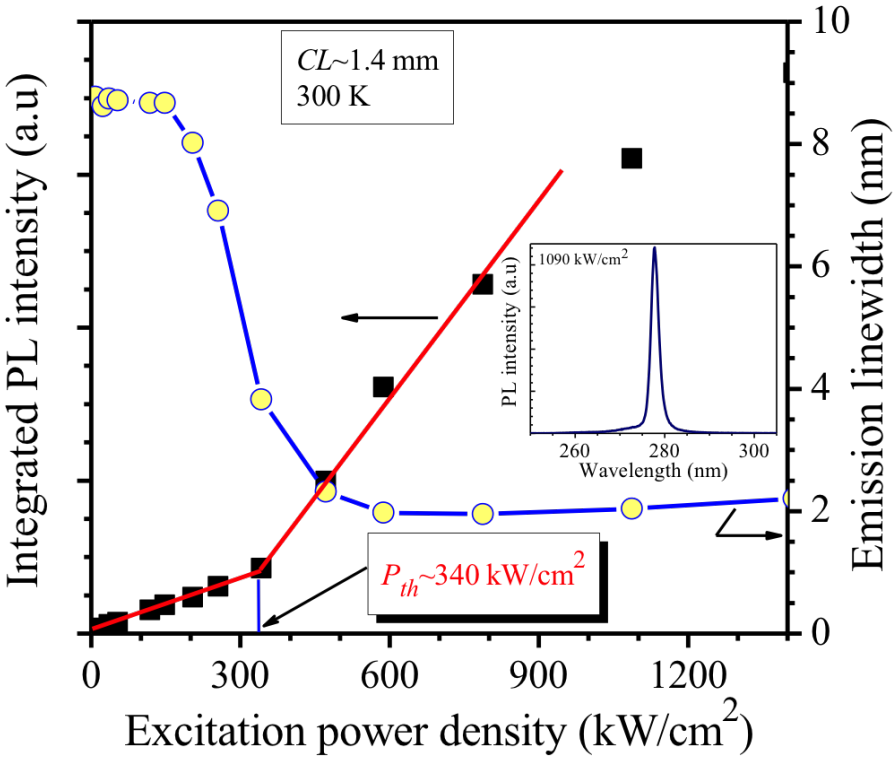

Figure 3.7: Output light intensity and emission line-width plotted vs the optical pump power density for a laser bar with a 1.4mm cavity length. The inset shows a PL spectrum measured for PD = 1.09 MW/cm^2.

bulk AlN substrate [90], [92], [94] or on sapphire substrates [94], [98]. The degree of polarization of UV-SE in QW active regions was found to depend on the materials compositions and level of strain relaxation in the active region [99], [100]. Such dependence or relationship can be exploited to prevent potential polarization switching phenomenon, especially at shorter emission wavelengths, and preserve the preferred TE mode light polarization for the reasons summarized elsewhere [90], [98]. The degree of polarization of the simulated emissions for our MQW structures was found to be of approximately 72%. In contrast, the spontaneous emission exhibited the same spectral profile irrespective of the polarizer orientation, which is consistent with the behavior of unpolarized light.

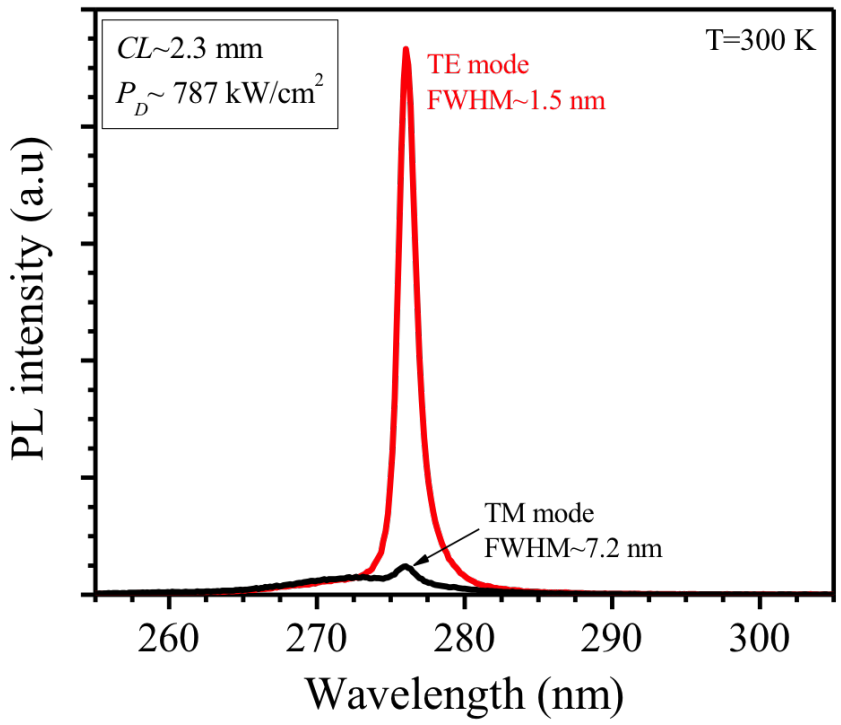

Figure 3.8: TE and TM mode edge PL spectra measured for the 276 nm MQW structure above the threshold power density (PD = 588 kW/cm^2).

Finally, it is worth mentioning that for the laser bars with 1.4 mm cavity length, the PL experiments could not resolve the longitudinal cavity modes because as the separation between two neighboring longitudinal modes, estimated to be well below 0.1 nm for peak wavelength $<$ 280 nm [91], was more than one order of magnitude smaller than the resolution of our detection system (i.e. 0.5 nm).

Summary

We achieved ~276 nm optically-pumped stimulated emission using non-optimized AlGaN MQW heterostructures grown over basal-plane sapphire substrates. The threshold power density of 240 kW/cm^2 compare favorably to the levels obtained for structures grown pseudomorphically on bulk AlN substrates and emitting in UV-C and better than fully relaxed structure for which the power density was 970 kW/cm^2. The

SE was TE polarized and the minimum emission line-width was 1.2 nm. Moreover, the emission peak wavelength shift and emission peak broadening were limited to ~0.5 nm above threshold, indicating stable characteristics of the emitted light. These results suggest that pseudomorphic structures grown over sapphire substrate can provide a low-cost and reproducible platform for the developments of deep UVLEDs.

3.2 Development of Pseudomorphic Deep Ultraviolet Light Emitting Diodes

In this section, the fabrication of the first pseudomorphic (PSM) deep UV LEDs on AlN/sapphire templates, with emissions at 275 nm, is presented. In the pseudomorphic growth mode, the thickness of bottom silicon doped n-AlGaN contact layer is limited to 0.6 μm. This growth constraint results in a relatively low-doping of the thin n-AlGaN with a high sheet resistance (R_s), which ultimately reduces the LEDs light output power and reliability. To mitigate these issues, a novel pulsed silicon modulation doping (PMD) technique [101] has been proposed, in combination with the micro-pixel design geometry [71] for the growth and fabrication of these devices, respectively.

LED Structure and Material Characterization

The LED epilayer structure was grown on c-plane sapphire substrate by low-pressure metalorganic chemical vapor deposition (MOCVD). A 2.4 μm-thick high quality AlN buffer layer was then deposited at ~1200°C. Typical linewidth values for the AlN (102) off-axis X-ray diffraction (XRD) rocking curves ranged from 280 to 330 arcsec. The FWHM of the (0002) XRD scan for AlN epilayer was measured to be 150 arcsec.

The LED epilayers structure consisted of a 0.6 μm thick, silicon doped $Al_{0.60}Ga_{0.40}N$, followed by a five-period $Al_{0.44}Ga_{0.56}N/Al_{0.60}Ga_{0.40}N$ multiple quantum wells, Mg-doped p-AlGaN electron blocking layers and p-$Al_{0.60}Ga_{0.40}N$/p-GaN hole injection

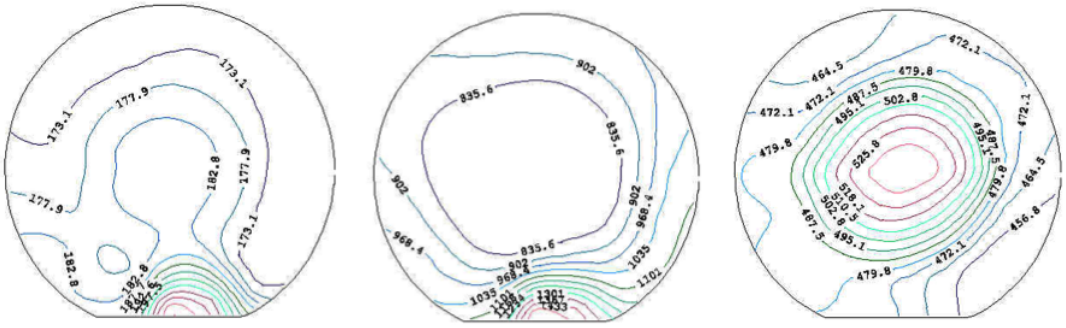

(a) (b) (c)

Figure 3.9: n-AlGaN sheet resistance for (a) standard SPSL LED, (b) pseudomorphic LED with standard doping and (c) pseudomorphic LED with PMD.

layers. The n-AlGaN layer was deposited using the conventional doping technique, where the silane (SiH_4) gas flow was kept open throughout the process. The layer sheet resistance was determined to be ~ 900Ω/sq. Next, a novel technique, called pulsed silicon modulation doping, was used where the SiH_4 gas supply was pulsed using a 50% duty cycle. The material sheet resistance dropped to ~500 Ω/sq, indicating a much better Si atoms incorporation leading to a higher doping level, and without sacrificing the material structural quality. The sheet resistance of n-contact layer for standard SPSL LEDs was measured to be 180 Ω/sq, this lower value is due to higher thickness of n-AlGaN layer. These sheet resistances are depicted in Figure 3.9.

To determine the threading dislocation density in the pseudomorphically grown n-AlGaN layers, the etch pit density analysis of the epiwafers, grown using conventional and pulsed n-type doping techniques, was carried out. Both samples were immersed in phosphoric acid solution heated at $130°C$ for 3 min. The samples were then characterized for the dislocations density using atomic force microscopy. The 2 μm x 2 μm AFM images shown in Figure 3.10 indicate that the PMD approach produced a better quality material with an EPD of the ~$2x10^8$ cm^{-2} versus ~$1.3x10^9$ cm^{-2} for the standard n-AlGaN layer, which represents significant improvement in the n-AlGaN

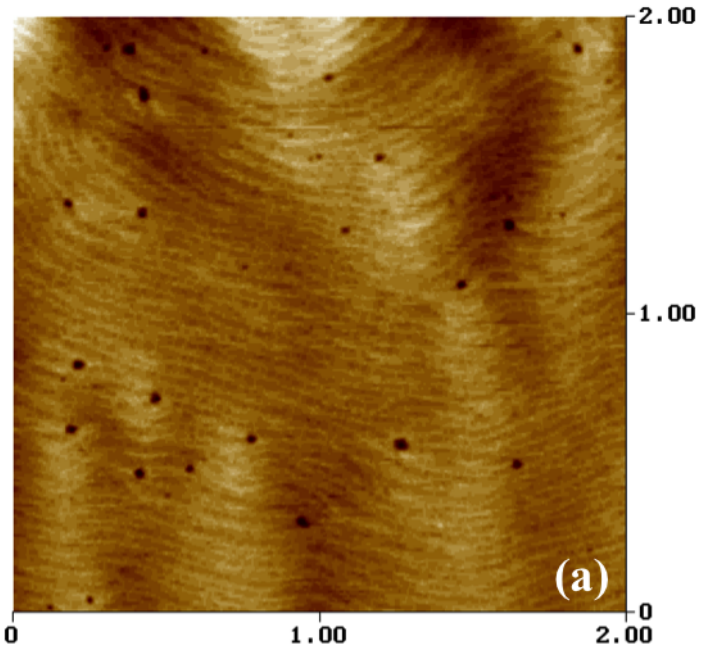

(a)

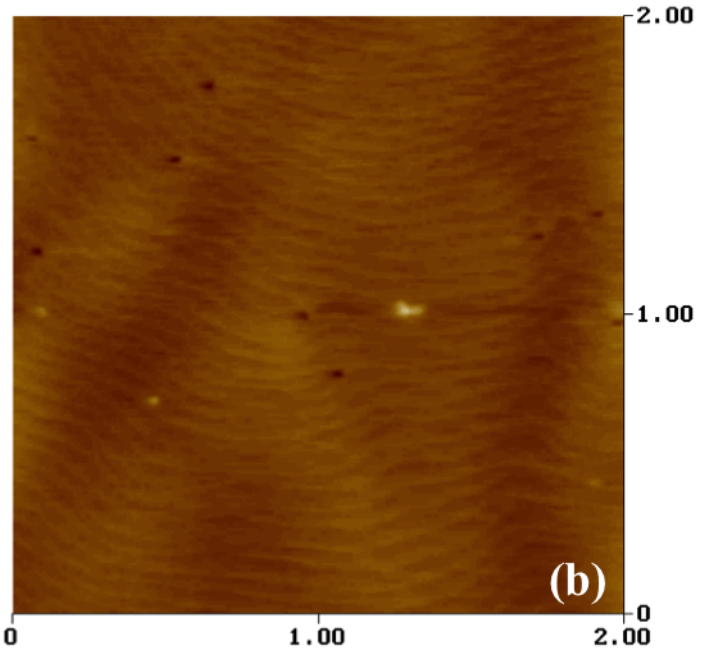

(b)

Figure 3.10: Study of Etch pit Density (EPD) after KOH etching for n-AlGaN with standard doping (a), and n-AlGaN with PMD doping (b).

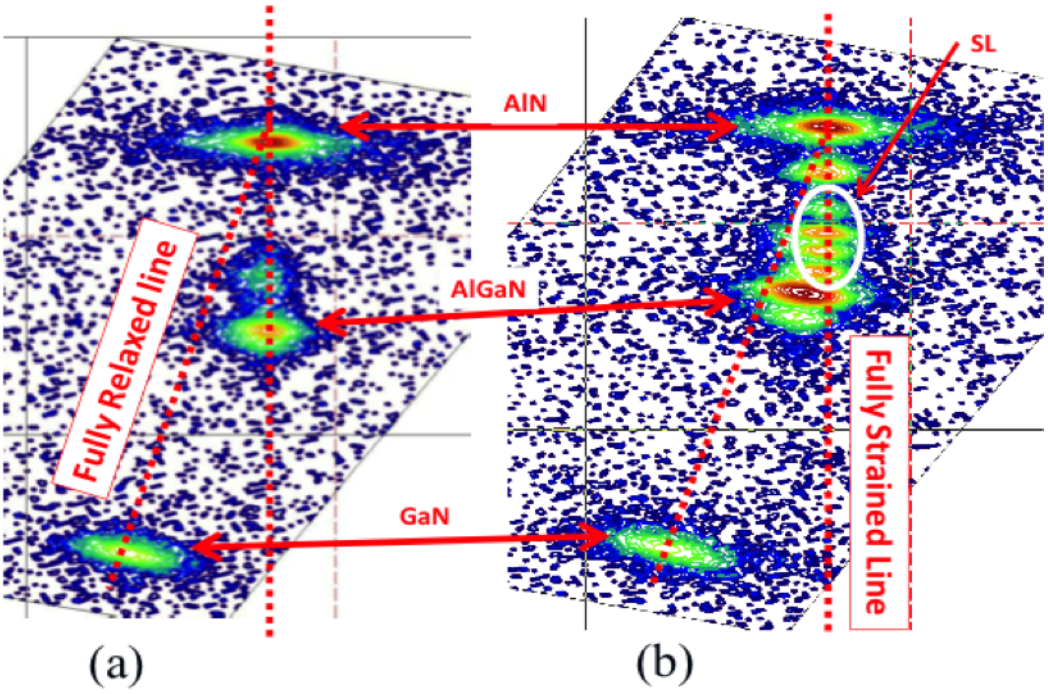

Figure 3.11: XRD reciprocal space mapping of pseudomorphic (a) and standard SPSL (b) DUV-LED structures.

crystal quality due to pseudomorphic growth.

High resolution X-ray diffraction reciprocal space maps of both LED structures grown over AlN/sapphire templates are shown in Figure 3.11. As seen in Figure 3.11(a), the AlN and AlGaN peaks are well aligned along the vertical axis, which indicates that the 0.6 μm n-AlGaN and the overlaying epilayers were pseudomorphically grown. On the other hand, for the relaxed UV LED (Figure 3.11(b)), the short period superlattice (SPSL) peak was aligned with that of the AlN, but not with that of the n-AlGaN. The SPSL structure is strained, but allows the subsequent AlGaN layers to grow partially relaxed. Note that the off-axis X-ray rocking curve measurements along the [102] direction also showed a reduction of the peak linewidth for the pseudomorphic n-AlGaN layer (~350 arcsec) when compared to the standard n-AlGaN layer (~480 arcsec).

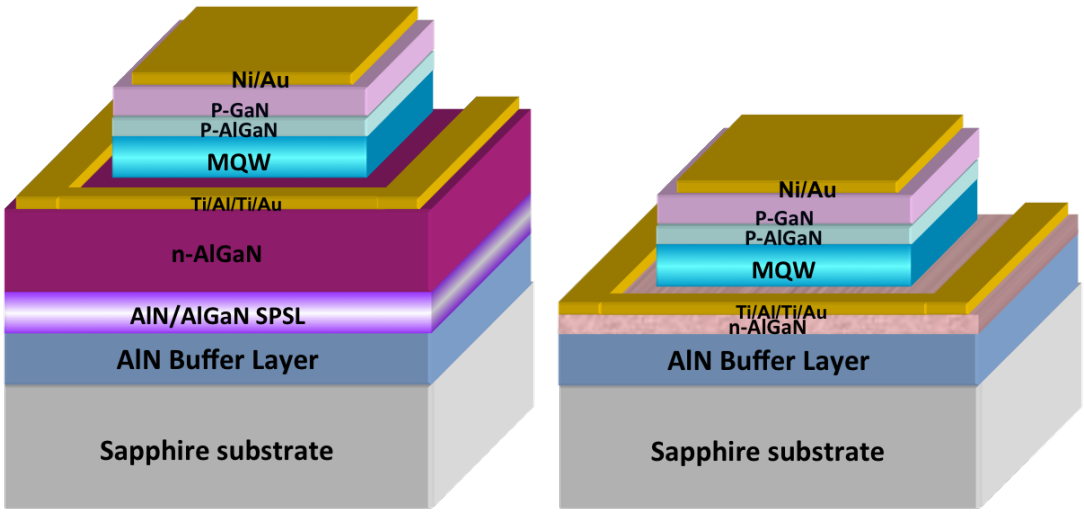

(a) (b)

Figure 3.12: Schematics of the DUV-LED epilayer structures: standard SPSL (relaxed) LED (left) and pseudomorphic LED (right).

Device Fabrication

The fabrication of the LED devices can be explained with the schematic diagram of a single pixel shown in Figure 3.12. Large area pixel array mesas were first defined using standard photolithography and reactive ion etching in chlorine plasma. Ti/Al/Ti/Au and Ni/Au metal stacks were used for the formation of n- and p-contacts, respectively. The n-contact was annealed at 950 ^{o}C for 30 sec in nitrogen ambient while p contact was annealed in ambient air at 550 ^{o}C. The pixel LEDs were then isolated using a planar layer of benzocyclobutene (BCB) followed by shorting of all the pixel p-contact areas in each device [102]. Each pixel size was 60 μm, which translates into a total p-active area of 360 x 360 μm^2. For comparison, a standard LED epiwafer grown using a thicker n-AlGaN layer (~2 μm) on top of AlGaN/AlN short-period superlattice structure was also investigated.

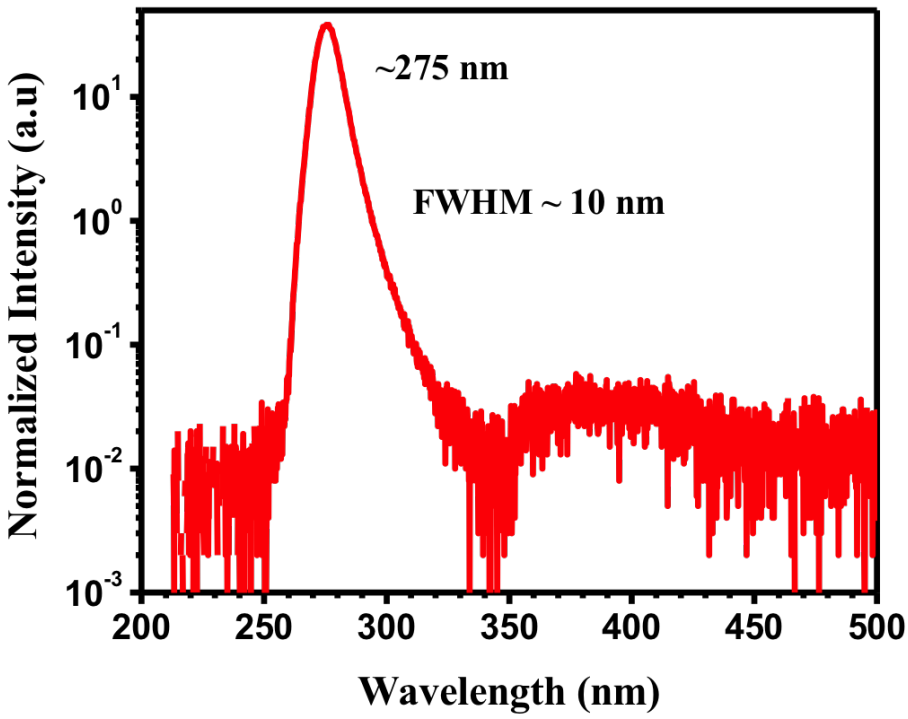

Figure 3.13: EL spectrum of pseudomorphic LED measured in dc mode.

Device Electrical and Optical Characterization

Electrical and optical characterization of flip-chip package LEDs were next performed in dc mode. Electroluminescence (EL) measurements were then carried out using a HORIBA Jobin Yvon spectrometer, Triax 550, which is equipped with a 600 gr/mm grating and a liquid nitrogen cooled Si CCD detector. The electroluminescence spectrum of the pseudomorphic LED can be seen in Figure 3.13 where the peak emission is at 275 nm with full width at half maximum of 10 nm. The EL intensity ratio between the main and the parasitic peaks was around 1000, which is an indication of good carrier confinement in the MQW active regions [103].

Typical RT current-voltage characteristics of the pseudomorphic and standard SPSL relaxed devices are illustrated in Figure 3.14 and were measured using a high-

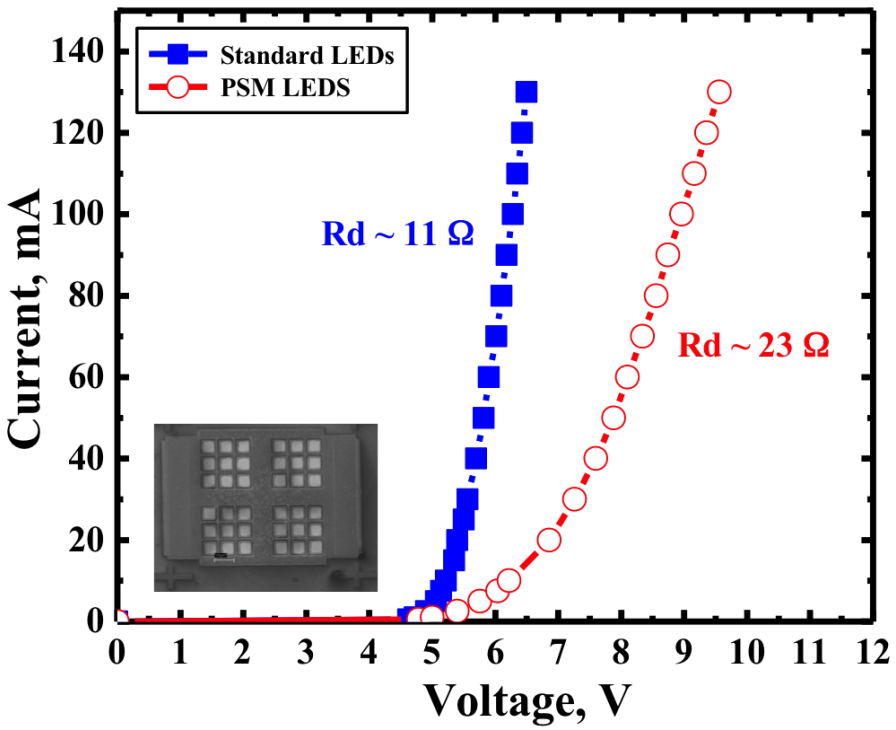

Figure 3.14: I-V characteristics of pseudomorphic and standard SPSL LEDs measured in dc mode. The inset represents SEM image of the pixel-LED device with 360 x 360 μm^2 p-active area.

resolution digital curve tracer, model Sony/Tektronix 370A. The corresponding diode series resistances were 23 Ω and 11 Ω, respectively. The high resistance of pseudomorphic LED is due to the thin n-AlGaN layer. the inset of Figure 3.14 depicts the SEM image of the pixel-LED device with 360 x 360 μm^2p-active area.

The devices RT output powers were then measured as a function of pump current. The measurements were carried out using a calibrated integrating sphere. The data is plotted in Figure 3.15. An output powers of ~7mW and 12mW were measured at 100 mA for the pseudomorphic and standard SPSL LEDs, respectively. The forward voltages were 8.8 V and 6.2 V, respectively. As a result the PSM LED device exhibits a lower power saturation current of ~125 mA.

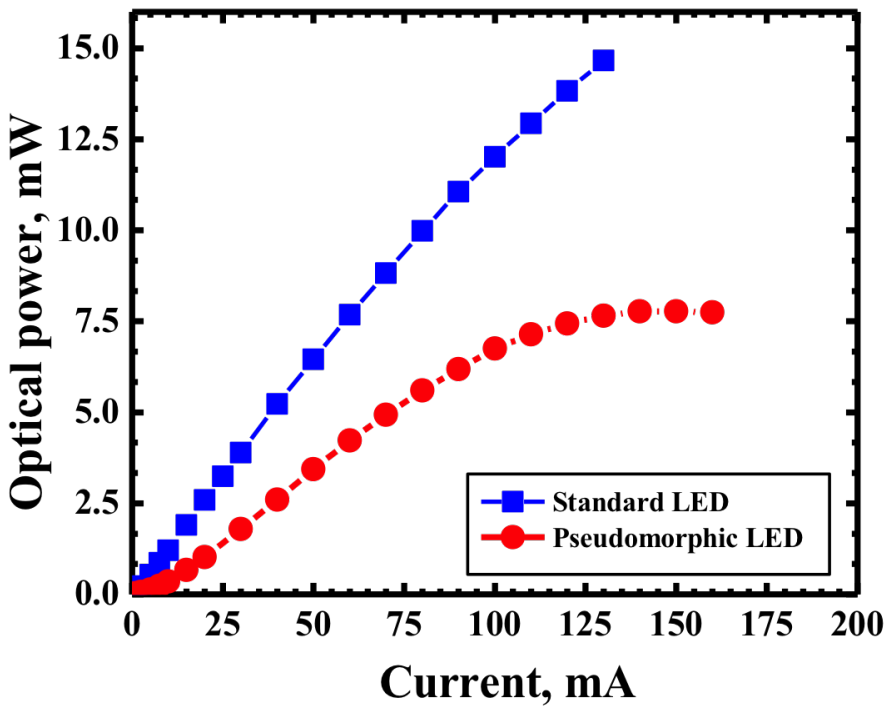

Figure 3.15: L-I characteristics measured in dc mode for pseudomorphic and standard SPSL LEDs with 360 x 360 μm^2 emission areas.

Reliability of Pseudomorphic DUV-LEDs

For reliability tests, an International Light integrating sphere with a calibrated silicon photodetector was used to measure the devices output powers, as a function of time under constant current conditions. Here, 100 x 100 μm^2 and 200 x 200 μm^2 square-shaped LED devices were stressed at 20mA dc injection current, which translates into current densities of 200 A/cm^2 and 50 A/cm^2, respectively. The lifetime data plots for several devices with different packaging schemes can be seen in Figure 3.16.

The results indicate an initial steep drop (of more than 30%) in the output power of the pseudomorphic devices due to self-heating effects resulting from the thin n-AlGaN layer, and the associated increase of the junction temperature [104]–[106]. The initial power drop thus becomes important with increasing the pump current density,

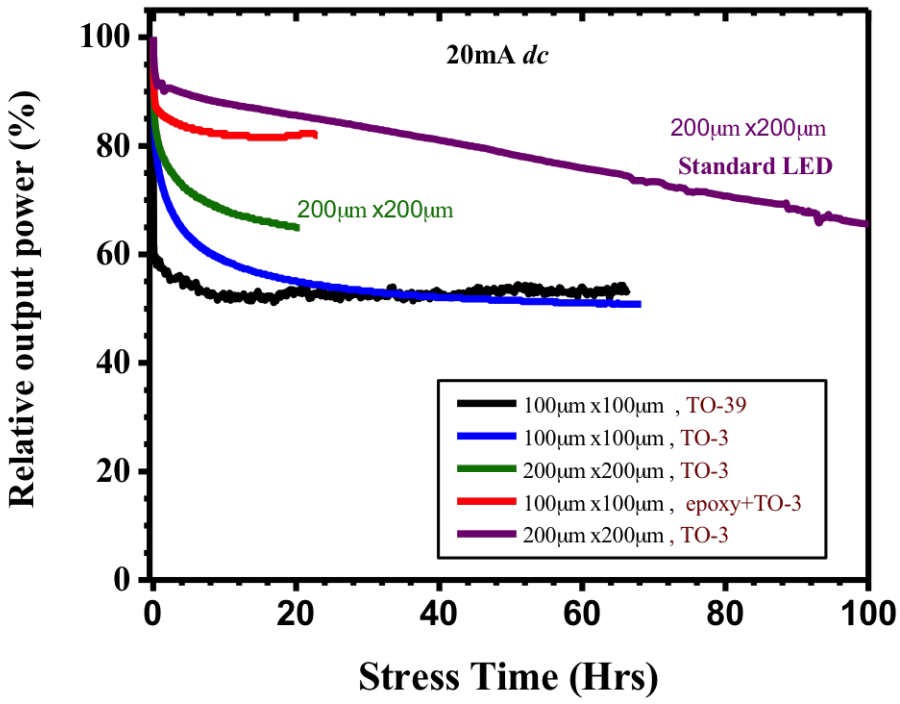

Figure 3.16: lifetime testing data for packaged pseudomorphic LEDs at RT with different packaging schemes. For comparison, reliability of a reference standard SPSL LED was also measured.

while keeping the other packaging parameters the same, and decreases with improving heat dissipation through efficient packaging schemes. For example, when the device is mounted on a TO-3 header and a higher thermal conductivity die attach epoxy (curve in red color), the output power drop was only 15%. The standard SPSL LED, also mounted on a TO-3 header, shows only 8% drop as the sheet resistance of n-AlGaN for standard SPSL LEDs is three times lower than that of pseudomorphic LEDs. The output power initial rapid decay is followed by a much slower decay over time. This slower degradation is believed to be due to gradual activation of dislocations in the active region of the device [107], [108]. These dislocations get activated under constant stress, leading to non-radiative recombination and hence decay of output power. However, in the case of pseudomorphic LEDs, the power appears to stabilize

(reach a constant level) after about 30 hours of stress, due to better materials quality, hence exhibiting better device reliability than standard SPSL LEDs.

Summary

In conclusion, the first pseudomorphic deep-UV LEDs has been grown on AlN/sapphire templates by incorporating a number of innovations in the growth process. A novel pulse modulation doping technique has been used to improve doping in the 0.6 μm thick n-AlGaN layer. LED devices with 360 x 360 μm^2 p-contact areas were then fabricated using pixel-LED design geometry. Output powers of ~7 mW at 100 mA current injection were measured together with a forward voltage of ~ 8.8 V.

The significant improvement in the device reliability of the pseudomorphic LED devices looks very promising. Although the reference (relaxed) LEDs output power was better than that of the pseudomorphic devices, more recent results reveal that there is still room for improvements in LED performance using a quasi-pseudomorphic growth approach, for which the results will be presented in Chapter 4.

Chapter 4

Quasi-Pseudomorphic Deep Ultraviolet Light Emitting Diodes over Sapphire

The thin n-AlGaN layer in pseudomorphic growth introduces a serious concern in the form of high sheet resistance due to its reduced thickness. This high sheet resistance proved to be a deterrent to device output power and reliability as was discussed in Chapter 3.

It is imperative to address the heating issues by growing thicker n-AlGaN while maintaining low dislocation density. This goal must be achieved by keeping the epilayers mostly strained, so that the dislocations density remain close to that of the starting template. The thicker n-AlGaN layer exhibits better sheet resistance, which alleviates the current crowding and device self heating issues, thereby, increasing the device output power and lifetime.

The main advantage of this approach over comparable strain management techniques comes from the straightforward growth process. For comparison, short-period superlattice structures, an alternate strain management scheme, require complex and time consuming steps that can lead to increased fabrication cost and lower commercial feasibility. Furthermore, thick superlattice structures also suffer from issues such as severe substrate bowing, further reducing the yield of these structures.

A novel quasi-pseudomorphic LED structure is introduced in this chapter that offers low sheet resistance, low dislocation densities, and a straightforward growth and fabrication process. In the following sections, the growth and fabrication pro-

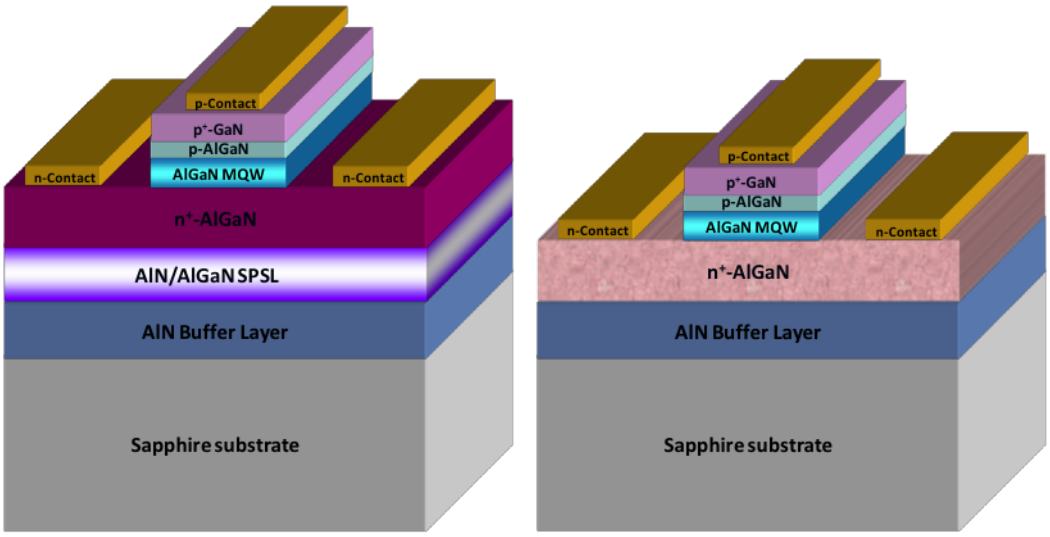

(a) (b)

Figure 4.1: Schematic diagram of DUV-LED epilayer structures: standard SPSL LED (a) and Quasi-pseudomorphic LED (b).

cesses for a quasi-pseudomorphic DUV-LED are presented along with a comprehensive comparisons of device performance with the short-period superlattice based LEDs, henceforth called the "standard" LEDs for sake of brevity.

4.1 Epilayer Structure

The schematic structures for standard (SPSL) and quasi-pseudomorphic LEDs are illustrated in Figure 4.1. The initial steps in the growth process for both techniques are similar. Both the samples were grown on c-plane sapphire substrate. A 2.4 μm thick, high quality AlN buffer layer was first deposited at ~1200 ^{o}C using pulsed MOCVD [61]. The dislocation density was measured to be 2 x10^{8}cm^{-2}.

Quasi-pseudomorphic LEDs have a simpler epilayer structure, with the AlN buffer layer followed by 2 μm thick silicon-doped n-$Al_{0.60}Ga_{0.40}N$ layer. A five-period multiple quantum wells is grown over the n-AlGaN layer. Then p-AlGaN/p-GaN p-contact layers were grown to complete the LED structure.

In comparison, for standard SPSL LEDs, a short period superlattice is also de-

posited before the growth of 3 μm silicon doped n-AlGaN layer.

4.2 Material Characterization

After the growth of the two samples, a detailed analysis of the characteristics of the two epiwafers was carried out.

Etch Pit Density

The n-AlGaN dislocation density of 5 x10^8 $cm^{-2}$and 2 x10^9 cm^{-2}were measured for quasi-pseudomorphic and standard SPSL LEDs respectively. Due to quasi growth, the dislocation density of n-AlGaN remain very close to the template, translating into four times lower dislocation density as compared to the standard LEDs with superlattice structure.

Sheet Resistances

The measured sheet resistances for these LED samples are shown in Figure 4.2. The sheet resistance for quasi-pseudomorphic LEDs decreases with increasing thickness of n-AlGaN layer. The average value for sheet resistance was 159 Ω/sq as compared to the 500 Ω/sq for the pseudomorphic LED wafer with 0.6 μm n-AlGaN layer. As expected the sheet resistance for standard SPSL LEDs was found to be 105 Ω/sq, owning to a thicker n-AlGaN layer.

XRD Reciprocal Space Mapping

Comparisons of the X-ray diffraction reciprocal space maps of quasi-pseudomorphic and standard SPSL DUV-LED structures are shown in Figure 4.3. As seen the AlN and n-AlGaN films reciprocal lattice points (RLP) are not exactly on the vertical line that is perpendicular to the q_x axis, indicating a partial relaxation of the n-

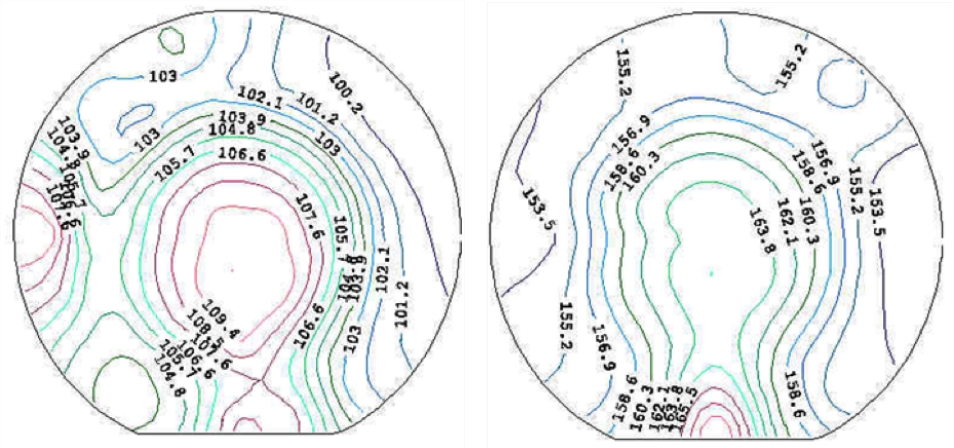

(a) (b)

Figure 4.2: Sheet resistance mapping of Standard SPSL LED (a) and Quasi-pseudomorphic LED (b).

AlGaN with respect to the underlying AlN layer, when grown to a thickness of 2 μm. However, it remains mostly strained as compared to the fully relaxed n-AlGaN for standard SPSL LEDs (see Figure 4.3b), indicating a better crystal quality for quasi-pseudomorphic LEDs, as the layer relaxation creates defects in LED epilayer.

Summary

The primary advantage of quasi-pseudomorphic epilayers are rooted into a simpler growth and fabrication process that can lead to significant reductions in manufacturing time and cost. The comparisons in the last sections reveal that despite having simpler growth and fabrication processes, quasi-pseudomorphic LEDs have higher quality crystals that exhibit lower dislocation densities than those with SPSL structures. The sheet resistances have improved significantly over pseudomorphic LED but still trail behind standard SPSL LEDs. However, the thickness of quasi-pseudomorphic n-AlGaN can be increased further to further reduce the sheet resistance, albeit at the cost of higher density of defects.

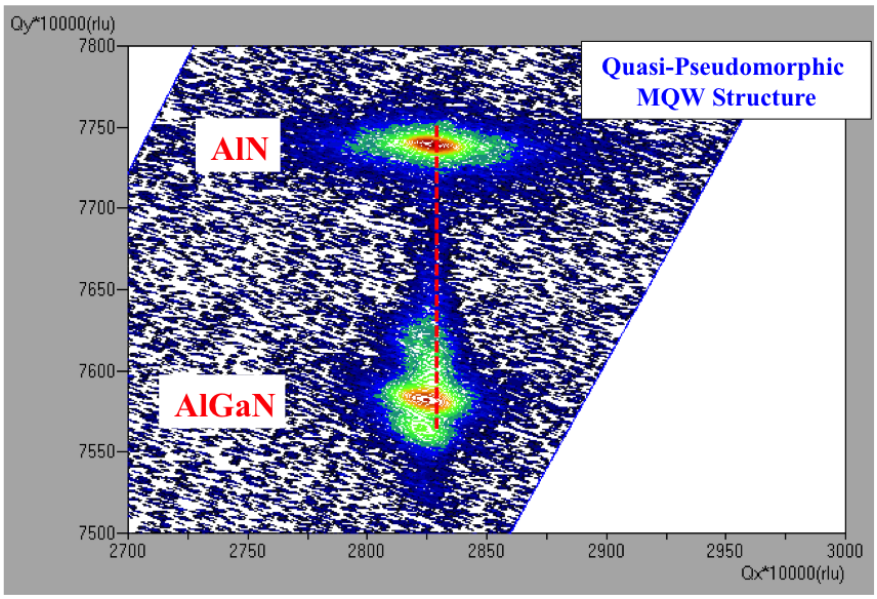

(a)

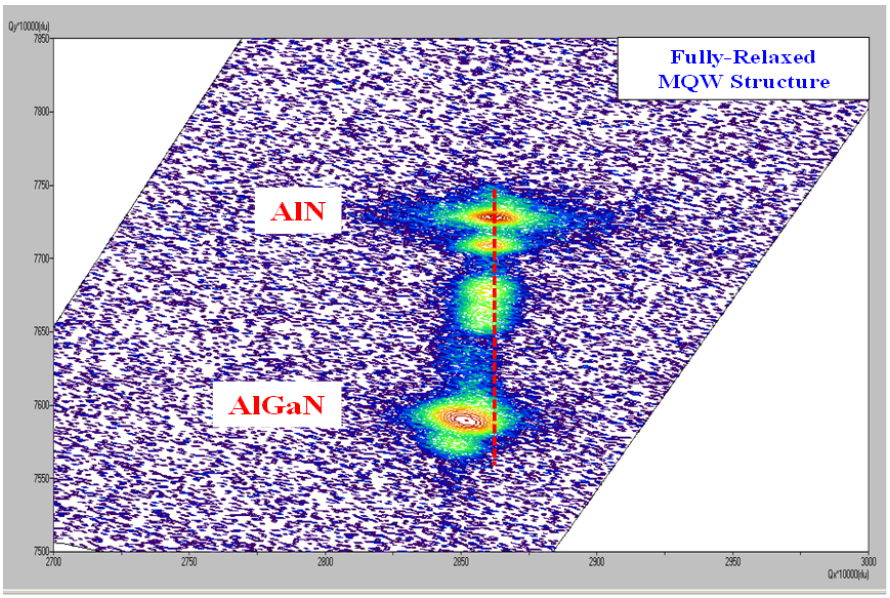

(b)

Figure 4.3: XRD reciprocal space mapping of quasi-pseudomorphic LEDs (a) and Standard SPSL LEDs (b).

4.3 Device Processing

After growth and material characterization, both the samples were processed and packaged before the final evaluation of their electrical and optical characteristics.

H-shaped mesas were defined to reach the bottom n-AlGaN layer by inductively coupled plasma reactive ion etching. Once these mesas were formed, n and p ohmic contacts were laid out by using electron beam evaporation technique. Ti/Al/Ti/Au and Ni/Au metal stacks were used for n and p ohmic contacts respectively. A probe contact containing Ti/Ni/Au was also deposited on n and p contacts to make the contacts thicker for probing purposes. Finally, electroplated Au layer was deposited on top of n and p contacts before the individual devices were diced.

UV light is collected from the sapphire side of the device, hence, the individual diced chips (devices) were flip-chip bonded to ceramic AlN submounts using Au bumps. The flip-chip devices were then mounted on TO-3 headers for device characterization.

The device total p-active area was equal to $200 \times 200\ \mu m^2$. The processing and packaging parameters of both devices, including the device active area, were kept constant for the sake of comparison.

4.4 Electrical and Optical Characterization of Devices

In the following sections, the measured electrical and optical characteristics of quasi-PSM and standard SPSL LEDs are presented and compared in detail.

Device Electroluminescence

The electroluminescence spectrum for quasi-pseudomorphic and standard SPSL LED devices are plotted in Figure 4.4. These measurements were carried out using Horiba

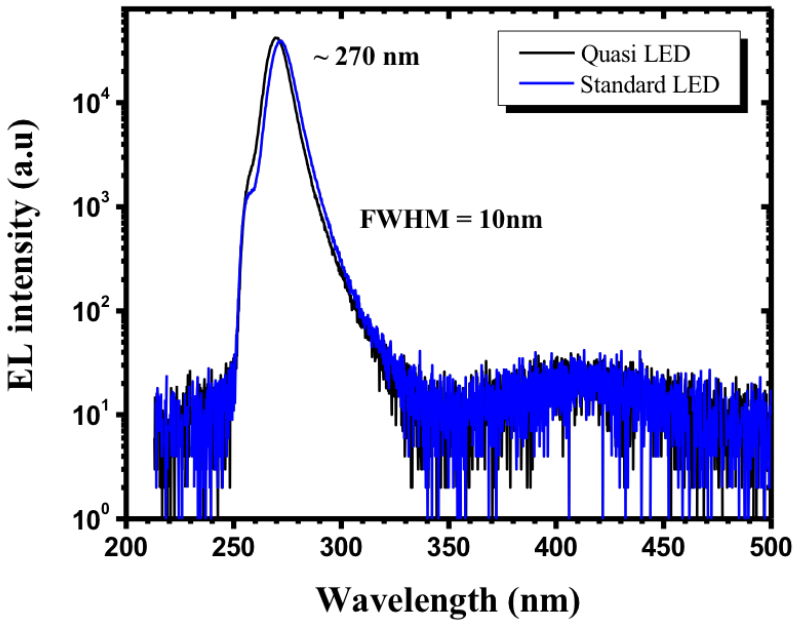

Figure 4.4: RT normalized EL spectra of Quasi-pseudomorphic and standard SPSL DUV-LEDs measured at 20mA pump current.

Jobin Yvon spectrometer, Triax 550, equipped with a 600 gr/mm grating and a liquid nitrogen cooled Si CCD detector.

It can be seen in Figure 4.4 that the dominant main peak for both devices occurred at approximately 270 nm. The value of full width at half maximum was 10 nm for both quasi-pseudomorphic and standard SPSL devices.

A long wavelength side peak centered at 410 nm can also be seen in both the EL spectra. This secondary peak is a result of an overflow of the injected electrons to the deep level of the p-GaN. This leakage can be mitigated by further optimization of the electron blocking layer. The rate of leakage can be controlled by changing the thickness and/or composition of the blocking layer. However, the ratio of main to parasitic emission peaks is measured to be greater than 1500, indicating very good carrier confinement in the active region [103]. The existence of a short wavelength emission shoulder centered at ~ 257 nm can be attributed to carrier recombinations

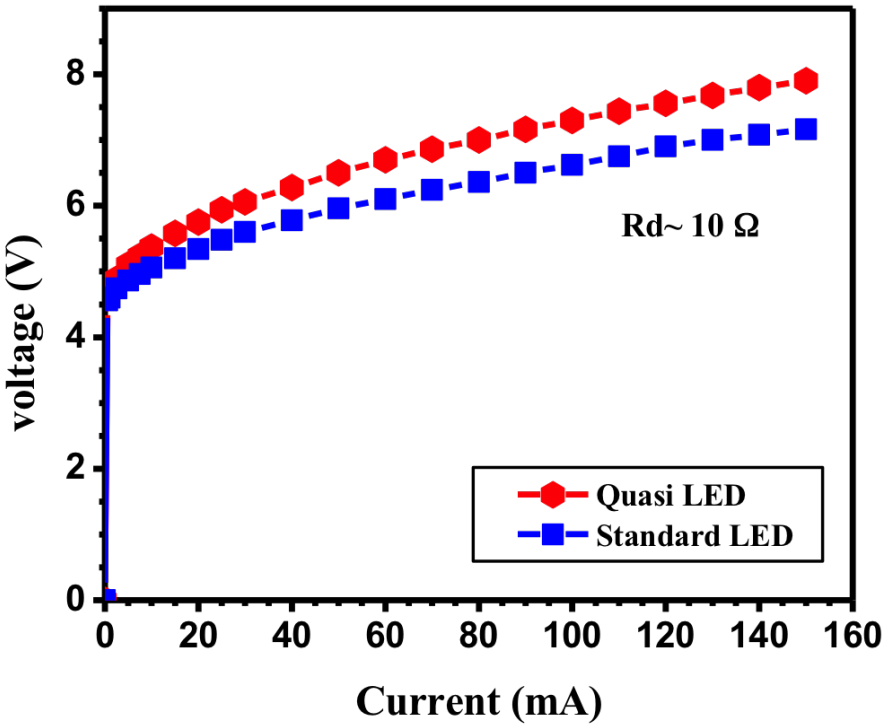

Figure 4.5: I-V characteristics of standard SPSL and quasi-pseudomorphic LEDs measured in dc mode.

in the AlGaN barrier layer.

Current-Voltage and Current-Power Relationships

The plots of current-voltage characteristics for the packaged standard SPSL and quasi-pseudomorphic LED devices are presented in Figure 4.5 and were measured in dc mode using a digital curve tracer (Sony/Tektronix 370A). The slightly higher forward voltage for quasi-pseudomorphic LEDs is a result of higher sheet resistance, due to a thinner n-AlGaN layer as compared to the standard SPSL LEDs. However, both the devices exhibited similar differential resistances of approximately 10 Ω. The similar values for differential resistance, in spite of quasi-pseudomorphic LEDs having a higher sheet resistance than the standard SPSL LEDs, can be attributed

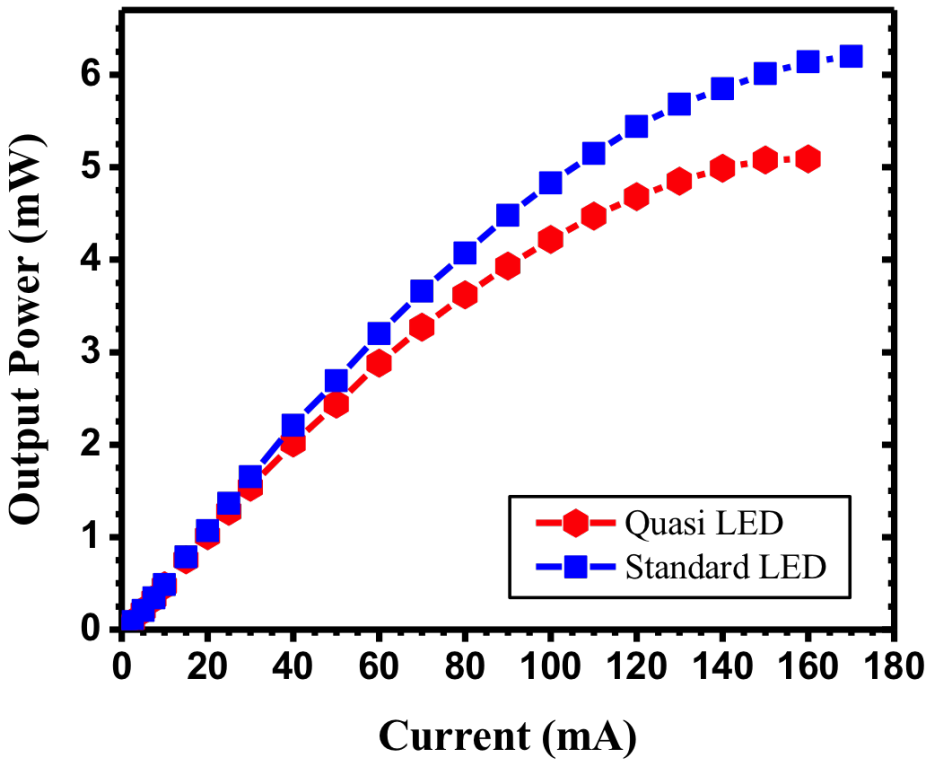

Figure 4.6: The plot of dc output power as a function of pump current for standard SPSL and quasi-pseudomorphic packaged LEDs measured at RT.

to higher carrier mobility in quasi-pseudomorphic epilayers, and is an indication of better crystal quality.

A comparison of output power versus injection current plots, measured at room temperature, for quasi-pseudomorphic and standard SPSL packaged LEDs can be seen in Figure 4.6. An integrating sphere with a calibrated UV-enhanced Si detector was used for these measurements.

The output power of the quasi-pseudomorphic LED was expected to be lower, at the same value of injection current, due to a higher operating voltage. The output powers at lower injection currents are very similar for both devices, with an output power of approximately 1 mW measured at a current of 20 mA. In this region, self-heating is not a serious issue and the quasi-pseudomorphic LED achieved comparable

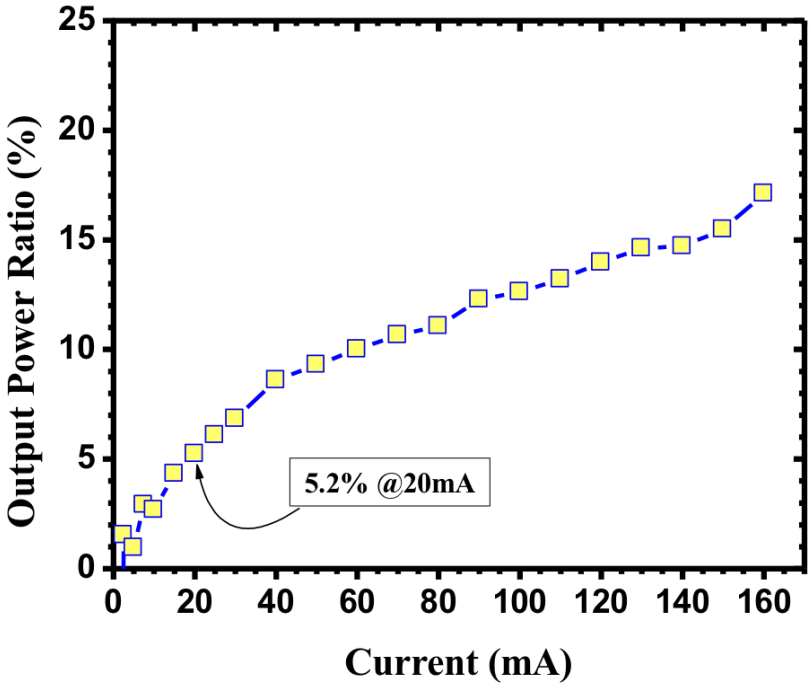

Figure 4.7: The ratio of standard SPSL LEDs output power over the quasi-pseudomorphic LEDs as a function of pump currents.

output power despite having a higher operating voltage.

At higher injection currents, however, the output power of quasi-pseudomorphic LEDs drops relatively due to higher rate of self-heating, caused by its higher sheet resistance. This sheet resistance can be further minimized by growing a thicker n-AlGaN layer. However, increasing the thickness of n-AlGaN layer can lead to higher defects in the crystal. The optimal value of n-AlGaN thickness, with regards to dislocation density and sheet resistance, is the subject of discussion in Chapter 5.

The L-I characteristics for both devices exhibit non-linear behavior due to self-heating. This self-heating subsequently raises the junction temperature, leading to early saturation of output power. The output power saturation for standard SPSL LEDs was at 160 mA as compared to 150 mA for quasi-pseudomorphic LEDs. The higher saturation current for standard SPSL LEDs can be attributed to better heat

dissipation due to thicker device structure. As discussed earlier, the saturation point for quasi-pseudomorphic LEDs can be improved by growing a thicker n-AlGaN layer.

The ratio of standard SPSL LEDs output power over the quasi-pseudomorphic LEDs is plotted in Figure 4.7. It has to be emphasized here that these devices are small area devices and are generally operated at low injection currents. For a typical dc input current of 20mA, the output power of standard SPSL LED is only 5.2% higher than that of a quasi-pseudomorphic LED.

Device External Quantum Efficiency

The external quantum efficiencies as a function of injection currents is plotted in Figure 4.8. The plots for both the devices exhibit similar characteristics and can be divided into two regions. In the first region, the EQE increases rapidly with an increase in the injection current until it reaches a maximum value. The peak values of 1.1% and 1.2% were observed for quasi-pseudomorphic and standard SPSL LEDs respectively, indicating very similar performance between both devices.

Once the maximum value of EQE is achieved, any further increase in the input current leads to higher rate of self heating rather than light emission, reducing the overall EQE.

Device Reliability Test

For the reliability measurements, the output power under constant dc current was monitored as a function of time using an integrating sphere with a calibrated Si photodiode. The measurements were carried out at room temperature. The H-shaped LED devices, with an area of 200x200 μm^2 each, were stressed at dc injection current of 20 mA, which corresponds to a current density of 50 A/cm^2. The plots for output power decay for quasi-pseudomorphic and standard SPSL DUV-LEDs are shown in Figure 4.9.

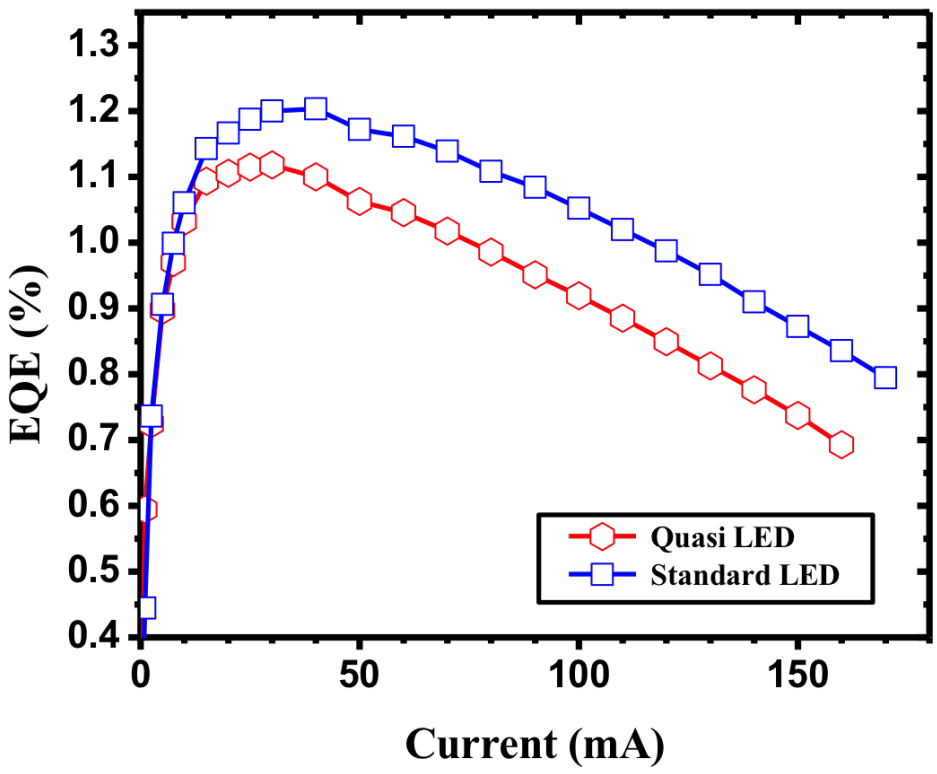

Figure 4.8: External quantum efficiency (EQE) for quasi-pseudomorphic and standard SPSL LEDs under dc pump currents.

A rapid drop of 9% in the output power was observed initially for both the devices due to self-heating, and the associated rise of junction temperatures [104][106].

The initial decay is then followed by a much slower degradation over time. This slower degradation is believed to be due the gradual activation of dislocations in the active region of the device [107][108]. These dislocations get activated under constant stress, leading to non-radiative recombination and hence decay of the output power.

Drops in output powers of 25% and 35% were observed for quasi-pseudomorphic and standard SPSL devices respectively, after 100 hours of stress. The fact that the quasi-pseudomorphic LED retained 75% of its original output power, compared to 65% for the standard SPSL LEDs, indicates a better material quality and longer life

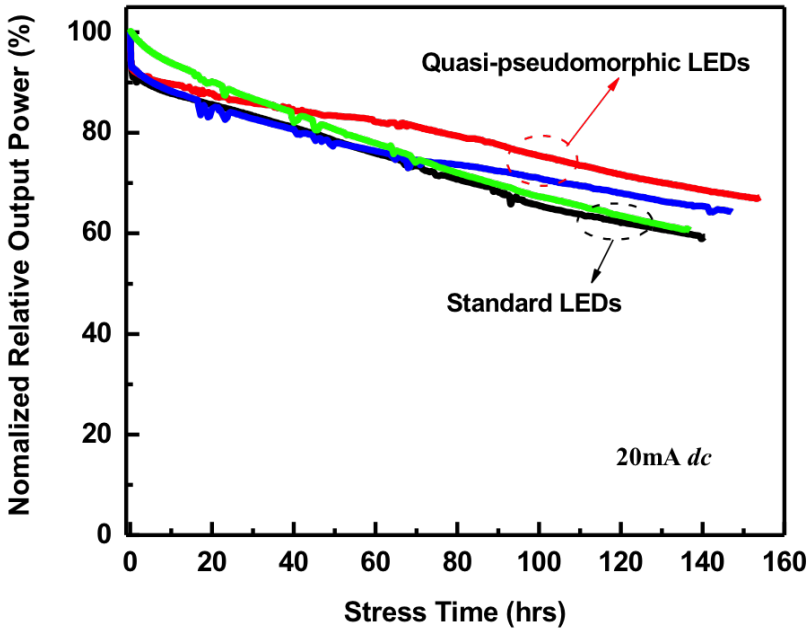

Figure 4.9: Reliability comparison of quasi-pseudomorphic versus standard SPSL LEDs, at room temperature, packaged on TO-3 headers.

spans for quasi-pseudomorphic DUV-LEDs. The higher reliability of QPSM DUV-LEDs in this study can be attributed to the improved materials quality, resulting from the mostly strained epilayer structure.

Summary

In conclusion, we demonstrated the feasibility of quasi-pseudomorphic epilayers over AlN/sapphire template, without compromising the device performance. The output power for these devices were observed to be slightly lower (5.2%) than that of reference standard SPSL LEDs at typical operating conditions (injection current of 20 mA). On the other hand, quasi-pseudomorphic LEDs easily surpassed the reference LEDs in reliability and crystal quality. The quasi-pseudomorphic DUV-LEDs addressed the issue of low output power of pseudomorphic LEDs by allowing the growth of thicker,

low resistance n-AlGaN layer without sacrificing the crystal quality resulting from a mostly strained layer. The proposed approach achieved these goals by simplifying the growth and fabrication processes leading to time and cost savings. Furthermore, by eliminating the need for short-period superlattices, this approach avoids the severe substrate bowing issues that plagued the fabrication of standard SPSL devices.

Chapter 5

Selective Area Deposition for Deep Ultraviolet Light Emitting Diodes over Sapphire

In Chapter 3, we presented the design, fabrication, and characterization of pseudomorphic LEDs. In these devices, the MQW structure is fully strained leading to low levels of dislocation density. As a result, these devices have higher reliability and longer life spans than fully relaxed SPSL LEDs. However, the output power was almost 50% less than that of SPSL LEDs owing to the thin AlGaN layer.

The output power limitations led to the development of quasi-pseudomorphic LEDs, with partially relaxed MQW structure. The quasi-pseudomorphic LEDs offer output power comparable to standard SPSL LEDs with significantly improved reliability. However, the higher value of sheet resistance, and its contribution to joule's heating, is an issue that must be resolved in order to develop efficient, high output DUV-LEDs.

In this chapter, efforts to grow even thicker n-AlGaN layers have been described. In Section 5.1, attempts were made to grow epilayers with thickness ranging from 2-4 μm. At these values of thickness, the epilayers are no longer strained. Although the sheet resistance is reduced by the increased thickness, the defect density increases significantly due to varying degree of relaxation in the epilayers. The object of these experiments was to estimate the optimal value of thickness that lead to maximum value of output power while preserving the quality of the crystals.

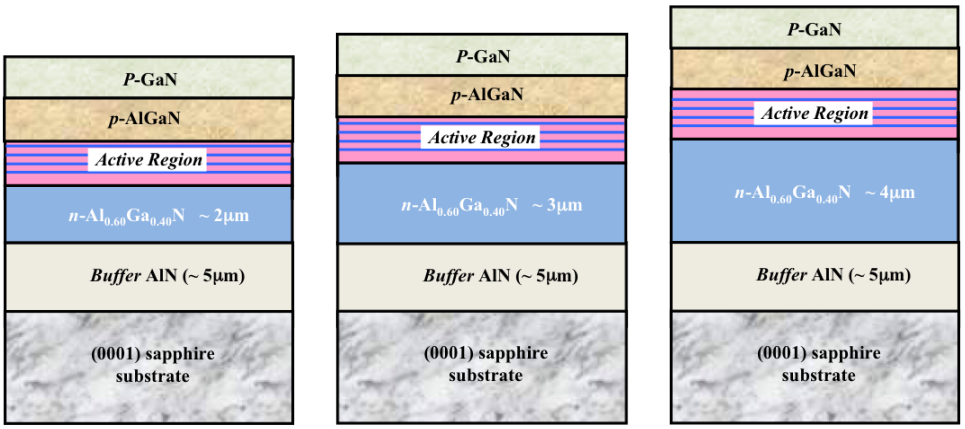

(a) (b) (c)

Figure 5.1: Schematic diagram of DUV-LEDs with different n-AlGaN thickness.

The results of these experiments led us to the next approach of using selective area deposition (SAD) for growing thick n-AlGaN epilayers. Selective area deposition have been successfully used on silicon substrate and Section 5.2 provides the details of our efforts to adapt this technique for DUV-LEDs over a sapphire substrate.

5.1 The Effects of n-AlGaN Thickness on Device Performance

To study the effects of n-AlGaN thickness on device performance, three LEDs structures of varying thicknesses were grown on a 5 μm AlN buffer layer, grown on sapphire substrate. The thickness of the n-AlGaN layers were kept at 2 μm, 3 μm and 4 μm for device A, B and C respectively. No additional strain relief superlattice layers were grown for any of these devices. The device schematics are illustrated in Figure 5.1. Other growth parameters were similar to those described in Chapter 3.

Sheet Resistance

The sheet resistance of n-AlGaN for each sample was measured using Lehighton contactless sheet resistance mapping system. The sheet resistance mappings for these LED samples are shown in Figure 5.2. The value of sheet resistances for device A,

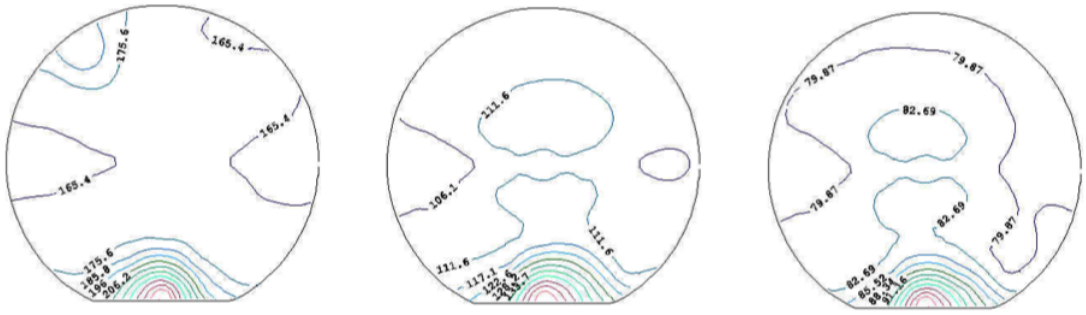

(a) (b) (c)

Figure 5.2: n-AlGaN Sheet resistance for (a) device A (b) device B and (c) device C..

with 2 μm thick n-AlGaN layer, is similar to quasi-pseudomorphic LEDs, with an average value of 174 Ω/sq. This value of sheet resistance is expected given both the compared devices have same thickness for the n-AlGaN layer. The sheet resistance for device B and device C were measured to be 112 Ω/sq and 82 Ω/sq respectively. This reduction in sheet resistance is primarily driven by an increase in the thickness of n-AlGaN layer, however, small variations in carrier mobility and concentrations can also contribute to the final value of sheet resistance.

Device I-V and I-L Characteristics

These LED structures were processed into devices, each with an active area of 100 × 100 μm^2, using the same processing techniques described in Chapter 3. The electrical and optical characterizations of unpackaged LED devices were carried out in dc mode. The I-V characteristics of these devices, measured at room temperature, are shown in Figure 5.3. Although, of varying thickness, all the devices exhibited similar series resistances. The high value of operating voltage is due to the non-ohmic n-contact and indicates the need for further optimizations in the fabrication process.

The measured output power versus dc pumping currents, at room temperature, are plotted in Figure 5.4. It can be seen from the figure that output powers of 1.2 mW, 1.03 mW and 0.93 mW were measured at a dc current of 20 mA for device A, B

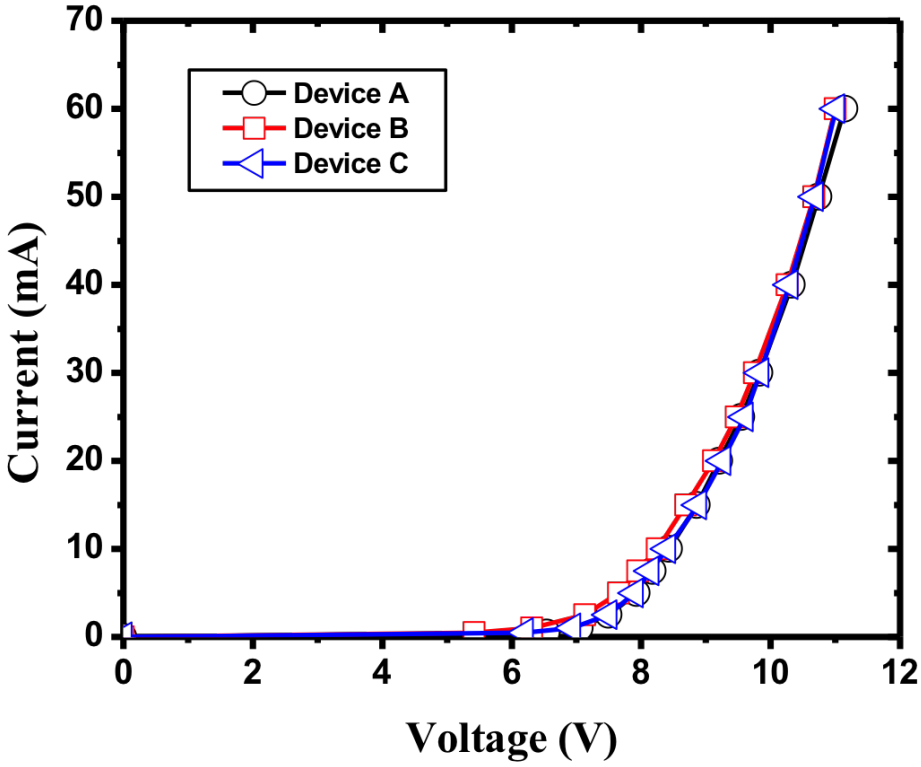

Figure 5.3: devices I-V characteristics measured at RT.

and C respectively. The result shows a decrease of LEDs output power with increase in n-AlGaN thickness.

It can be hypothesized that an increase in the n-AlGaN thickness beyond 2 μm, which was the thickness for our quasi-pseudomorphic LEDs, results in the relaxation of epilayer structure, leading to the formation of dislocations throughout the AlGaN layers. These dislocations upon penetration to the active region increase the non-radiative recombination. As a result, devices B and C exhibit lower output power.

It is evident that the planar growth technique leads to high levels of defects when the thickness of n-AlGaN epilayer is increased beyond a certain threshold. In order to increase the thickness of n-AlGaN without compromising the epilayer crystal quality, the growth of n-AlGaN by selective area deposition approach was next investigated.

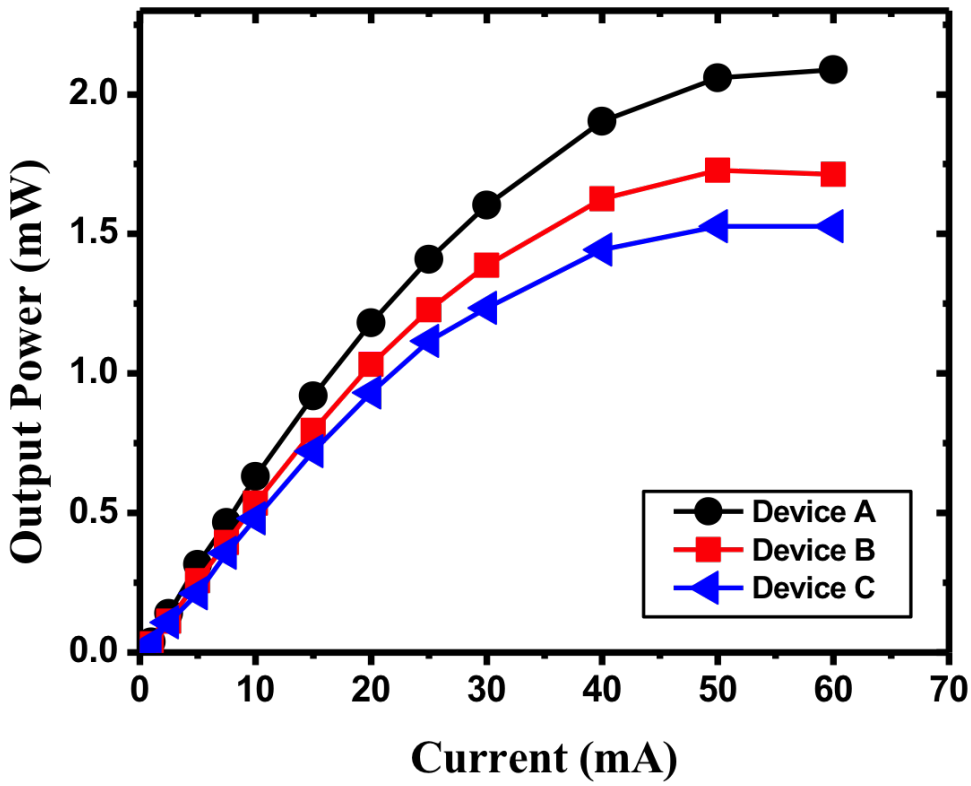

Figure 5.4: RT current- output Power (I-L) characteristics of the devices measured in dc mode.

This approach is described in detail in the following section.

5.2 Selective Area Deposition of n-AlGaN and MQW Structure

For DUV-LEDs, the strain in the epilayers is much higher and more difficult to manage than in their visible counterparts due to large lattice mismatch between AlN/AlGaN and sapphire. Consequently, the growth of crack-free, thick, doped AlGaN epitaxial layers faces a number of unique challenges. In the previous chapters, two alternate schemes were presented to grow high quality, reliable AlGaN epilayers. These approaches suffered from self-heating due to higher sheet resistances.

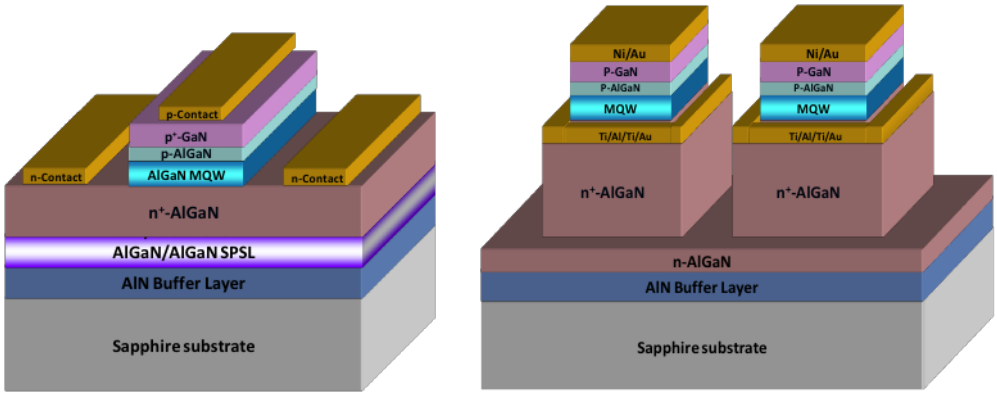

(a) (b)

Figure 5.5: Schematic diagram of standard SPSL (left) and SAD (right) LEDs.

The outcome of the experiments in the last section revealed that any attempts to reduce the sheet resistance by increasing the thickness of the epilayer result in higher dislocation densities in these devices, hence impacting their EQE.

The selective area deposition technique has been used previously for deposition of III-Nitride materials over silicon substrates [109]. This approach has been proven to be effective in minimizing the micro-cracks formations by localizing the growth of nitride epilayers.

In this section, the growth of n-AlGaN epilayers over sapphire substrate, using selective area deposition, is presented. The schematic diagram of the selective area deposited LEDs versus standard SPSL LEDs is shown in Figure 5.5.

Sample Preparation Process

A thin un-doped n-AlGaN layer is initially deposited on top of AlN/sapphire template. Then 0.2-0.3 μm thick SiO_2 mask pattern is transferred to this layer using plasma-enhanced chemical vapor deposition (PECVD), photolithography and reactive-ion etching (RIE). The wafer is then thoroughly cleaned before loading it in the MOCVD chamber for regrowth. The silicon doped n-AlGaN contact layer, active region, p-AlGaN, p-GaN are selectively deposited in two steps. A step by step

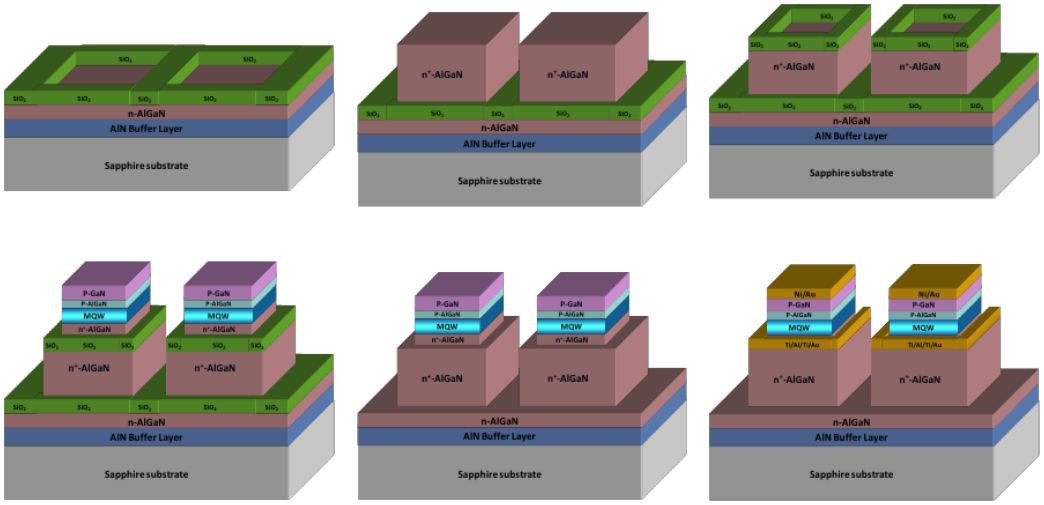

(a) (b) (c)

Figure 5.6: Process-flow for selective area deposition (SAD) approach

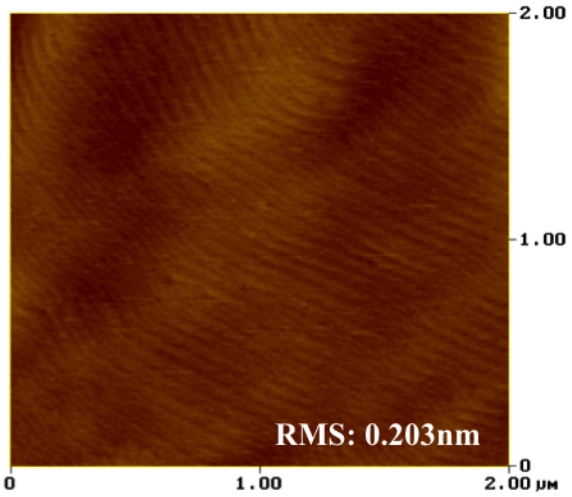

Figure 5.7: AFM image of SAD n-AlGaN.

depiction of the entire process is shown in Figure 5.6.

Preliminary Results

The surface morphology for selective area deposited n-AlGaN is illustrated in Figure 5.7. A surface RMS of 0.203 nm is observed for SAD. which is comparable with RMS value of 0.35 nm for conventionally grown n-AlGaN.

The electroluminescence spectrum for the LEDs grown with selective area de-

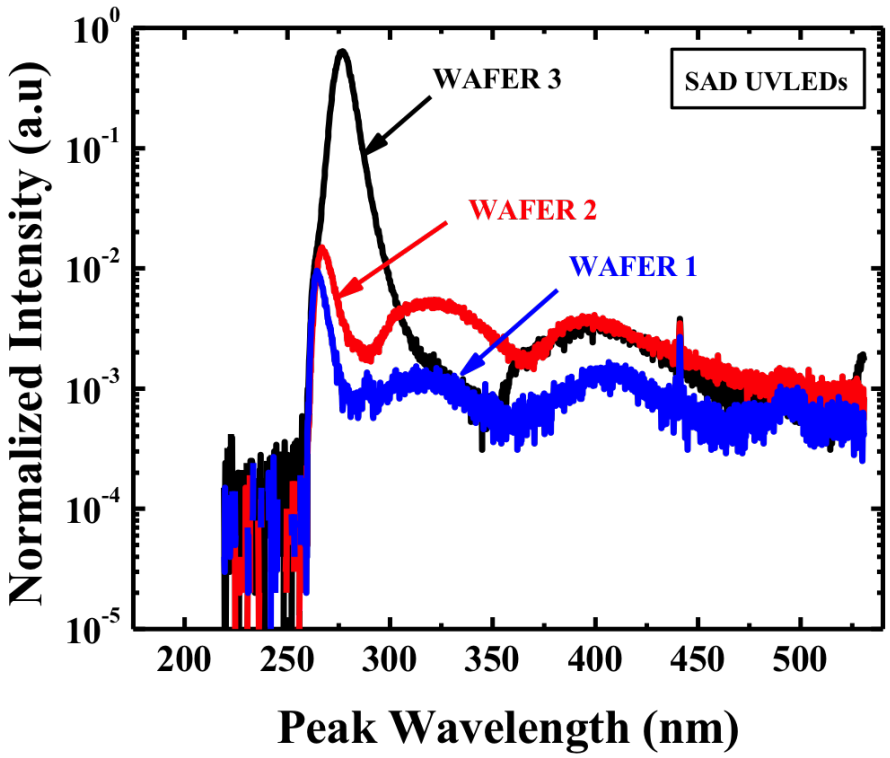

Figure 5.8: EL spectrum of SAD LEDs

position method, is plotted in Figure 5.8. For the first 2 growth runs, a shoulder and longer wavelength emission bands were observed around 320 nm and 410 nm in addition to the primary peak at approximately 275 nm.

After further optimizations in the electron blocking layer, the parasitic peak at 320 nm was eliminated and a much higher ratio of main to parasitic peaks was achieved, as can be seen from the plot of wafer 3 in Figure 5.8.

The use of different metal schemes were investigated for the n-ohmic contacts. The same metal stacks were evaporated on the n-AlGaN grown by selective area deposition method and conventionally grown method. The results are shown in Figure 5.9. It is evident from the plot that unetched SAD samples exhibit ohmic contacts with very small barrier, as compared to the etched samples for the same metal stacks.

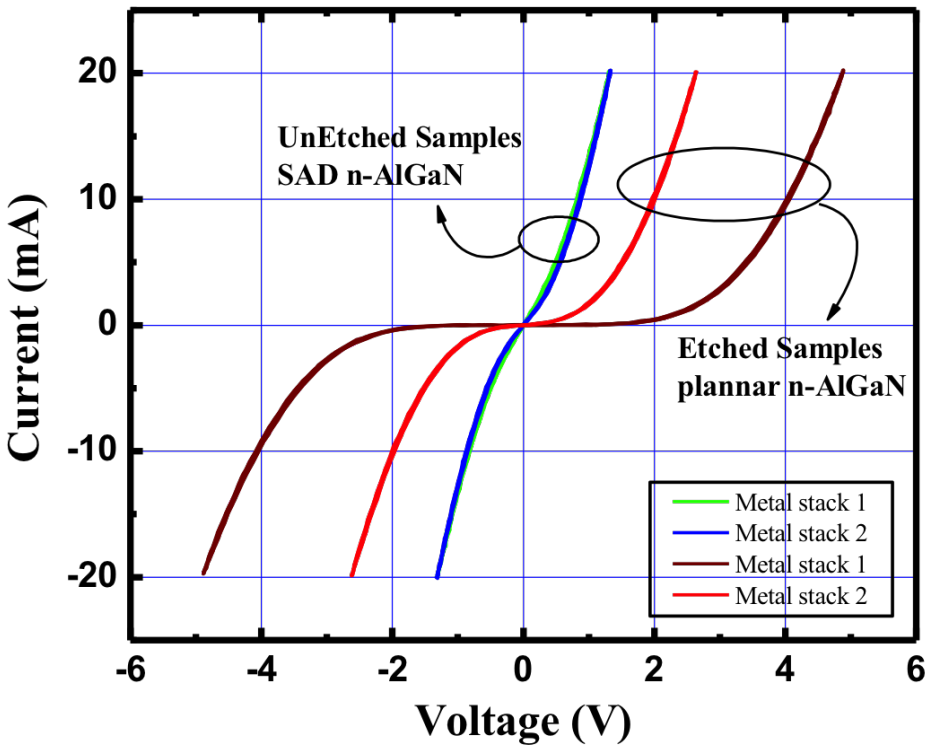

Figure 5.9: I-V characteristics for unetched SAD samples versus etched samples with different metal schemes.

Selective area deposition is a promising technique that must be investigated further to evaluate its feasibility for the development of DUV-LEDs over sapphire. The preliminary results reveal excellent morphology of the surfaces developed using this process, and there is plenty of room for further optimizations.

The SAD approach has the added advantage of enabling the fabrication of optical devices without the need for post-growth etching for device definition. This simplification can lead to further reductions in the processing costs.

Summary

In this chapter, it was shown that the sheet resistance of n-AlGaN decreases with an increase in n-AlGaN thickness, but the optical output power does not follow this trend. Beyond a certain threshold for thickness (2 μm for QPSM), the epilayers strain is relieved in the form of dislocations. The increase in the crystal defects offsets any advantages from a lower sheet resistance, resulting in a decline in the optical output power of the device.

Selective area deposition technique is expected to decrease the dislocations density and enable the deposition of thick n-AlGaN, thereby improving both the material crystal quality and conductivity. This technique has the potential to facilitate fabrication of large area single chip DUV-LEDs due to the elimination of current crowding by allowing the growth of thick n-AlGaN current spreading layers. Initial results are promising for this approach but require further growth and processing optimization.

Chapter 6

Conclusions and Future Work

Due to their long life spans, robust nature, high efficiencies and low operating voltages, light emitting diodes have emerged as an ideal candidate to dethrone the traditional incandescent light bulb. Similarly, III-nitrides based light emitting diodes are poised to completely replace bulky, fragile, environmentally hazardous UV mercury lamps. In this research, a number of novel techniques have been proposed to improve the reliability and output power of DUV-LEDs. In the following sections, the conclusions derived from the outcome of the experiments are discussed and future directions for further research are presented.

6.1 Conclusions

A major impediment to the development of commercially feasible DUV-LED is the availability of a well-behaved native substrate that is both readily available and cost effective. III-nitride light emitting diodes are generally grown on a sapphire substrate. Sapphire substrates are inexpensive, abundant, and offer adequate transparency to radiations down to 150 nm range. However, sapphire suffers from a number of serious limitations. The large lattice mismatch between sapphire and AlN/AlGaN layers creates high levels of strain in the epitaxial layer of the device. The resulting strain reduces the likelihood of growing crack-free AlGaN layers.

Devices produced using a mismatched AlN/AlGaN layer on top of a sapphire substrate often exhibit large number of dislocations. These defects lead to the creation of non-radiative recombination centers for the injected carriers, lowering the overall

output power and efficiency of these device.

Short period superlattice structures have been successfully used to minimize and mitigate the strain between the mismatched adjacent layers, allowing for the growth of thick n-AlGaN layers. The fabrication of the superlattice structures is a complex process that involves lengthy preparation and requires large amount of materials. Furthermore, the growth of thick superlattice structures introduces bowing problems for the resultant wafer. The bowing of the wafer introduces alignment problems during the application of masks in the lithography process, which further reduces the yield during fabrication.

In this dissertation, DUV-LEDs have been developed pseudomorphically on low defect density AlN/sapphire template without the superlattice structures. This technique was initially introduced for bulk AlN substrates but its commercial applications are limited due to concerns related to the cost and availability of bulk AlN. By replacing the bulk AlN with a high quality AlN/sapphire template, the overall manufacturing cost of the resulting devices are significantly reduced while retaining the many advantages offered by pseudomorphic layers.

For the first time, pseudomorphic DUV-LEDs have been fabricated with peak emission wavelength of 275 nm. These devices exhibit better reliability scores as compared to SPSL relaxed LEDs owing to the lower dislocation density in the pseudomorphically grown epitaxial layers.

The optical output power of pseudomorphic UV LEDs is observed to be lower than standard UV LEDs with superlattice structures. The thickness of n-AlGaN layer must be increased to reduce its sheet resistance and hence, increase its output power. The maximum thickness that can be achieved in high-strain n-AlGaN layer is limited in pseudomorphic LEDs. Increasing the thickness of the n-AlGaN layer beyond a certain threshold significantly increases the dislocation density, reducing the reliability as well as lowering the optical output power of the device.

To resolve the limitation of pseudomorphic LEDs, an alternate approach, based on quasi-pseudomorphic n-AlGaN over AlN/sapphire, has also been developed in this research. The thickness of n-AlGaN current spreading layer has been increased to 2 μm in the proposed approach as compared to the 0.6 μm for pseudomorphic LEDs. The quasi-pseudomorphic LEDs have a partially relaxed structure compared to the fully-strained structures in pseudomorphic LEDs. The reduced strain between the adjacent layers allow for the growth of thicker n-AlGaN layers that can result in the development of higher optical output devices. The optical output power achieved by quasi-pseudomorphic LEDs, developed in this research, rivaled that of SPSL LEDs. Device reliability, although lower than pseudomorphic LEDs, was considerably better than standard superlattice LEDs, owing to the better epilayer crystal quality.

Comprehensive analysis of the devices revealed a ~25% drop in initial output power for quasi-pseudomorphic versus ~35% for SPSL LEDs after 100 hours of constant stress. The outcomes of these experiments have revealed the pseudomorphic and quasi-pseudomorphic LEDs to be a serious contender to traditional, superlattice based UV LEDs. These devices offer comparable output power and reliability with a simpler growth and fabrication processes that can significantly reduce the unit cost of DUV-LEDs for high volume production.

6.2 Future Work

A thicker n-AlGaN current spreading layer can mitigate the effects of current crowding, and can lead to the development of cost effective, large area, DUV-LEDs on a single chip, without the need for intricate micro-pixel fabrication processes. Selective area deposition techniques for the growth of high quality thick n-AlGaN current spreading layers have yielded promising preliminary results. Further research into selective area deposition techniques and the optimization of the current pseudomorphic and quasi-pseudomorphic growth schemes can result in the development of a wide

range of DUV-LEDs that can satisfy a wide range of reliability and output power requirements.

Bibliography

[1] A. Khan, K. Balakrishnan, and T. Katona, "Ultraviolet light-emitting diodes based on group three nitrides", *Nature photonics*, vol. 2, no. 2, pp. 77–84, 2008.

[2] W. Morison, *Phototherapy and Photochemotherapy of Skin Disease 2nd edn.* 1991.

[3] N. Aeronautics and S. Administration. (). UV exposure has increased over the last 30 years, but stabilized since the mid-1990s, [Online]. Available: `http://www.nasa.gov/topics/solarsystem/features/uv-exposure.html`.

[4] M. H. Crawford, M. A. Banas, M. P. Ross, D. S. Ruby, J. S. Nelson, R. Boucher, and A. A. Allerman, "Final LDRD report: ultraviolet water purification systems for rural environments and mobile applications", *Sandia Report*, 2005. [Online]. Available: `http://prod.sandia.gov/techlib/access-control.cgi/2005/057245.pdf`..

[5] S. Vilhunen, H. Särkkä, and M. Sillanpää, "Ultraviolet light-emitting diodes in water disinfection", *Environmental Science and Pollution Research*, vol. 16, no. 4, pp. 439–442, 2009.

[6] M. Würtele, T. Kolbe, M. Lipsz, A. Külberg, M. Weyers, M. Kneissl, and M. Jekel, "Application of GaN-based ultraviolet-C light emitting diodes–UV LEDs–for water disinfection", *water research*, vol. 45, no. 3, pp. 1481–1489, 2011.

[7] I. Sensor Electronic Technology. (). Product overview, [Online]. Available: `http://www.s-et.com/products.html`.

[8] P. Sandvik, K. Mi, F. Shahedipour, R. McClintock, A. Yasan, P. Kung, and M. Razeghi, "$Al_xGa_{1-x}N$ for solar-blind UV detectors", *Journal of crystal growth*, vol. 231, no. 3, pp. 366–370, 2001.

[9] K. Davitt, Y.-K. Song, W. Patterson III, A. Nurmikko, M. Gherasimova, J. Han, Y.-L. Pan, and R. Chang, "290 and 340 nm UV LED arrays for fluorescence detection from single airborne particles", *Optics express*, vol. 13, no. 23, pp. 9548–9555, 2005.

[10] A. Khan, Q. Fareed, and V. Adivarahan. (2010). Lamps boost output in the deep ultraviolet, [Online]. Available: `http://www.compoundsemiconductor.net/article/86449-lamps-boost-output-in-the-deep-ultraviolet.html`.

[11] Y. Muramoto, M. Kimura, and S. Nouda, "Development and future of ultraviolet light-emitting diodes: UV-LED will replace the UV lamp", *Semiconductor Science and Technology*, vol. 29, no. 8, pp. 84 004–84 011, 2014.

[12] A. Khan and K. Balakrishnan, "Present status of deep UV nitride light emitters", in *Materials Science Forum*, Trans Tech Publ, vol. 590, 2008, pp. 141–174.

[13] J. Pankove, E. Miller, and J. Berkeyheiser, "GaN electroluminescent diodes", in *Electron Devices Meeting, 1971 International*, IEEE, vol. 17, 1971, pp. 78–78.

[14] H. Amano, N. Sawaki, I. Akasaki, and Y. Toyoda, "Metalorganic vapor phase epitaxial growth of a high quality GaN film using an AlN buffer layer", *Applied Physics Letters*, vol. 48, no. 5, pp. 353–355, 1986.

[15] H. Amano, M. Kito, K. Hiramatsu, and I. Akasaki, "P-type conduction in Mg-doped GaN treated with low-energy electron beam irradiation (LEEBI)", *Japanese Journal of Applied Physics*, vol. 28, no. 12A, p. L2112, 1989.

[16] S. Nakamura, "GaN growth using GaN buffer layer", *Japanese Journal of Applied Physics*, vol. 30, no. 10A, p. L1705, 1991.

[17] S. Nakamura, T. Mukai, M. Senoh, and N. Iwasa, "Thermal annealing effects on p-type Mg-doped GaN films", *Japanese Journal of Applied Physics*, vol. 31, no. 2B, p. L139, 1992.

[18] S. Nakamura, M. Senoh, and T. Mukai, "High-power InGaN/GaN double-heterostructure violet light emitting diodes", *Applied Physics Letters*, vol. 62, no. 19, pp. 2390–2392, 1993.

[19] S. Nakamura, M. Senoh, N. Iwasa, and S.-i. Nagahama, "High-power InGaN single-quantum-well-structure blue and violet light-emitting diodes", *Applied Physics Letters*, vol. 67, no. 13, pp. 1868–1870, 1995.

[20] S. Nakamura, M. Senoh, S.-i. Nagahama, N. Iwasa, T. Yamada, T. Matsushita, H. Kiyoku, and Y. Sugimoto, "InGaN multi-quantum-well-structure laser diodes with cleaved mirror cavity facets", *Japanese journal of applied physics*, vol. 35, no. 2B, p. L217, 1996.

[21] S. Nakamura, M. Senoh, S.-i. Nagahama, N. Iwasa, T. Yamada, T. Matsushita, Y. Sugimoto, and H. Kiyoku, "Room-temperature continuous-wave operation of InGaN multi-quantum-well structure laser diodes", *Applied Physics Letters*, vol. 69, no. 26, pp. 4056–4058, 1996.

[22] M. Krames, O. Shchekin, R. Mueller-Mach, G. O. Mueller, L. Zhou, G. Harbers, and M. Craford, "Status and future of high-power light-emitting diodes for solid-state lighting", *Display Technology, Journal of*, vol. 3, no. 2, pp. 160–175, Jun. 2007, ISSN: 1551-319X. DOI: 10.1109/JDT.2007.895339.

[23] M. A. Khan, R. Skogman, J. Van Hove, S. Krishnankutty, and R. Kolbas, "Photoluminescence characteristics of AlGaN-GaN-AlGaN quantum wells", *Applied physics letters*, vol. 56, no. 13, pp. 1257–1259, 1990.

[24] J. Han, M. Crawford, R. Shul, J. Figiel, M. Banas, L. Zhang, Y. Song, H. Zhou, and A. Nurmikko, "AlGaN/GaN quantum well ultraviolet light emitting diodes", *Applied physics letters*, vol. 73, no. 12, pp. 1688–1690, 1998.

[25] T. Nishida and N. Kobayashi, "346 nm emission from AlGaN multi-quantum-well light emitting diode", *physica status solidi (a)*, vol. 176, no. 1, pp. 45–48, 1999.

[26] M. A. Khan, J. Yang, G. Simin, R. Gaska, M. Shur, H.-C. zur Loye, G. Tamulaitis, A. Zukauskas, D. J. Smith, D. Chandrasekhar, *et al.*, "Lattice and energy band engineering in AlInGaN/GaN heterostructures", *Applied Physics Letters*, vol. 76, no. 9, pp. 1161–1163, 2000.

[27] V. Adivarahan, A. Chitnis, J. Zhang, M. Shatalov, J. Yang, G. Simin, M. A. Khan, R. Gaska, and M. Shur, "Ultraviolet light-emitting diodes at 340 nm using quaternary AlInGaN multiple quantum wells", *Applied Physics Letters*, vol. 79, no. 25, pp. 4240–4242, 2001.

[28] A. Kinoshita, H. Hirayama, M. Ainoya, Y. Aoyagi, and A. Hirata, "Room-temperature operation at 333 nm of $Al_{0.03}Ga_{0.97}N/Al_{0.25}Ga_{0.75}N$ quantum-well light-emitting diodes with Mg-doped superlattice layers", *Applied Physics Letters*, vol. 77, no. 2, pp. 175–177, 2000.

[29] M. A. Khan, V. Adivarahan, J. P. Zhang, C. Chen, E. Kuokstis, A. Chitnis, M. Shatalov, J. W. Yang, and G. Simin, "Stripe geometry ultraviolet light emitting diodes at 305 nanometers using quaternary AlInGaN multiple quantum wells", *Japanese Journal of Applied Physics*, vol. 40, no. 12A, p. L1308, 2001.

[30] V. Adivarahan, S. Wu, A. Chitnis, R. Pachipulusu, V. Mandavilli, M. Shatalov, J. Zhang, M. A. Khan, G. Tamulaitis, A. Sereika, *et al.*, "AlGaN single-

quantum-well light-emitting diodes with emission at 285 nm", *Applied Physics Letters*, vol. 81, no. 19, pp. 3666–3668, 2002.

[31] J. Zhang, A. Chitnis, V. Adivarahan, S. Wu, V. Mandavilli, R. Pachipulusu, M. Shatalov, G. Simin, J. Yang, and M. A. Khan, "Milliwatt power deep ultraviolet light-emitting diodes over sapphire with emission at 278 nm", *Applied physics letters*, vol. 81, no. 26, pp. 4910–4912, 2002.

[32] K. Mayes, A. Yasan, R. McClintock, D. Shiell, S. Darvish, P. Kung, and M. Razeghi, "High-power 280 nm AlGaN light-emitting diodes based on an asymmetric single-quantum well", *Applied physics letters*, vol. 84, no. 7, pp. 1046–1048, 2004.

[33] A. Fujioka, T. Misaki, T. Murayama, Y. Narukawa, and T. Mukai, "Improvement in output power of 280-nm deep ultraviolet light-emitting diode by using AlGaN multi quantum wells", *Applied physics express*, vol. 3, no. 4, p. 041 001, 2010.

[34] Y. Liao, C. Thomidis, C.-k. Kao, and T. D. Moustakas, "AlGaN based deep ultraviolet light emitting diodes with high internal quantum efficiency grown by molecular beam epitaxy", *Applied Physics Letters*, vol. 98, no. 8, p. 081 110, 2011.

[35] Y. Taniyasu, M. Kasu, and T. Makimoto, "An aluminium nitride light-emitting diode with a wavelength of 210 nanometres", *Nature*, vol. 441, no. 7091, pp. 325–328, 2006.

[36] N. Otsuka, A. Tsujimura, Y. Hasegawa, G. Sugahara, M. Kume, and Y. Ban, "Room temperature 339 nm emission from $Al_{0.13}Ga_{0.87}N/Al_{0.10}Ga_{0.90}$ double heterostructure light-emitting diode on sapphire substrate", *Japanese Journal of Applied Physics*, vol. 39, no. 5B, p. L445, 2000.

[37] A. Chitnis, J. Zhang, V. Adivarahan, M. Shatalov, S. Wu, R. Pachipulusu, V. Mandavilli, and M. A. Khan, "Improved performance of 325-nm emission AlGaN ultraviolet light-emitting diodes", *Applied physics letters*, vol. 82, no. 16, pp. 2565–2567, 2003.

[38] K. Lee, P. Parbrook, T. Wang, J. Bai, F. Ranalli, R. Airey, and G. Hill, "Effect of the AlGaN electron blocking layer thickness on the performance of AlGaN-based ultraviolet light-emitting diodes", *Journal of Crystal Growth*, vol. 311, no. 10, pp. 2857–2859, 2009.

[39] E. F. Schubert, T. Gessmann, and J. K. Kim, *Light emitting diodes*. Wiley Online Library, 2005.

[40] C. Pernot, M. Kim, S. Fukahori, T. Inazu, T. Fujita, Y. Nagasawa, A. Hirano, M. Ippommatsu, M. Iwaya, S. Kamiyama, *et al.*, "Improved efficiency of 255-280 nm AlGaN-based light-emitting diodes", *Applied physics express*, vol. 3, no. 6, p. 061 004, 2010.

[41] T. Fujii, Y. Gao, R. Sharma, E. Hu, S. DenBaars, and S. Nakamura, "Increase in the extraction efficiency of GaN-based light-emitting diodes via surface roughening", *Applied physics letters*, vol. 84, no. 6, pp. 855–857, 2004.

[42] O. Shchekin, J. Epler, T. Trottier, T. Margalith, D. Steigerwald, M. Holcomb, P. Martin, and M. Krames, "High performance thin-film flip-chip InGaN-GaN light-emitting diodes", *Applied Physics Letters*, vol. 89, no. 7, pp. 071 109–071 109, 2006.

[43] R.-H. Horng, H.-L. Hu, M.-T. Chu, Y.-L. Tsai, Y.-J. Tsai, C.-P. Hsu, and D.-S. Wuu, "Performance of flip-chip thin-film GaN light-emitting diodes with and without patterned sapphires", *Photonics Technology Letters, IEEE*, vol. 22, no. 8, pp. 550–552, 2010.

[44] H. Aoshima, K. Takeda, K. Takehara, S. Ito, M. Mori, M. Iwaya, T. Takeuchi, S. Kamiyama, I. Akasaki, and H. Amano, "Laser lift-off of AlN/sapphire for UV light-emitting diodes", *physica status solidi (c)*, vol. 9, no. 3-4, pp. 753–756, 2012.

[45] P. Dong, J. Yan, J. Wang, Y. Zhang, C. Geng, T. Wei, P. Cong, Y. Zhang, J. Zeng, Y. Tian, *et al.*, "282-nm AlGaN-based deep ultraviolet light-emitting diodes with improved performance on nano-patterned sapphire substrates", *Applied Physics Letters*, vol. 102, no. 24, p. 241 113, 2013.

[46] M. Shatalov, A. Lunev, X. Hu, O. Bilenko, I. Gaska, W. Sun, J. Yang, A. Dobrinsky, Y. Bilenko, R. Gaska, *et al.*, "Performance and applications of deep UV LED", *International Journal of High Speed Electronics and Systems*, vol. 21, no. 01, 2012.

[47] X. Hu, J. Deng, J. Zhang, A. Lunev, Y. Bilenko, T. Katona, M. Shur, R. Gaska, M. Shatalov, and A. Khan, "Deep ultraviolet light-emitting diodes", *physica status solidi (a)*, vol. 203, no. 7, pp. 1815–1818, 2006.

[48] W. Sun, M. Shatalov, J. Deng, X. Hu, J. Yang, A. Lunev, Y. Bilenko, M. Shur, and R. Gaska, "Efficiency droop in 245-247 nm AlGaN light-emitting diodes with continuous wave 2 mW output power", *Applied Physics Letters*, vol. 96, no. 6, p. 061 102, 2010.

[49] H. Hirayama, Y. Tsukada, T. Maeda, and N. Kamata, "Marked enhancement in the efficiency of deep-ultraviolet AlGaN light-emitting diodes by using a multiquantum-barrier electron blocking layer", *Applied Physics Express*, vol. 3, no. 3, p. 031 002, 2010.

[50] M. Kneissl, T. Kolbe, C. Chua, V. Kueller, N. Lobo, J. Stellmach, A. Knauer, H. Rodriguez, S. Einfeldt, Z. Yang, *et al.*, "Advances in group III-nitride-

based deep UV light-emitting diode technology", *Semiconductor Science and Technology*, vol. 26, no. 1, p. 014 036, 2011.

[51] C. Sun, P. Kung, A. Saxler, H. Ohsato, K. Haritos, and M. Razeghi, "A crystallographic model of (00.1) aluminum nitride epitaxial thin film growth on (00.1) sapphire substrate", *Journal of applied physics*, vol. 75, no. 8, pp. 3964–3967, 1994.

[52] T. Kolbe, *Private communication*, 2010.

[53] J. Zhang, H. Wang, M. Gaevski, C. Chen, Q. Fareed, J. Yang, G. Simin, and M. Asif Khan, "Crack-free thick AlGaN grown on sapphire using AlN/AlGaN superlattices for strain management", *Applied physics letters*, vol. 80, no. 19, pp. 3542–3544, 2002.

[54] H.-M. Wang, J.-P. Zhang, C.-Q. Chen, Q. Fareed, J.-W. Yang, and M. A. Khan, "AlN/AlGaN superlattices as dislocation filter for low threading dislocation thick AlGaN layers on sapphire", *Applied physics letters*, vol. 81, no. 4, pp. 604–606, 2002.

[55] J. Zhang, X. Hu, A. Lunev, J. Deng, Y. Bilenko, T. M. Katona, M. S. Shur, R. Gaska, and M. A. Khan, "AlGaN deep-ultraviolet light-emitting diodes", *Japanese journal of applied physics*, vol. 44, no. 10R, p. 7250, 2005.

[56] C. Pernot, S. Fukahori, T. Inazu, T. Fujita, M. Kim, Y. Nagasawa, A. Hirano, M. Ippommatsu, M. Iwaya, S. Kamiyama, *et al.*, "Development of high efficiency 255-355 nm AlGaN-based light-emitting diodes", *physica status solidi (a)*, vol. 208, no. 7, pp. 1594–1596, 2011.

[57] H. Hirayama, T. Yatabe, N. Noguchi, T. Ohashi, and N. Kamata, "231-261 nm AlGaN deep-ultraviolet light-emitting diodes fabricated on AlN multilayer buffers grown by ammonia pulse-flow method on sapphire", *Applied Physics Letters*, vol. 91, no. 7, pp. 071 901–071 901, 2007.

[58] H. Hirayama, S. Fujikawa, N. Noguchi, J. Norimatsu, T. Takano, K. Tsubaki, and N. Kamata, "222-282 nm AlGaN and InAlGaN-based deep-UV LEDs fabricated on high-quality AlN on sapphire", *physica status solidi (a)*, vol. 206, no. 6, pp. 1176–1182, 2009.

[59] F. Brunner, H. Protzmann, M. Heuken, A. Knauer, M. Weyers, and M. Kneissl, "High-temperature growth of AlN in a production scale 11 × 2' MOVPE reactor", *physica status solidi (c)*, vol. 5, no. 6, pp. 1799–1801, 2008.

[60] W. Sun, J. Zhang, J. Yang, H. Maruska, M. Asif Khan, R. Liu, and F. Ponce, "Fine structure of AlN/AlGaN superlattice grown by pulsed atomic-layer epitaxy for dislocation filtering", *Applied Physics Letters*, vol. 87, no. 21, pp. 211 915–211 915, 2005.

[61] I. Ahmad, B. Krishnan, B. Zhang, Q. Fareed, M. Lachab, J. Dion, and A. Khan, "Dislocation reduction in high Al-content AlGaN films for deep ultraviolet light emitting diodes", *physica status solidi (a)*, vol. 208, no. 7, pp. 1501–1503, 2011.

[62] J. Yan, J. Wang, P. Cong, L. Sun, N. Liu, Z. Liu, C. Zhao, and J. Li, "Improved performance of UV-LED by p-AlGaN with graded composition", *physica status solidi (c)*, vol. 8, no. 2, pp. 461–463, 2011.

[63] L. Zhou, J. Epler, M. Krames, W. Goetz, M. Gherasimova, Z. Ren, J. Han, M. Kneissl, and N. Johnson, "Vertical injection thin-film AlGaN/AlGaN multiple-quantum-well deep ultraviolet light-emitting diodes", *Applied physics letters*, vol. 89, no. 24, pp. 241 113–241 113, 2006.

[64] V. Adivarahan, A. Heidari, B. Zhang, Q. Fareed, M. Islam, S. Hwang, K. Balakrishnan, and A. Khan, "Vertical injection thin film deep ultraviolet light emitting diodes with AlGaN multiple-quantum wells active region", *Applied physics express*, vol. 2, no. 9, p. 092 102, 2009.

[65] S. Hwang, D. Morgan, A. Kesler, M. Lachab, B. Zhang, A. Heidari, H. Nazir, I. Ahmad, J. Dion, Q. Fareed, *et al.*, "276 nm substrate-free flip-chip AlGaN light-emitting diodes", *Applied physics express*, vol. 4, no. 3, p. 032 102, 2011.

[66] F. Asif, H.-C. Chen, A. Coleman, M. Lachab, I. Ahmad, B. Zhang, Q. Fareed, V. Adivarahan, and A. Khan, "Substrate lifted-off AlGaN/AlGaN lateral conduction thin-film light-emitting diodes operating at 285 nm", *Japanese Journal of Applied Physics*, vol. 52, no. 8S, 08JG14, 2013.

[67] M. Lachab, F. Asif, B. Zhang, I. Ahmad, A. Heidari, Q. Fareed, V. Adivarahan, and A. Khan, "Enhancement of light extraction efficiency in sub-300nm nitride thin-film flip-chip light-emitting diodes", *Solid-State Electronics*, vol. 89, pp. 156–160, 2013.

[68] N. Lobo, H. Rodriguez, A. Knauer, M. Hoppe, S. Einfeldt, P. Vogt, M. Weyers, and M. Kneissl, "Enhancement of light extraction in ultraviolet light-emitting diodes using nanopixel contact design with Al reflector", *Applied Physics Letters*, vol. 96, no. 8, p. 081 109, 2010.

[69] M. Shatalov, W. Sun, A. Lunev, X. Hu, A. Dobrinsky, Y. Bilenko, J. Yang, M. Shur, R. Gaska, C. Moe, *et al.*, "AlGaN deep-ultraviolet light-emitting diodes with external quantum efficiency above 10%", *Applied Physics Express*, vol. 5, no. 8, p. 082 101, 2012.

[70] S. Nakamura, "The roles of structural imperfections in InGaN-based blue light-emitting diodes and laser diodes", *Science*, vol. 281, no. 5379, pp. 956–961, 1998.

[71] V. Adivarahan, A. Heidari, B. Zhang, Q. Fareed, S. Hwang, M. Islam, and A. Khan, "280 nm deep ultraviolet light emitting diode lamp with an AlGaN multiple quantum well active region", *Applied Physics Express*, vol. 2, no. 10, p. 102 101, 2009.

[72] M. Shatalov, J. Yang, W. Sun, R. Kennedy, R. Gaska, K. Liu, M. Shur, and G. Tamulaitis, "Efficiency of light emission in high aluminum content AlGaN quantum wells", *Journal of Applied Physics*, vol. 105, no. 7, p. 073 103, 2009.

[73] M. A. Khan, "AlGaN multiple quantum well based deep UV LEDs and their applications", *physica status solidi (a)*, vol. 203, no. 7, pp. 1764–1770, 2006.

[74] S. G. Mueller, R. T. Bondokov, K. E. Morgan, G. A. Slack, S. B. Schujman, J. Grandusky, J. A. Smart, and L. J. Schowalter, "The progress of AlN bulk growth and epitaxy for electronic applications", *physica status solidi (a)*, vol. 206, no. 6, pp. 1153–1159, 2009.

[75] R. Dalmau, B. Moody, R. Schlesser, S. Mita, J. Xie, M. Feneberg, B. Neuschl, K. Thonke, R. Collazo, A. Rice, *et al.*, "Growth and characterization of AlN and AlGaN epitaxial films on AlN single crystal substrates", *Journal of The Electrochemical Society*, vol. 158, no. 5, H530–H535, 2011.

[76] L. Schowalter, S. Schujman, W. Liu, M. Goorsky, M. Wood, J. Grandusky, and F. Shahedipour-Sandvik, "Development of native, single crystal AlN substrates for device applications", *physica status solidi (a)*, vol. 203, no. 7, pp. 1667–1671, 2006.

[77] J. R. Grandusky, J. Chen, S. R. Gibb, M. C. Mendrick, C. G. Moe, L. Rodak, G. A. Garrett, M. Wraback, and L. J. Schowalter, "270 nm pseudomorphic ultraviolet light-emitting diodes with over 60 mw continuous wave output power", *Applied Physics Express*, vol. 6, no. 3, p. 032 101, 2013.

[78] T. Kinoshita, T. Obata, T. Nagashima, H. Yanagi, B. Moody, S. Mita, S.-i. Inoue, Y. Kumagai, A. Koukitu, and Z. Sitar, "Performance and reliability of deep-ultraviolet light-emitting diodes fabricated on AlN substrates prepared by hydride vapor phase epitaxy", *Applied Physics Express*, vol. 6, no. 9, p. 092 103, 2013.

[79] G. Miller, D. Robinson, and J. Wiley, "Contactless measurement of semiconductor conductivity by radio frequency-free-carrier power absorption", *Review of Scientific Instruments*, vol. 47, no. 7, pp. 799–805, 1976.

[80] B. I. for Advanced Science and T. U. of Illinois at Urbana-Champaign. (). Scanning probe microscopy, [Online]. Available: `http://virtual.itg.uiuc.edu/training/AFM_tutorial/`.

[81] U. O. S. Florida. (). Thin films, [Online]. Available: `http://www.eng.usf.edu/~tvestgaa/ThinFilm/`.

[82] N. A. Geisse, "AFM and combined optical techniques", *Materials today*, vol. 12, no. 7, pp. 40–45, 2009.

[83] MIT. (). Xray diffraction, [Online]. Available: `http://prism.mit.edu/xray/`.

[84] J. A. Dion, "Reduced defect density nAlGaN template layer for improved output deep-UV LED", PhD thesis, UNIVERSITY OF SOUTH CAROLINA, 2011.

[85] W. Sun, V. Adivarahan, M. Shatalov, Y. Lee, S. Wu, J. Yang, J. Zhang, and M. A. Khan, "Continuous wave milliwatt power AlGaN light emitting diodes at 280 nm", *Japanese journal of applied physics*, vol. 43, no. 11A, p. L1419, 2004.

[86] M. Shatalov, W. Sun, Y. Bilenko, A. Sattu, X. Hu, J. Deng, J. Yang, M. Shur, C. Moe, M. Wraback, *et al.*, "Large chip high power deep ultraviolet light-emitting diodes", *Applied physics express*, vol. 3, no. 6, p. 062 101, 2010.

[87] J. Grandusky, J. Smart, M. Mendrick, L. Schowalter, K. Chen, and E. Schubert, "Pseudomorphic growth of thick n-type $Al_xGa_{1-x}N$ layers on low-defect-density bulk AlN substrates for UV LED applications", *Journal of Crystal Growth*, vol. 311, no. 10, pp. 2864–2866, 2009.

[88] J. Matthews and A. Blakeslee, "Defects in epitaxial multilayers: i. misfit dislocations", *Journal of Crystal Growth*, vol. 27, pp. 118–125, 1974.

[89] M. Shatalov, M. Gaevski, V. Adivarahan, and A. Khan, "Room-temperature stimulated emission from AlN at 214 nm", *Japanese journal of applied physics*, vol. 45, no. 12L, p. L1286, 2006.

[90] T. Wunderer, C. Chua, J. Northrup, Z. Yang, N. Johnson, M. Kneissl, G. Garrett, H. Shen, M. Wraback, B. Moody, *et al.*, "Optically pumped uv lasers grown on bulk AlN substrates", *physica status solidi (c)*, vol. 9, no. 3-4, pp. 822–825, 2012.

[91] J. Xie, S. Mita, Z. Bryan, W. Guo, L. Hussey, B. Moody, R. Schlesser, R. Kirste, M. Gerhold, R. Collazo, *et al.*, "Lasing and longitudinal cavity modes in photo-pumped deep ultraviolet AlGaN heterostructures", *Applied Physics Letters*, vol. 102, no. 17, p. 171 102, 2013.

[92] Z. Lochner, T.-T. Kao, Y.-S. Liu, X.-H. Li, M. M. Satter, S.-C. Shen, P. D. Yoder, J.-H. Ryou, R. D. Dupuis, Y. Wei, *et al.*, "Deep-ultraviolet lasing at 243 nm from photo-pumped AlGaN/AlN heterostructure on AlN substrate", *Applied Physics Letters*, vol. 102, no. 10, p. 101 110, 2013.

[93] V. Jmerik, E. Lutsenko, and S. Ivanov, "Plasma-assisted molecular beam epitaxy of AlGaN heterostructures for deep-ultraviolet optically pumped lasers", *physica status solidi (a)*, vol. 210, no. 3, pp. 439–450, 2013.

[94] M. Martens, F. Mehnke, C. Kuhn, C. Reich, V. Kueller, A. Knauer, C. Netzel, C. Hartmann, J. Wollweber, J. Rass, T. Wernicke, M. Bickermann, M. Weyers, and M. Kneissl, "Performance characteristics of UV-C AlGaN-based lasers grown on sapphire and bulk AlN substrates", *Photonics Technology Letters, IEEE*, vol. 26, no. 4, pp. 342–345, Feb. 2014, ISSN: 1041-1135. DOI: 10.1109/LPT.2013.2293611.

[95] M. Lachab, F. Asif, A. Coleman, I. Ahmad, B. Zhang, V. Adivarahan, and A. Khan, "Optically-pumped 285 nm edge stimulated emission from AlGaN-based led structures grown by MOCVD on sapphire substrates", *Japanese Journal of Applied Physics*, vol. 53, no. 11, p. 112 101, 2014.

[96] S. M. Sze and K. K. Ng, *Physics of semiconductor devices*. John Wiley & Sons, 2006.

[97] D. Brunner, H. Angerer, E. Bustarret, F. Freudenberg, R. Hopler, R. Dimitrov, O. Ambacher, and M. Stutzmann, "Optical constants of epitaxial AlGaN films and their temperature dependence", *Journal of applied physics*, vol. 82, no. 10, pp. 5090–5096, 1997.

[98] S. Ivanov, D. Nechaev, A. Sitnikova, V. Ratnikov, M. Yagovkina, N. Rzheutskii, E. Lutsenko, and V. Jmerik, "Plasma-assisted molecular beam epitaxy of Al(Ga)N layers and quantum well structures for optically pumped mid-UV lasers on c-Al_2O_3", *Semiconductor Science and Technology*, vol. 29, no. 8, p. 084 008, 2014.

[99] R. Banal, M. Funato, and Y. Kawakami, "Optical anisotropy in [0001]-oriented Al_x $Ga_{1-x}N$/AlN quantum wells (x>0.69)", *Physical Review B*, vol. 79, no. 12, p. 121 308, 2009.

[100] J. Northrup, C. Chua, Z. Yang, T. Wunderer, M. Kneissl, N. Johnson, and T. Kolbe, "Effect of strain and barrier composition on the polarization of light emission from AlGaN/AlN quantum wells", *Applied Physics Letters*, vol. 100, no. 2, p. 021 101, 2012.

[101] H.-C. Chen, I. Ahmad, B. Zhang, A. Coleman, M. Sultana, V. Adivarahan, and A. Khan, "Pulsed modulation doping of $Al_xGa_{1-x}N$ (x>0.6) AlGaN epilayers for deep UV optoelectronic devices", *physica status solidi (c)*, vol. 11, no. 3-4, pp. 408–411, 2014.

[102] S. Wu, S. Chhajed, L. Yan, W. Sun, M. Shatalov, V. Adivarahan, and M. A. Khan, "Matrix addressable micro-pixel 280 nm deep UV light-emitting diodes", *Japanese journal of applied physics*, vol. 45, no. 4L, p. L352, 2006.

[103] M. Shatalov, A. Chitnis, V. Mandavilli, R. Pachipulusu, J. Zhang, V. Adivarahan, S. Wu, G. Simin, M. A. Khan, G. Tamulaitis, *et al.*, "Time-resolved electroluminescence of AlGaN-based light-emitting diodes with emission at 285 nm", *Applied physics letters*, vol. 82, no. 2, pp. 167–169, 2003.

[104] A. Khan, S. Hwang, J. Lowder, V. Adivarahan, and Q. Fareed, "Reliability issues in AlGaN based deep ultraviolet light emitting diodes", in *Reliability Physics Symposium, 2009 IEEE International*, IEEE, 2009, pp. 89–93.

[105] J. Grandusky, Y. Cui, S. Gibb, M. Mendrick, and L. Schowalter, "Performance and reliability of ultraviolet-C pseudomorphic light emitting diodes on bulk AlN substrates", *physica status solidi (c)*, vol. 7, no. 7-8, pp. 2199–2201, 2010.

[106] Z. Gong, M. Gaevski, V. Adivarahan, W. Sun, M. Shatalov, and M. Asif Khan, "Optical power degradation mechanisms in AlGaN-based 280 nm deep ultraviolet light-emitting diodes on sapphire", *Applied physics letters*, vol. 88, no. 12, pp. 121 106–121 106, 2006.

[107] A. Pinos, S. Marcinkevičius, J. Yang, R. Gaska, M. Shatalov, and M. Shur, "Optical studies of degradation of AlGaN quantum well based deep ultraviolet light emitting diodes", *Journal of Applied Physics*, vol. 108, no. 9, p. 093 113, 2010.

[108] M. Shatalov, Z. Gong, M. Gaevski, S. Wu, W. Sun, V. Adivarahan, and M. A. Khan, "Reliability of AlGaN-based deep UV LEDs on sapphire", in *Integrated Optoelectronic Devices 2006*, International Society for Optics and Photonics, 2006, 61340P–61340P.

[109] J. Yang, A. Lunev, G. Simin, A. Chitnis, M. Shatalov, M. A. Khan, J. E. Van Nostrand, and R. Gaska, "Selective area deposited blue GaN-InGaN multiple-quantum well light emitting diodes over silicon substrates", *Applied Physics Letters*, vol. 76, no. 3, pp. 273–275, 2000.

Appendix A

Permission to Reprint

AIP PUBLISHING LLC LICENSE
TERMS AND CONDITIONS

Apr 17, 2015

All payments must be made in full to CCC. For payment instructions, please see information listed at the bottom of this form.

License Number	3604390135349
Order Date	Apr 08, 2015
Publisher	AIP Publishing LLC
Publication	Journal of Vacuum Science & Technology B
Article Title	Deep ultraviolet photopumped stimulated emission from partially relaxed AlGaN multiple quantum well heterostructures grown on sapphire substrates
Author	Fatima Asif,Mohamed Lachab,Antwon Coleman, et al.
Online Publication Date	Oct 24, 2014
Volume number	32
Issue number	6
Type of Use	Thesis/Dissertation
Requestor type	Author (original article)
Format	Print and electronic
Portion	Excerpt (> 800 words)
Will you be translating?	No
Title of your thesis / dissertation	Design, Fabrication and Characterization of Pseudomorphic and Quasi-Pseudomorphic AlGaN based Deep Ultraviolet Light Emitting Diodes over Sapphire
Expected completion date	Apr 2015
Estimated size (number of pages)	110
Total	0.00 USD

JOHN WILEY AND SONS LICENSE
TERMS AND CONDITIONS

Apr 17, 2015

This Agreement between Fatima Asif ("You") and John Wiley and Sons ("John Wiley and Sons") consists of your license details and the terms and conditions provided by John Wiley and Sons and Copyright Clearance Center.

License Number	3604391250360
License date	Apr 08, 2015
Licensed Content Publisher	John Wiley and Sons
Licensed Content Publication	physica status solidi (c) Current topics in solid state physics
Licensed Content Title	Pseudomorphic AlxGa1-xN MQW based deep ultraviolet light emitting diodes over sapphire
Licensed Content Author	Fatima Asif,Hung-Chi Chen,Antwon Coleman,Iftikhar Ahmad,Bin Zhang,Joe Dion,Ahmad Heidari,Vinod Adivarahan,Asif Khan
Licensed Content Date	Feb 27, 2014
Pages	4
Type of use	Dissertation/Thesis
Requestor type	Author of this Wiley article
Format	Print and electronic
Portion	Full article
Will you be translating?	No
Title of your thesis / dissertation	Design, Fabrication and Characterization of Pseudomorphic and Quasi-Pseudomorphic AlGaN based Deep Ultraviolet Light Emitting Diodes over Sapphire
Expected completion date	Apr 2015
Expected size (number of pages)	110
Requestor Location	Fatima Asif 301 S. Main Street, Room 3A80 Columbia, SC 29208 COLUMBIA, SC 29208 United States Attn: Fatima Asif
Billing Type	Invoice
Billing Address	Fatima Asif 301 S. Main Street, Room 3A80 Columbia, SC 29208 COLUMBIA, SC 29208 United States Attn: Fatima Asif
Total	0.00 USD